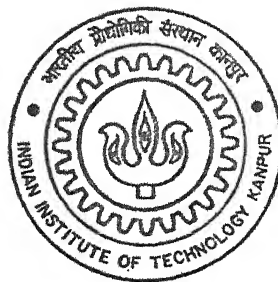# SUPERIORITY OF ELLIPTICAL JETS

by

K. N. Murugan

DEPARTMENT OF AEROSPACE ENGINEERING

Indian Institute of Technology Kanpur
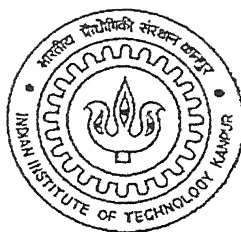
DECEMBER, 2002

SUPERIORITY OF ELLIPTICAL JETS

A Thesis Submitted in Partial Fulfillment of the Requirements
for the Degree of

MASTER OF TECHNOLOGY

by

K. N. MURUGAN

Department of Aerospace Engineering
Indian Institute of Technology Kanpur, India
December 2002

CERTIFICATE

It is certified that the work contained in the thesis entitled "**SUPERIORITY OF ELLIPTICAL JETS**" by K. N. Murugan, has been carried out under my supervision and that this work has not been submitted elsewhere for a degree.

December 30, 2002

Prof. E. Rathakrishnan
Department of Aerospace Engineering
Indian Institute of Technology Kanpur

TO MY
BELOVED SENIORS

ACKNOWLEDGEMENT

K. N. Murugan.

Abstract

Elliptical jets with aspect ratios (AR) 2, 3 and 4 were studied experimentally to understand its superiority over circular jet. The experiments were conducted for Mach numbers of 1.0, 0.8 and 0.6. Decay of the jet and its growth at different axial locations were investigated quantitatively by measuring pressure in jet field and qualitatively by visualizing the jet with a flat plate coated with lamp black. The study clearly brings out this superiority of the elliptical jet over circular jet from mixing point of view. The quantitative and qualitative results of present study bring out that the generation of vortices from largest to smallest size with continuous variation in their size. The variations of the size of the vortices are due to the continuous variation of the radius of curvature of the elliptical orifice along its azimuth. This is responsible for the enhanced mixing in the elliptical jet compared to circular one. Among the different aspect ratios tested, elliptical jet with AR = 2 experiences significantly higher mixing.

The study on correlation between axis-switching, mixing enhancement, and mass entrainment along the axial direction of the jet is also studied for all the Mach numbers (1.0, 0.8 and 0.6).

Contents

Nomenclature

AR   Aspect ratio (Ratio of major to minor diameter)

D   Nozzle exit diameter

D_e Equivalent diameter

M   Exit Mach number

m_{exit} Mass flow rate at nozzle exit

m_j Mass flow rate in the X-direction at various locations

P_a Ambient pressure

P_e Centre line pressure

P_t Pitot Pressure in the flow field

P_0 Stagnation pressure

V   Local velocity

Vc   Velocity along centerline

X   Co-ordinate perpendicular to exit plane

Y   Transverse co-ordinate parallel to plane of symmetry

Z   Span wise (lateral) co-ordinate perpendicular to plane of symmetry

List of Figures

Chapter 1

Introduction

Jets are free shear flows driven by the momentum introduced at the exit of, usually, a nozzle or an orifice. It can be defined as a pressure driven unrestricted flow of a fluid into quiescent ambience. Jets find a wide range of application both in Aerospace, commercial industry and domestic life and its use in the modern world with improved technology, various mixing and thrust producing devices. Research in the field of jets in order to gain insight of the flow-field has been the focus of study to experimentalist since 1940's. Several extensive investigations are going on in the field of jets. Extensive work has been carried out on plane and axisymmetric jets. However, not much of experimental work has been done on three-dimensional elliptical jets. Because elliptical jets has got excellent characteristics of mixing compared to the conventional circular jets. Therefore, it is very essential to characterize the elliptical jets experimentally. The jet flow studies have been mostly motivated by two important considerations, namely (1) proper understanding of the jet flow physics (2) controlling the characteristics of the evolving jet. Here, control may be defined as the ability to modify the development of the flow field by directing the energy into selected turbulence scale. Control of a jet can be either active or passive. Active control of jet require additional or auxiliary energy source. The most commonly employed active control technique is acoustic forcing. Passive control techniques do not require any additional energy; the control is generally achieved by means of special configurations like notches tabs and slots, the controlling energy drawn directly from the flow itself which is to be controlled.

Elliptical or non–axisymmetric or three-dimensional jets are emerging as a new class of jet flow control mechanism. Techniques, either passive or active, that can

accentuate the asymmetry of the vortices, which will be able to promote entrainment. For instance, small aspect ratio elliptic jets have been found to have entrainment rates several times larger than either plane symmetric or axisymmetric jets [1]. This high entrainment has been attributed to the dynamics of non-circular vortex rings that form as coherent structures in the jet shear layer. This dynamics governed by self induction, the effect of one portion of the vortex ring on another. This causes the regions of the vortex rings with higher curvature to convect ahead of the rest, which in turn, increase the curvature of the lagging portions. These portions then overtake and decrease the curvature of the initial is high curvature sections. As a result the elliptic shape is restored, but the axis that was initially the minor axis has become major axis, and the motion then begins again. This phenomenon is generally referred to as *axis-switching*. Up to seven cycles of axis switching has been observed in the evaluation of isolated free elliptic vortex rings. This behavior is also seen in vortex rings formed in shear layers of elliptic and rectangular jets. The azimuthal deformation of the vortices increases the interfacial area and engulfs more ambient fluid into the mixing layer. Therefore, the entrainment and spreading of an elliptic jet is faster than that of two-dimensional jets.

Elliptical jets having more advantage compared to other axisymmetric jets, it given below

➢ Elliptical jets having the azimuthal variation, this will help for mixing and more mass entrainment.

1.1   Applications

The detailed dynamics of jet entrainment and mixing is of fundamental importance to various applications such as noise suppression, combustion, lift augmentation, heat transfer, and chemical reactors.

1.1.1 Jet noise

The noise produced by elliptical jets was lower compared to that of the circular jet, with a higher level emitted at the wider side.

1.1.2 Heat Transfer

An impinging elliptic jet with AR=2 was used to augment heat transfer between the jet and flat plate. The maximum heat transfer at the stagnation point for the elliptic jet occurred at a shorter nozzle-to-plate distance compared to a circular jet due to the elliptical jet potential core. The Nusselt number in the impingement region for the elliptic jet was larger than that of the circular jet due to the larger entrainment and the dynamics of the large scale coherent structures

1.1.3 Combustion and mixing control

Understanding the detailed dynamics of jet entrainment and mixing is of fundamental importance for achieving efficient and environmentally clean combustion. The mixing between the reactants in diffusion flames or between the hot reaction products and the fresh reactants needed to sustain combustion are the crucial part of the combustion process. The mixing occurs in two stages. The initial stage bring relatively large amount of the reactants together (large-scale string) and is associated with the entrainment process through vortex dynamics. The second stage involves small-scale turbulent mixing, which accelerates the molecular contact between the reactants. Non-circular jets can be used to enhance both the large-sale and small-scale mixing necessary for efficient combustion.

1.1.4 Thrust Vector Control (TVC)

TVC methods have the potential to be simpler than mechanical means with lower weight penalty, thrust loss and cost. Elongated jets, such as rectangular and elliptic shaped, are better suited for aerodynamic based control than circular nozzles due to the inherent lateral instability in their wide dimension.

1.2 Aim of the Present Investigation

The present investigation is mainly concentrated on studying the following aspects of the elliptical jet flow field,

1. Overall centerline pressure decay for different Mach number with different aspect ratio (AR) of orifice

2. Evaluation of axis-switching for different elliptical orifices and circular orifice
3. Flow visualizations for all elliptical orifices and circular orifice impingement on flat plate.
4. Mass entrainment for different aspect ratio (AR) of orifices with various Mach numbers.

Chapter 2

Literature Survey

Abramovich wrote the first monograph on turbulent jets in 1936. Since that time, the theory of turbulent jets has been further developed and enriched with a large amount of experimental material has been applied in different branch of engineering. The first monograph of Abromovich dealt solely with the submerged jet, i.e., the jet that spreads through a medium at rest. In 1963, an exhaustive monograph on turbulent jets of different classes, written by Abromovich [2] was published. "Fluid Dynamics of Jets" by Pai [3] discussed both incompressible and compressible jets. Rajaratanam's [4] book on "Turbulent Jets" presents a detailed treatment of mean flow characteristics of the incompressible turbulent jets. Schlitching [5] in his well known treatise on boundary layer theory devoted a full chapter on free turbulent flows. "Physical Fluid Dynamics" by Trittan [6] discussed jet and mass entrainment into the jets. The most popular book on "Turbulence" by Hinze [7] also contains an important chapter on free turbulent shear flows. Thus jet studies have became an integral part of Fluid Mechanics.

Extensive studies have been carried out on the mean flow characteristics of both axisymmetric and plane incompressible jets. A brief description of the general feature of an incompressible jet is considered necessary at this juncture. Immediately upon exiting, the jet fluid begins to entrain the stagnant ambient fluid. The momentum is exchanged with more entrained fluid as the jet propagates. Thus in the shear flow velocity gradient is set up at a direction perpendicular to the flow direction. Helmohltz was the first person to examine theoretically, flows with mean velocity gradients, to show that the arrangement is unstable to disturbances of frequency or wavelength. The exponential amplification of

these lead to the 'roll up' of the initial thin layer immediately downstream of the nozzle (or orifice) lips into vortices. These vortices engulf the irrotational ambient fluid into jet. These vertical structures can be viewed as large-scale organized coherent structures within the turbulent shear flow. Amalgamation between these vortices also referred to as pairing in which two consecutive vortices roll over each other, causes the local shear to increase its thickness (see Figure. 2.1). The successive amalgamations between these structures produce the classical random, small-scale turbulence. Therefore the turbulent jet may be viewed as double structured in nature: Large-scale coherent structures and small-scale random structures. While the large-scale structures are periodic, the small-scale structures are random. The coherent structures are primarily responsible for entrainment of the irrotational ambient fluid and small-scale structures, for the fine scale mixing and eventual assimilation of the ambient fluid into the jet. At some distance from the nozzle exit, the mixing region becomes wide enough to penetrate the centerline of the jet. Up to this point, the centerline velocity is unaffected by the mixing and remains equal exist is called the '*Potential Core*'. Beyond this potential core, the centerline velocity begins to decay while the turbulence intensity grows. Further downstream, the jet becomes 'self preserving' i.e. it is possible to reduce all velocities by one velocity scale and all dimension by one length scale, both the scales being functions of the coordinate in the main flow direction. The general structure of free jet is shown in Figure 2.2.

Elliptical or three-dimensional jets have been found to spread and mix faster than axisymmetric jets. Ho and Gutmark [8] investigated flow characteristics of an elliptic jet with an AR 2. The mass entrainment before the end of the potential core was found to be three to eight times higher than that in an axisymmetric or a two dimensional jet. The large entrainment of the elliptic jet was found to be mainly produced in the portion near minor axis. In the region of major axis, the entrainment was approximately the same as that of the circular or the two dimensional jet for $X < 5D_e$. Through flow visualization, they observed that the self-induction of the vorticity distributed around an asymmetric contour azimuthally distorts the vortex ring; the portion of the vortex near the minor axis moves outward, a large amount of the surrounding fluid is then induced towards the axis and entrained into the jet. Elangovan S. [9] discussed axis-switching mechanism for both

sonic and supersonic flows. He concluded, up to seven cycles of axis-switching has been observed in the evaluation of isolated free elliptical rings. The axis-switching phenomenon explained here provides the elliptic jets with a capability of to control the dynamics of the coherent structures passively as well as actively.

From the literature, it is seen that jets from non-circular geometries result in enhanced mixing, a characteristics mixing is far superior to the conventional circular jet. All the literature mainly focuses on a particular geometry and/or Mach number. Further there is no literature available to address the answer to the questions that what is nature of entrained mass variation with axial distance and whether this variation is influenced by the compressibility effect. With the above aspects in mind, the present study aims at addressing the issues of efficient mixing by proper combination of large and small-scale vortices. In the subsonic Mach number region which is not wave dominated, but highly compressible.

In addition to above aspect, it has to be kept in mind that for efficient mixing it is essential not only to have proper combination of larger and small vortex structures, but the distance between the structure also should be of some limiting value in order to have entrainment and efficient mixing. To investigate these aspects elliptical orifices with aspect ratio (AR = major axis/minor axis) 2, 3 and 4 were consider in the present study. In addition to these elliptical shapes the circular orifices was also studied for comparison.
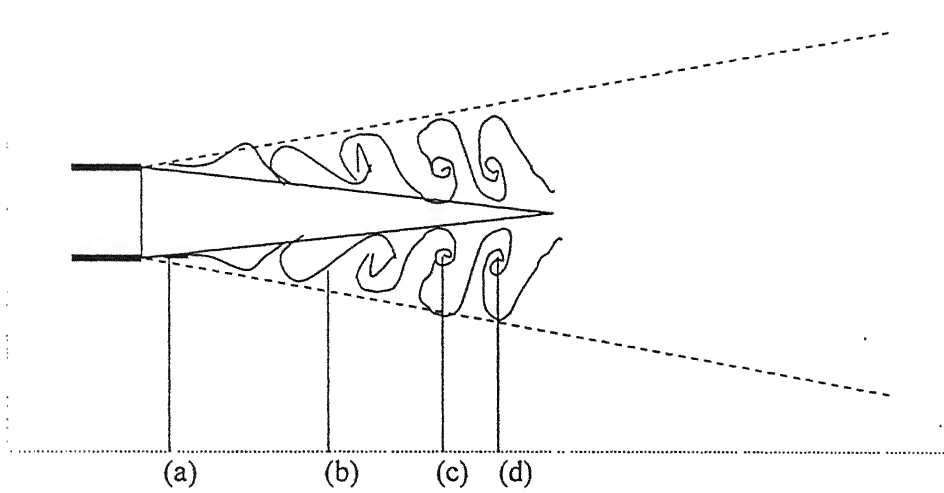
Figure. 2.1 Schematic diagram of development of shear layer
(a) Shear layer oscillates. (b) Air becomes entrained. (c) and (d) Vortices form pairs and so increase axial spacing.
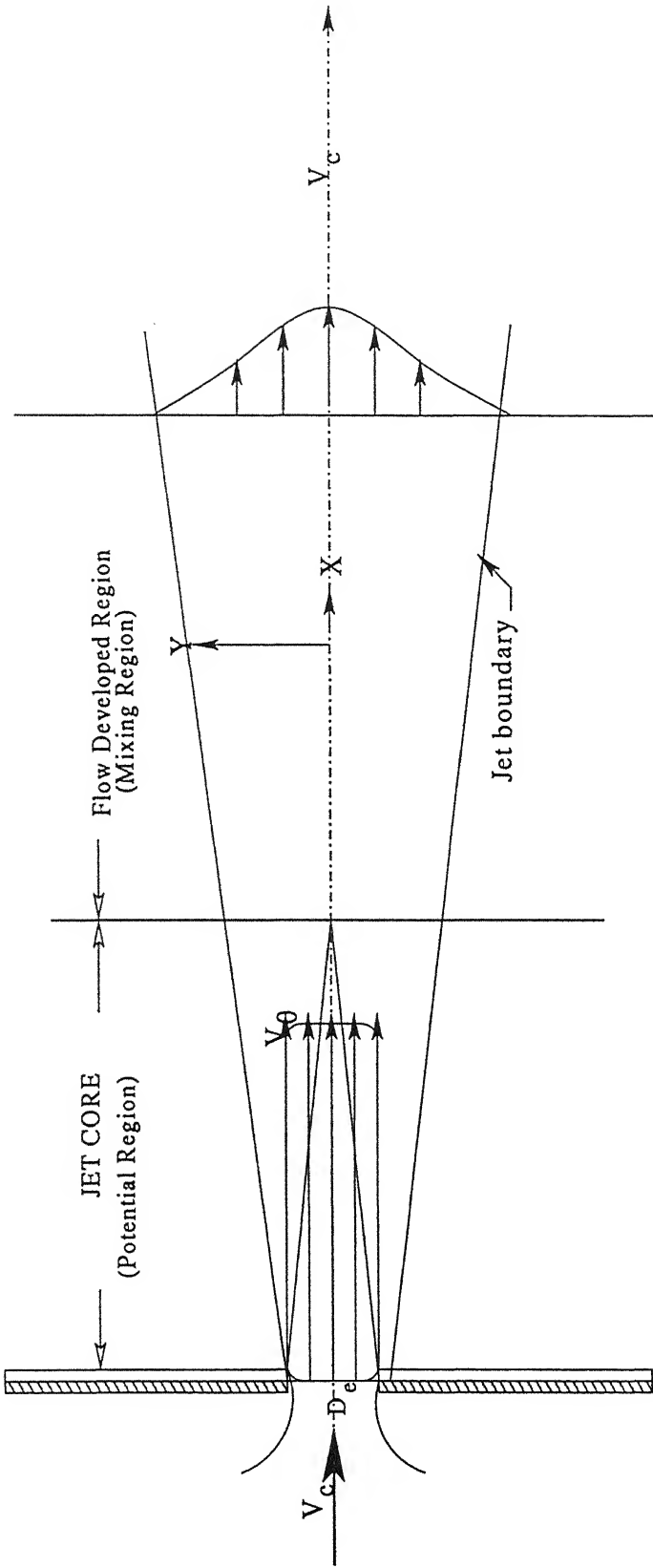
Figure. 2.2 Schemetic Diagram of Jet structure.

9

Chapter 3

Experimental Setup and Procedure

3.1 Experimental Setup

The experimental facility consists of the following components:

- ➢ Jet test facility
- ➢ Compressed air tanks
- ➢ Compressor
- ➢ Pressure measuring system
- ➢ Flow visualization

3.1.1 Jet Test Facility

Setup of the jet test facility is shown schematically in Figure.3.1a and a photographic view shown in Figure 3.1b. It consists of a settling chamber, with a provision to mount the jet nozzles on its end plate. The settling chamber is fed with the compressed dry air at high pressure through PRV (Pressure Regulating Valve) which controls the settling chamber pressure at any desired level. The settling chamber is provided with wire mesh screens to control the flow entering it to attain settled equilibrium before expansion through the jet nozzles.

3.1.2 Compressed Air Tanks

The storage system consists of 3 vessels of volume 1000 ft^3 each. The Compressed air stored in these tanks at a pressure of about 250 psi is used to drive the jet.

3.1.3 Compressor

A reciprocating compressor with a discharge of 360 cfm, driven by 150 hp electrical motor, is used to charge the storage tanks. Compressed air from the compressor is passed through a filter unit to remove the impurities and oil contamination, and then passed through drier units containing silica gel with electrical heating before reaching the storage tank.

3.1.4 Pressure Measuring System

It has dial type bourdon pressure gauge for the rough monitoring of settling chamber pressure, multi-tube water manometer and 16 channels PSI (Pressure System International) make pressure transducer with 0 – 300 psi range. The pressure probe used is pitot in the jet field, a rigid 3D traverse with 6 degrees of freedom (3 translation and 3 rotational) and having the least count of 0.10 mm in linear motion and 0.5 degree in angular motion is used.

3.1.5 Flow Visualization System

Jet flow field has been visualized by making jet impinge on a flat surface which is coated with diesel carbon and pump oil paste. The surface was a perspective plate. The plate was kept normal to the jet axis at different axial locations. After exposing the jet impingement on a plate, it was taken out and the pattern on the surface was photographed.

3.2 Experimental Models

Four types of experimental models were tested in the present investigation. They are listed below:

1. Circular orifice
2. Elliptical orifice AR = 2
3. Elliptical orifice AR = 3
4. Elliptical orifice AR = 4

All models were fabricated out of circular aluminum plates with 2 mm thickness. The circular orifice with diameter of 10 mm was drilled with smooth finishing. All elliptical

orifices were fabricated with equivalent diameter of 10 mm. The experimental models view and geometry are shown. (Figure. 3.2a to Figure. 3.2b)

3.3   Experimental Procedure

3.3.1   Center line Pressure Decay

The model was mounted on the settling chamber and all the joints were leak tested. The required pressure at the settling chamber (P_0) was maintained by controlling the PRV. The pressure tap at the settling chamber was connected to a port of PSI system and P_0 was monitored constantly. The pitot probe mounted on the traverse was aligned to face the jet axis at the orifice exit. The pitot pressure was recorded by connecting the pitot tube to another port of the PSI system. Since the jet Mach number is subsonic, the pitot pressure (P_t) measured is the pressure downstream of the jet at the pitot probe mouth. Using isentropic relation given below the jet Mach number has been calculated.

$$\frac{P_t}{P} = \left[1 + \frac{\gamma - 1}{2} M^2\right]^{\frac{\gamma}{\gamma-1}}$$

The probe is moved along the core jet axis and positioned at different stations from the orifice exit, at intervals of 1 mm from 0 to $2D_e$, 2 mm from $2D_e$ to $5D_e$, 5 mm from $5D_e$ to $10D_e$ and 10 mm beyond 10De. The jet field centerline pitot pressures at these points were recorded for a settling chamber pressure (P_0). Upon completing one measurement set, the settling chamber pressure was changed to the next Mach number level and the measurement was repeated.

3.3.2   Jet Pressure Field

After completing the centre line pressure distribution, the pressure grid measurements were made. For this, one quadrant of the jet cluster has been chosen. At a given axial location pressure at different grid points in the quadrant has been surveyed by positioning the pitot probe with the help of the traverse at the grid points. The grid points used for pressure survey is given in Table 3.1

Axial location	ΔX mm	ΔY mm	ΔZ mm
0D - 5D	10 mm	1mm	1 mm
5D - 10D	10 mm	1mm	1 mm
10D - 15D	10 mm	1 mm	1 mm

Table 3.1: Jet pressure field grid points

Pressure measurements were made at all grid points for all the levels of settling chamber pressure tested. Upon completing the centre line pressure and the jet pressure field measurements, the next model was mounted on the settling chamber and similar measurements were done.

3.3.3 Experimental Precaution

During the experimental runs the following precautions were observed.

1. The nozzle centre line was aligned longitudinally for every model.
2. The settling chamber was kept in a horizontal position to align the flow in the horizontal direction.
3. The model was carefully adjusted and checked with a sprit level to keep the measuring plane in the desired position.
4. The probe was aligned with the flow direction facing the orifice exit.
5. Before the experimental runs the leakage test was performed so that the experimental setup was leak free even at the maximum working pressure.
6. The apparatus was placed in a large room with constant ambient temperature.
7. The stagnation pressure and the air flow rate in the settling chamber were kept constant during the experiments by adjusting the PRV.

3.3.4 Data Accuracy

The possible source of error of the present investigation is due to

➤ Linear movement of the traverse along X, Y, and Z direction.
➤ Settling chamber stagnation pressure measuring pressure transducer.
➤ Error in the measurement of pitot pressure in the jet field.
➤ Possible inaccuracies in the orifices dimensions

The traverse is provided with a vernier scale of 0.1 mm. Hence, all the length dimensions measured were accurate up to 0.1 mm. The pressure measuring transducers and manometers were provided with graduations with a resolution of 1 mm. The variation of the temperature throughout on set of experimental run was less than 2%. All the pressures measured were found to be repeatable within ±3%. The maximum uncertainty involved in the pitot pressure was estimated to be ±3.5 %.

1. Settling chamber

2. Traversing system

3. Pressure measurement instrument
   (transducer)

4. Model
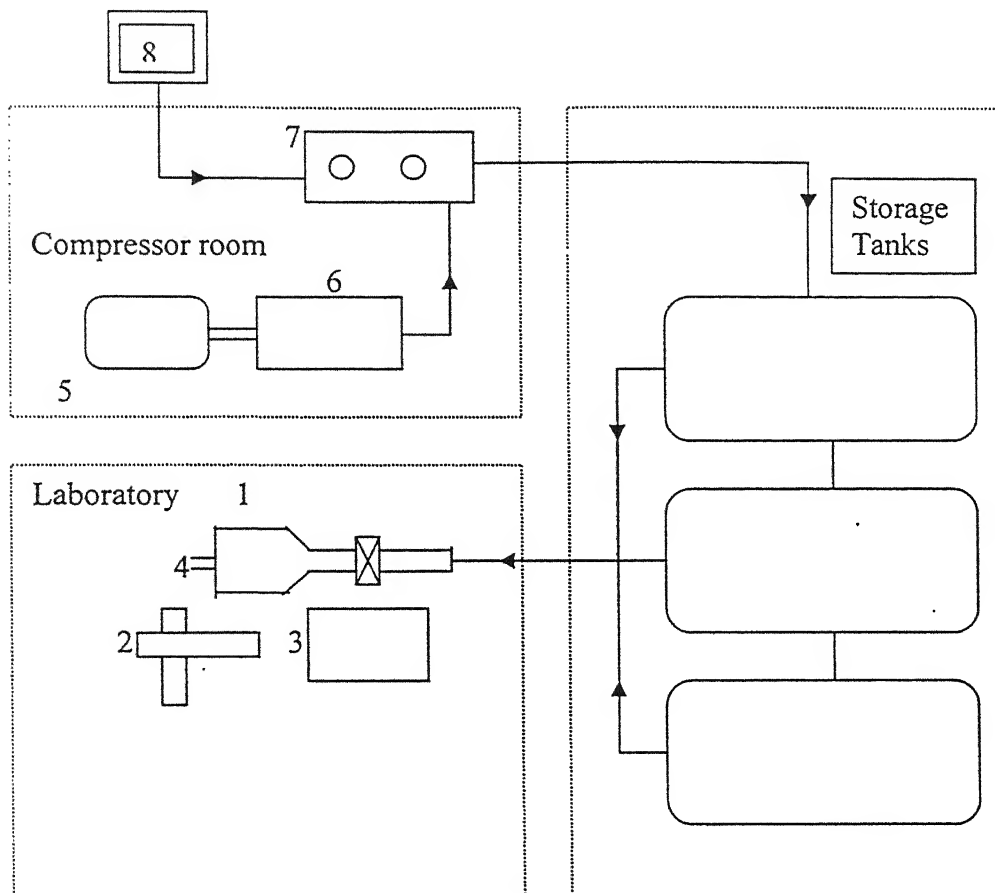
5. 150hp electric induction motor

6. Ingersoll Rand 2-stage
   Reciprocating compressor

7. Activated Charcoal Filter and
   Silica Gel drier units

8. Water-cooling unit

Figure 3.1a Schematic view of lab facility
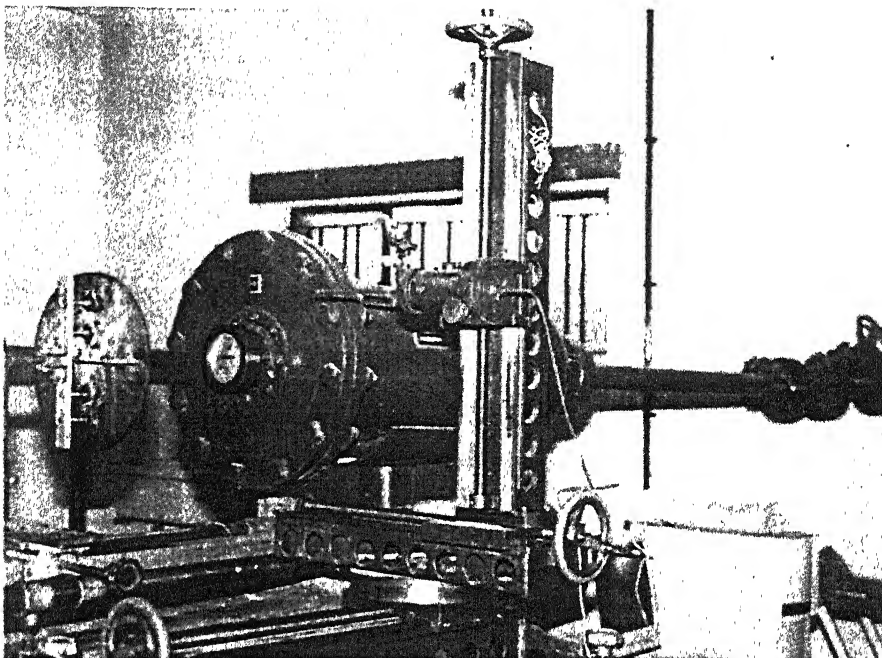
Figure. 3.1b A view of Experimental Setup (High Speed Lab. I.I.T Kanpur.)
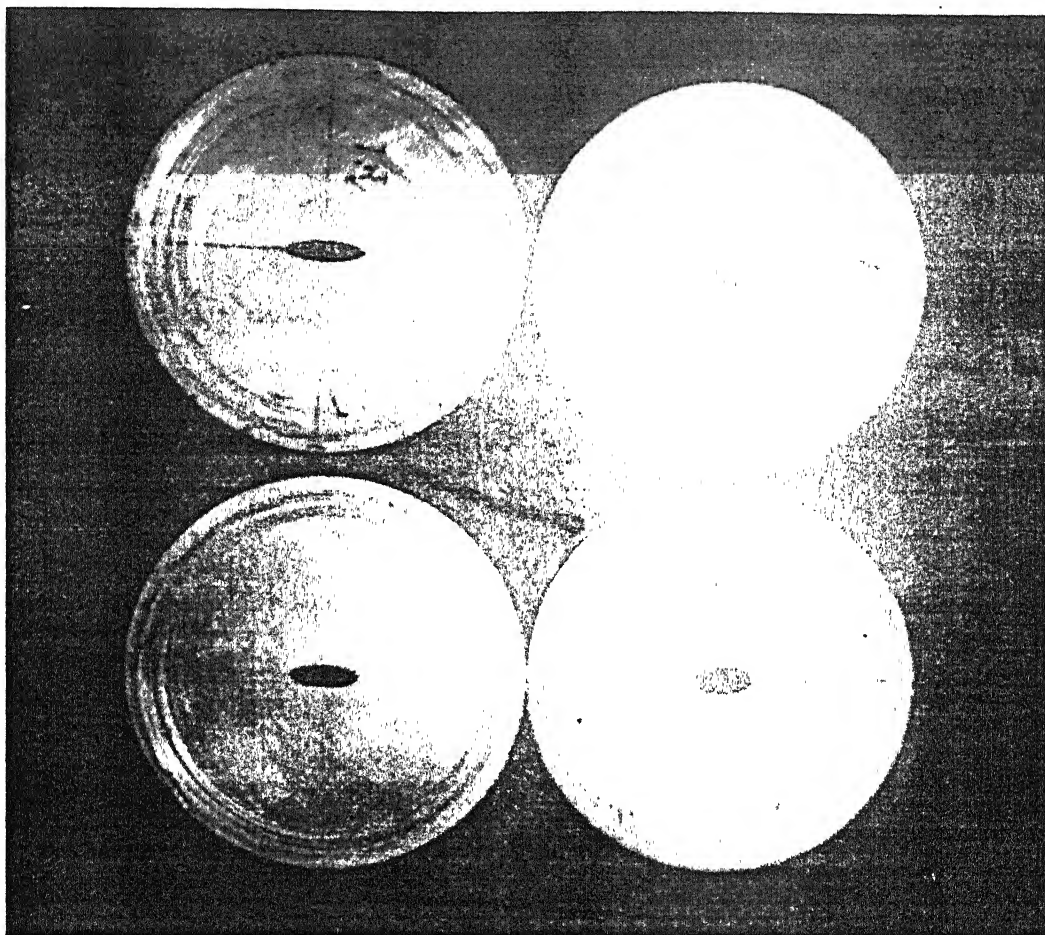
Figure 3.2a A view of experimental Models
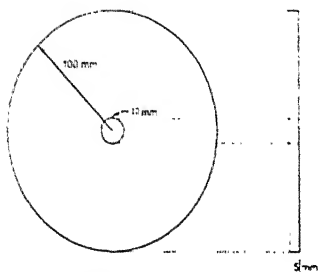
CIRCULAR ORIFICE
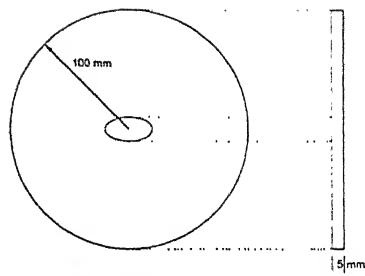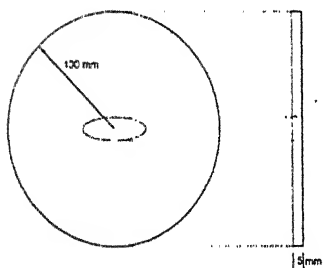
AR = 2 ORIFICE
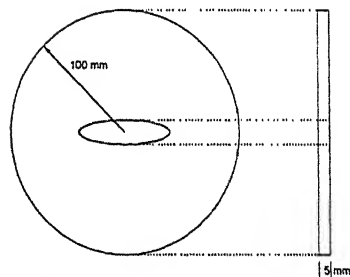
AR = 3 ORIFICE

AR = 4 ORIFICE

Figure. 3.2b Model Geometry

Chapter 4

Results and Discussion

4.1 Introduction

As it was seen in the chapter on introduction, the primary objective of the present investigation is to understand the efficacy behind superiority of elliptical jet over circular and other non-circular jets. Before, getting into the analysis of this results it is essential to recapitulate the following vital future of vortex dynamics. It is well established that the vortex size is directly proportional to the radius of curvature of the passage from which the flow is coming out. Thus the vortex generated from an orifice or nozzle will depend on the radius of the curvature of the nozzle or orifice exit [10]. Also large size vortices are very good at entraining the surrounding mass but their life is very short. As the move into the jet field, they will get fragmented into smaller vortices and get mixed up with the main flow. It is observed that the large size eddies are capable of traveling only few diameter/width of the passage from which they are getting generated. In contrast small-scale vortices are capable of traveling distance of the order of $10-15D_e$ of the passage from which they are existing. Further, small-scale structures are very efficient mixing promoters. Thus for an efficient mixing a jet with surrounding environment, both the mass entrainer mainly large-scale vortices and mixing promoters, mainly small scale vortices must coexist in proper proportion. From the literature survey, it was evident that all the researcher in the area of jet, trivial hard to identify, passage which can deliver high speed jet and the same time generate large and small scale eddies to result in efficient mixing. To achieve this goal, various technique like nozzle exit modification

(cut-outs [11], tabs [12], slots [13], cross-wire [14]) and different non-circular shape have been studied in literature. However most of the available literature mainly focuses on a particular geometry and/or Mach number. Further there is no literature available to address the answer to the questions that what is nature of entrained mass variation with axial distance and whether this variation is influenced by the compressibility effect? With the above aspects in mind, the present study aims at addressing the issues of efficient mixing by proper combination of large and small-scale vortices. In the subsonic Mach number region which is not wave dominated, but highly compressible. In the present study, the elliptical orifice was used to generate vortices from maximum to minimum size with continuous variation. Orifices avoid the growth of the boundary layer and hence jet issuing out is not influenced by the boundary layer as in the case of nozzle. It is evident that the vortex structure generate at the eccentric of minor axis are largest and those at eccentric of major axis are small for given ellipse. The continuous variation in the size of radius of curvature from minor axis end to major axis will ensure generation of vortices.

In addition to above aspect, it has to be kept in mind that for efficient mixing it is essential not only to have proper combination of larger and small vortex structures but the distance between the structure also should be of some limiting value in order to have entrainment and efficient mixing. To investigate these aspects elliptical orifices with aspect ratio (AR = major axis/minor axis) 2, 3 and 4 were consider in the present study. In addition to these elliptical shapes the circular orifices was also studied for comparison.

4.2   Centre line Pressure Decay

In the measured data consists of pitot pressure (P_t) along the jet axis as well as at different grid location in the Y, Z plane at various axial locations. All the measured pressure (P_t) were made non-dimensional with the chamber pressure (P_o) and all the distances in X, Y and Z were made non-dimensional by dividing them with equalent diameter (D_e).

It is well established that the jet centre line decay is a measure of jet mixing. Centre line pressure decay for all the orifices are given in Figures 4.1 to 4.3 for M = 1.0, 0.8 and 0.6 respectively. The results (Figure 4.1) shows that for M = 1.0 the core length is about X/De = 5 for circular orifice. For elliptical of AR = 2 and AR = 3 , the core length is about X/De = 2.0, where as for AR = 4, the core length is about X/D_e = 2.0. After the

20

core, elliptical jet with AR = 2 shows better mixing when compared with AR = 3 and circular jet and continuous superior over all other jet mixing. Even though AR = 4 shows minimum core length, the decay is much lower than AR = 2 for X/D_e more than 8.0. The reason for this may be due to the largest near field entrainment experienced by AR = 4 jet. This is because of the generation of larger eddies near minor axis ends compared to other orifices. But this advantage diminishes as the jet progresses since the interaction of the small size eddies generated at the major axis ends, it is making the larger sized eddies fragmented into tiny ones. For the smaller aspect ratio cases, even though the mass entrained by larger eddies are lesser than that of AR = 4. They have capability to travel far the distance compare to large-scale eddies generated by the AR = 4. This enables that jet from lower aspect ratio to enjoy continued combination of entrainment and efficient mixing as long as X/D_e is equal to 20. Also, it is seen that the circular jet does not have any of the advantages of mixed vortex size as in the case of elliptical shape and hence less efficient mixing compared to elliptical jet.

The centre line pressure decay for M = 0.8 jet is shown in Figure. 4.2. Here again, the AR = 4 jet exhibit the lowest core length also the core length of other jets of much smaller than those said for M = 1.0. This is because the combined effect of vortex motion and the jet velocity compared to M = 1.0 jet, the residential direction of vortices, Mach number 0.8 jet is much longer and hence the core lengths are relatively lesser. Here again AR = 2 jet experiences the best mixing compared to other jet in the far field.

The centre line pressure decay for M = 0.6 jet is shown Figure 4.3. The trend of the decay is similar to those discussed previously. However the core length slightly lesser than that of M = 1.0 and 0.8. From these discussion, it is interesting to note that as the jet Mach number decreases, the centre line velocity/pressure has a higher value at given axial distance. Further, beyond axial distance X/D_e = 25 the jet behaves almost identical.

For non-circular jet, the faster decay is also associated with early switching axis, which the major axis becomes minor axis and vice versa. The aspect of axis-switching is quantitatively analysed in the section to follow.

From above discussions it is seen that the elliptical jets are superior in mixing compared to circular jet. Also, the aspect ratio and the Mach number (compressibility) have a dominant role playing the jet propagation.

4.3 Axis-Switching

Axis-switching is phenomenon in which, for the case of elliptical jets, the initially major and minor axis cross over to become minor and major axis at downstream distance that is the jet grows rapidly along the minor axis side and very slowly (in some cases zero or negatively) along the major axis side. This differential growth makes initially elliptical jet to become axis-symmetry and subsequently to an ellipse of major and minor axis interchanged. This is because of the large-size vortex structure generated around minor axis entrains considerable amount of surrounding fluid and pushes the mass towards the jet axis. The entrained mass takes energy from fluid elements of the jet which are the higher velocity and tries to mix with the jet mass. In this process, the jet core (potential region) progressively gets reduced in size and ultimately becomes zero in size. Axial extent of the potential zone length from orifice exit. It is popularly known as *jet core*. When the mixing is enhanced, the core length will come down and thus prediction of core length is an indication of enhanced mixing.

To understand the axis-switching phenomenon, associated with shear activities of the large and small-scale structures generated and thier functional depends on jet Mach number and orifice aspect ratio (AR). The pressure measurement carried out at different location in the plane to normal to jet axis, at different axial locations. When converted to velocity refusing the following isentropic relation

$$\frac{P_t}{P} = \left[1 + \frac{\gamma - 1}{2} M^2\right]^{\left(\frac{\gamma}{\gamma - 1}\right)}$$

$$V = M \text{ x } a$$

$$V = M\sqrt{\gamma RT}$$

The calculated velocity made non-dimensional by dividing the local centre line velocity (V/Vc) and constant value of V/Vc contours in the Y, Z planes at different X/D_e are plotted in Figures 4.4 to 4.12. The inner most profile is with V/Vc = 1.0 and the outer most is V/Vc = 0.2.

4.3.1 Elliptical Jet with AR = 2

Figures 4.4 to 4.6 gives the iso-velocity profile for elliptical jet with AR = 2 at M = 1.0, 0.8, and 0.6 respectively. For M = 1.0 (Figure 4.4), the initial elliptic shape of the jet with major axis (horizontal) grows faster along the minor axis side as the jet flows downstream. Between X/D_e = 2.0 and 3.0 the jet becomes axis-symmetric and at X/D_e = 3.0 the axis-switching occurs. After that jet grows major axis (vertical) further downstream.

For M = 0.8 (Figure. 4.5), the jet growth is similar to the previous case but the axis-switching is taking place between X/D_e = 2 and 3. After that jet grows with major axis vertical and ultimately becomes a very low speed jet far downstream.

For M = 0.6 (Figure.4.6) jet proportion (growth) is identical to the previous case, and the axis-switching is experiencing around X/D_e = 2.3.

4.3.2 Elliptical Jet with AR = 3

Iso-velocity contours for AR = 3 elliptical jets are shown in Figures. 4.7 to 4.9 for M = 1.0, 0.8, and 0.6 respectively. The qualitative nature of jet propagation is that of AR = 2, but the axis-switching taking place only at about X/D_e = 6.0. This is because the azimuthal distance between minor axis and major axis end are larger than AR = 2 and hence the interaction between the mass entraining large structure mass distributing small structure is delayed. After axis-switching the jet to continuous with as major axis vertical.

For M = 0.8 (Figure 4.8), the iso-velocity contour with that of M = 1.0, expecting the axis-switching taking place at X/D_e = 5.0. That is $1D_e$ is prior to M = 1.0 jet. Jet grows with major axis normal as in the case of M = 1.0.

Iso-velocity contours for M = 0.6 are shown in Figure 4.9. For this case, the axis-switching takes place as early as possible X/D_e = 4.5.

4.3.3 Elliptical Jet with AR = 4

For iso-velocity contour for this case shown in Figures 4.10 to 4.12. For M = 1.0, the axis-switching is at X/D_e = 6.5 where as for M = 0.8 the axis-switching at X/D_e = 6.0. For M = 0.6, axis-switching taking place approximately at X/D_e = 6.0. This gives an

indication that for large aspect ratio the effect of Mach number on the axis-switching phenomenon is less pronounced compared to small aspect ratio (AR) jets. This clearly implies that the axis-switching dictating the combined effect of aspect ratio (AR) and compressibility as one can anticipated.

To quantify the above discussed details about axis-switching the variation of axis-switching with aspect ratios (AR), for the Mach numbers are shown in Figure 4.13.

As we saw, elliptical jet with AR = 2 experiences the highest mixing, and exhibits earlier axis-switching compared to AR = 3 and 4. Also, it is seen that the axis-switching distance increases with increase of aspect ratio (AR) for all Mach numbers.

4.4   Flow Visualization

To support the argument given for the axis-switching for previous section, the jet flow field has been visualized by making jet impinge on a flat surface, which is coated with diesel-carbon and pump oil paste. The surface was a perspective plate. The jet, when impinging on the surface coating was removed due to the shearing. The plate was kept normal to the jet axis at different axial locations. After exposing to plate to the jet it was taken out and the pattern on the surface was photographed with a diffused light projected from the opposite side of the plate. Visualization carried out larger number of station what is presented in the section those which appropriate with axis-switching phenomenon.

4.4.1   Elliptical Jet with AR = 2

At X/D_e = 1.0 for Mach 1.0 (Figure.4.14a) it's seen that the shape of the elliptical jet with major axis along the Y axis. Further it is seen that the jet spreads faster along the minor axis side, compared to major axis. At X/D_e = 2, the jet has grown rapidly along the minor axis and almost ready to switch over the axis. At X/D_e = 3.0, the axis-switching is over. The minor axis become major axis and vice versa. Similar results for M = 1.0 and 0.6 is shown from Figure 4.15a to 4.16c. It has been noted that these axis-switching over takes place in the region of X/D_e = 2 to 3.

From the above visualistion study, it is observed that the amount of shearing of lamb black coating on the flat plate is depends with jet Mach numbers.

4.4.2 Elliptical Jet with AR = 3

The visualization for M = 1.0 is shown in Figures 4.17a to 4.17d. It's seen that jet grows rapidly along the minor axis become axis-symmetric around at X/D_e = 3.0 and it becomes axis-switching X/D_e = 6.0. For M = 0.8, visualization picture from Figures 4.18a to 4.18e. The axis-switching taking place at X/D_e = 5.0. For M = 0.6 visualization Figures 4.19a to 4.19e shows that the axis-switching takes place at X/D_e = 4.5. Here again shear activity at the jet boundary are seen.

4.4.3 Elliptical Jet with AR = 4

The flow visualization for M = 1.0 is shown in Figures 14.20a to 4.20g. It is interesting to note that at X/D_e = 1.0, the small-scale eddies were unable to interact with large eddies eccentric of the minor axis as indicated by non-removal of the black coating at this zones. This is because of the tiny eddies generated at eccentric major axis considerably far away from the large eddy zone, for this aspect ratio compared to the lower cases. At X/D_e = 2.0, the vortex structure interaction all the periphery of the jet, because of the delayed interaction axis switching takes place between X/D_e = 6 to 7 as seen in the Figures.

The visualization for M = 0.8 jet is shown in Figures 4.21a to 4.21f. As like in the pervious case, there also large-scale eddies interact at X/D_e = 1.0. However, for this case as seen from the result the axis switching taking place around $6D_e$. The results for M = 0.6 jet are given in Figures 4.22a to 4.22f. The jet behaves similar to M = 0.8, the axis-switching nearly at $6D_e$.

4.4.4 Circular Jet

The visualization for the circular jet is shown in Figures 4.23a to 4.23d. The uniformity of the vortex structures at the jet periphery it seen as uniform shearing at all azimuthal locations. The jet is axis-symmetric at all axial location in contrast to the elliptical jet. There is no axis-switching taking place for axis-symmetric jet.

From above visualization, the axis-switching of elliptical or non-circular jet is highly depends on the orifices aspect ratio.

4.5 Pressure Profiles

To have a better understanding about the jet grows and axis-switching the pressure profiles along the transverse (Y, major axis) and normal (Z, minor axis) have been made for the different axial locations (X). The measured profile are discussed in this section.

4.5.1 Elliptical Jet with AR = 2

The pressure profile for elliptical jets with AR = 2 are presented from Figure 4.24a to 4.24c. The pressure profile along the major and minor axis at different axial locations shown (in Figure 4.24a) for M =1.0 jet. It's seen from these results the jet grows along the minor axis much faster than much along the major axis. The reason for this are explained in the previous sections, is the generation of vortices of continuous size variation from the largest minor axis end to smallest in major axis end. From the iso-velocity plots, it was seen that the axis-switching is taking place at X/D_e = 3.0. Here again the same thing is exhibited. The pressure plots for M = 0.8 are shown in Figure.4.24b. The axis-switching is at about X/D_e = 2.5 has observed in the iso-velocity contours.

The pressure plots for M = 0.6 are given in the 4.24c. Here again it seen that jet growth along the minor axis side much faster than that of the major axis side. The axis- switching taking place at X/D_e = 2.3.

4.5.2 Elliptical Jet with AR = 3

The pressure profile for AR = 3 elliptical jet given in Figure 4.25a to 4.25c. From these result as discussed in the iso-velocity section and flow visualization section, the jet grows faster along the minor axis side and the growth along the major axis side is very shallow. The axis-switching is taking place at X/D_e = 6.0, 5.0 & 4.5 for M = 1.0, 0.8 and 0.6 jets respectively.

4.5.1 Elliptical Jet with AR = 4

The results for AR = 4 elliptical jet are shown in Figure 4.26. Here again faster growth along minor axis side and the growth along minor axis side shallow are seen explicitly the axis-switching taking places at X/D_e = 6.5 and 6.0 respectively for M = 1.0 & 0.8.

4.6 Mass Entrainment

The induction of the surrounding mass into the jet field by the eddies at the jet periphery is termed as *mass entrainment* (i.e. entrained mass from zero momentum surrounding zone). When moved into the jet field, the jet acquires momentum from the jet flow thereby reducing the momentum of the original fluid, since momentum is conserved. The mass entrainment is a direct influence on the jet decay through the momentum exchange process. Higher the entrainment, faster the decay.

The mass at different cross section of the jet field (m_j) is computed from the measured pitot pressure at different grid points. The difference between m_j and m_{exit} is made non-dimensional with m_{exit}. The variation of non-dimensionalized mass flow rate $(m_j - m_{exit})/m_{exit}$ along the axial distance (X/D_e) for the elliptical jet with various Mach numbers are shown in Figure 4.27.

The entrainment results for M = 1.0 for circular jet, elliptical jet with AR = 2 and elliptical jet with AR = 4 are compared in Figure 4.27. The superiority of elliptical jet in mixing is seen in all axial locations. The entrainment is significantly larger for the case of elliptical jet with AR = 2 compared to AR = 4 and circular jet. This mixing phenomena can offer significant advantage in terms of base heating attenuation and stealth capability for launch vehicles and missiles. In the far field, AR = 2 and circular jet behaves almost identical mass entrainment.

The entrainment results for M = 0.8 jets from different orifices are compared in Figure 4.28. These result showed at all axial location the mass entrainment is much larger compared to M = 1.0 jet. Also, the elliptical jet with AR = 2 shows much higher superiority in mixing than elliptical jet with AR = 4 and circular jet at M = 0.8 compared to M = 1.0. The reason for this is that at lower Mach number the large-scale structure eddies gets a longer time to entrain the surrounding mass.

The result for M = 0.6 has been shown Figure 4.29. In this case shows much higher entrainment efficiency for AR = 2 elliptical jet did significantly augmented over the circle.

From above discussion its evident that the combined effect of azimuthal variation in the radius of curvature of the orifice and compressibility, as dominant role to play in the mass entrainment of jet.

Chapter 5

Summary and Conclusions

The superiority of the elliptical jet over circular jet is highlighted with physical reasoning in the present investigation.

    1. The generation of vortices of various sizes along the azimuth of elliptical cross section was observed from the flow pattern obtained by surface coating.

    2. The axis switching which is typical of non-circular jet, responsible of enhanced mixing over axis-symmetric jet, is captured both quantitatively and qualitatively.

    3. The axis-switching of elliptical or non-circular jet strongly depends on the orifice aspect ratio.

    4. The combined effect by compressibility and aspect ratio on the jet propagation process has been quantified and found to have dominant role to play on the jet propagation.

    5. AR = 2 elliptical jet experiences higher mixing compared to other aspect ratio jets of present study. In the axial location at which axis-switching takes place increases with increase of aspect ratio for all Mach numbers of the present study. The shearing action at the periphery is found to depend on the jet Mach number.

    From the above discussions its evident that, combined effect of azimuthal variation of radius of curvature of the orifice and compressibility has a dominant role to play in the mass entrainment of jet.

Bibliography

[1] E.J.Gutmark and F.F.Griestein, 'Flow Control with Non-circular Jets', Annual Review of Fluid Mechanics (1999), Vol. 31, pp.239-272.

[2] Abromovich G.N, 'The Theory of Turbulent Jets', M.I.T. Press, Massachusetts U.S.A., 1963.

[3] Pai S, 'Fluid Dynamics of Jets', Van Nostrand, New York, 1954.

[4] Rajaratnam N, 'Turbulent Jets', Elsevier Scientific publishing Company, Netherlands, 1976.

[5] Schliching H, 'Boundary Layer Theory', McGraw-Hill, New York, 1968.

[6] Trittan, 'Physical fluid Dynamics' Elsevier Scientific publishing Company, Netherlands

[7] Hinze J. O. Turbulence. McGraw-Hill, New York, 1968.

[8] Chin-Ming Ho and Ephraim Gutmark, 'Vortex induction and mass entrainment in a small-aspect-ratio on elliptic jet', J. Fluid Mech. (1987), vol.179, pp.383-405.

[9] Elangovan S 'Studies on Passive-Controlled Sonic and Underexpanded Free Jet' PhD Thesis, Department Aerospace Engineering, I. I. T. Kanpur. India. 1996.

[10] Rathakrishnan E, 'Fluid Mechanics'. Book to be published.

[11] S.Elangovan and Rathakrishnan E, 'Effect of cut-outs on underexpanded rectangular Jets', The Aeronautical Journal (May 1998), pp.267-275.

[12] Navin Kumar Singh and Rathakrishnan E, 'Sonic Jet Control with Tabs', Journal of Turbo and Jet Engines, Vol. 19 No. 1-2 (2002), pp. 107-106.

[13] Verma S B and Rathakrishnan E, 'Flow and Acoustic Properties of Underexpanded Elliptic-Slot Jets', AIAA Journal of Propulsion and Power, Vol. 17, No. 1(2001), pp. 49-57.

[14] Sreejith R B and Rathakrishnan E, 'Cross-Wire as Passive Device for Supersonic Jet Control', AIAA Paper No. 2002-4059. 38th JPC, Indianapolis, July 7-11, 2002.

[15] Rathakrishnan E, 'Instrumentation, Measurements and Experiments in Fluids'. Book to be published.

[16] Rathakrishnan E, 'Gas Dynamics' Prentice-Hall of India, 1995.
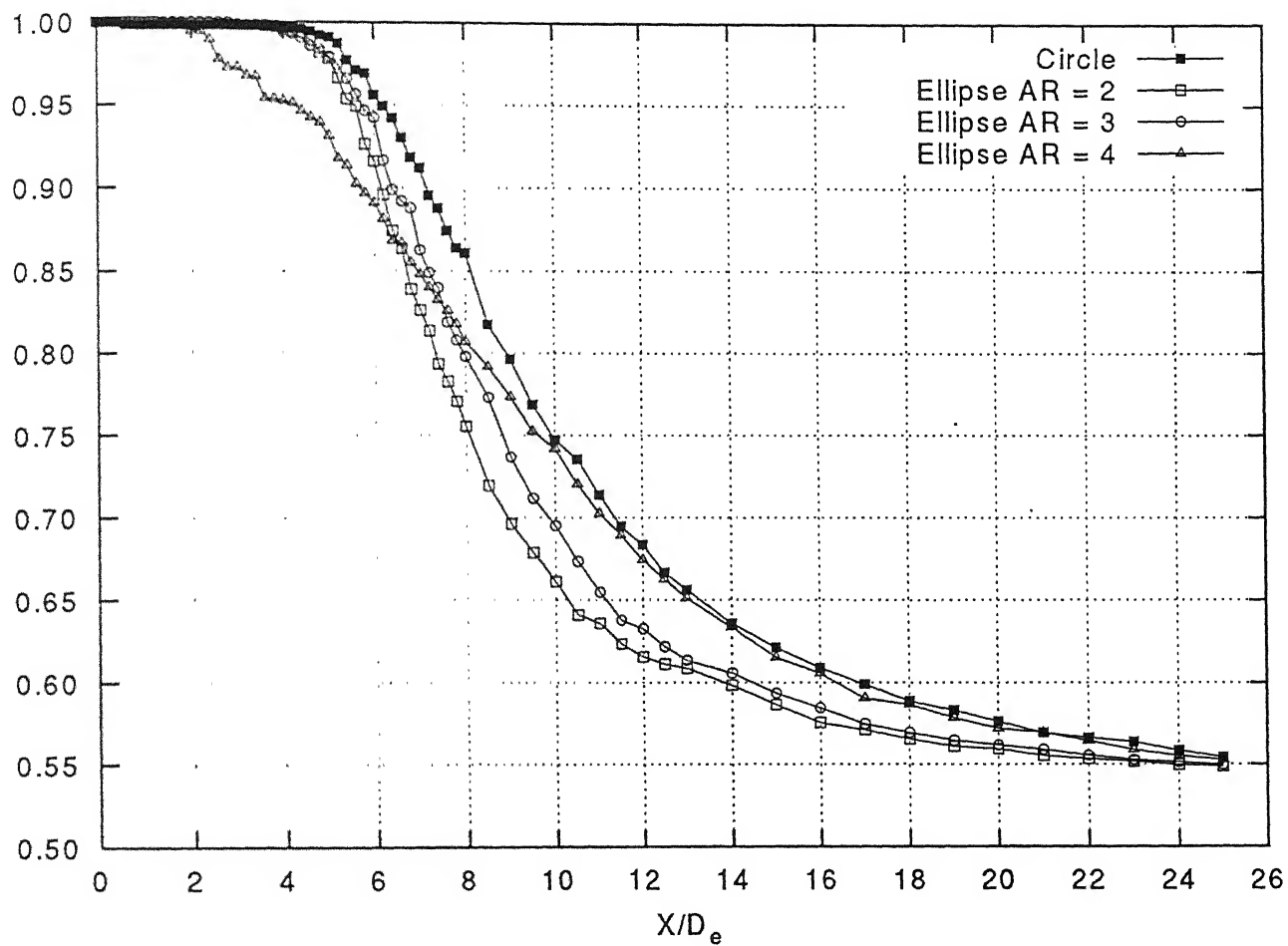
Figure. 4.1 Centerline Pressure Decay for M = 1.0
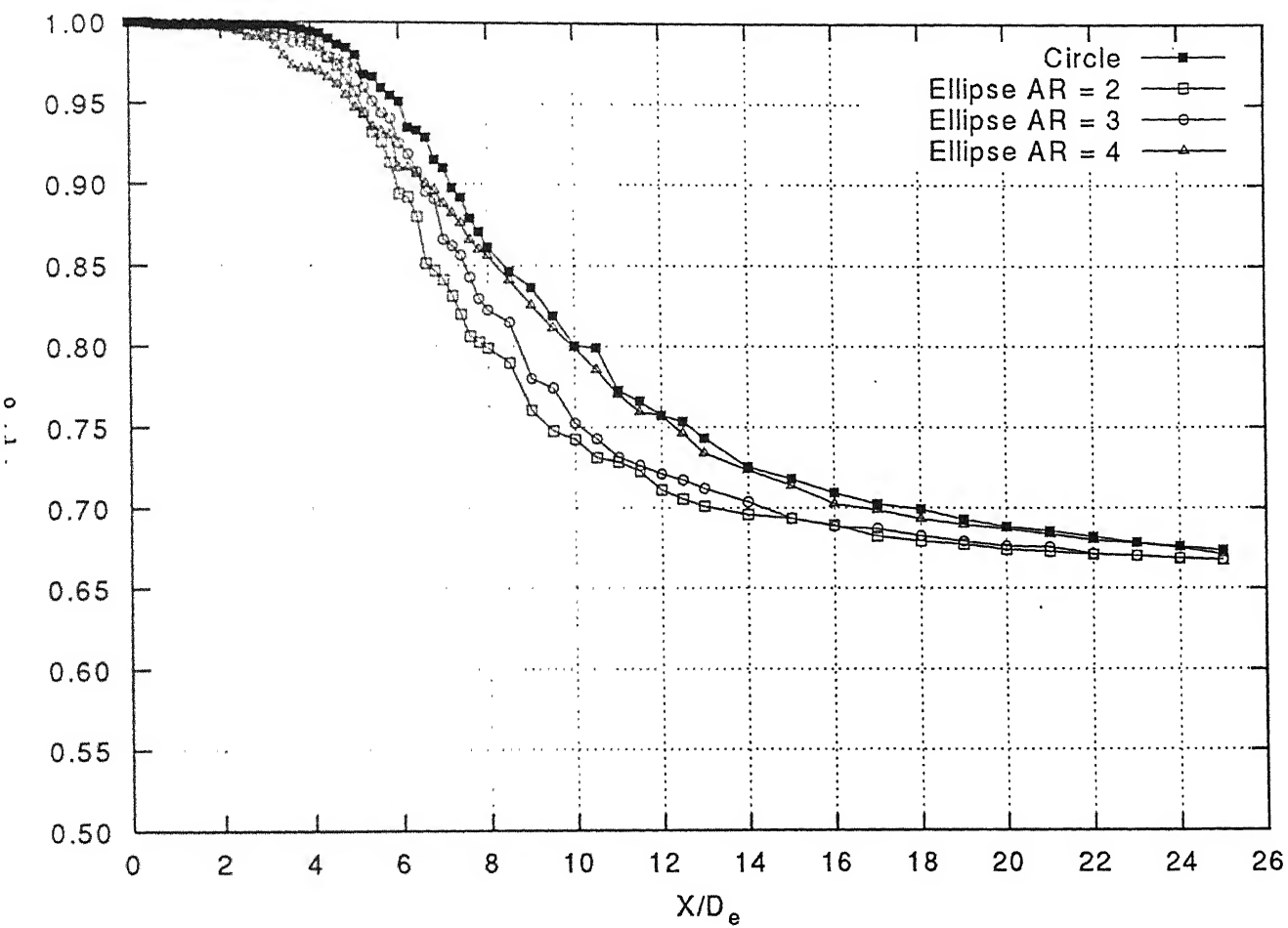
Figure. 4.2 Centerline Pressure Decay for M = 0.8
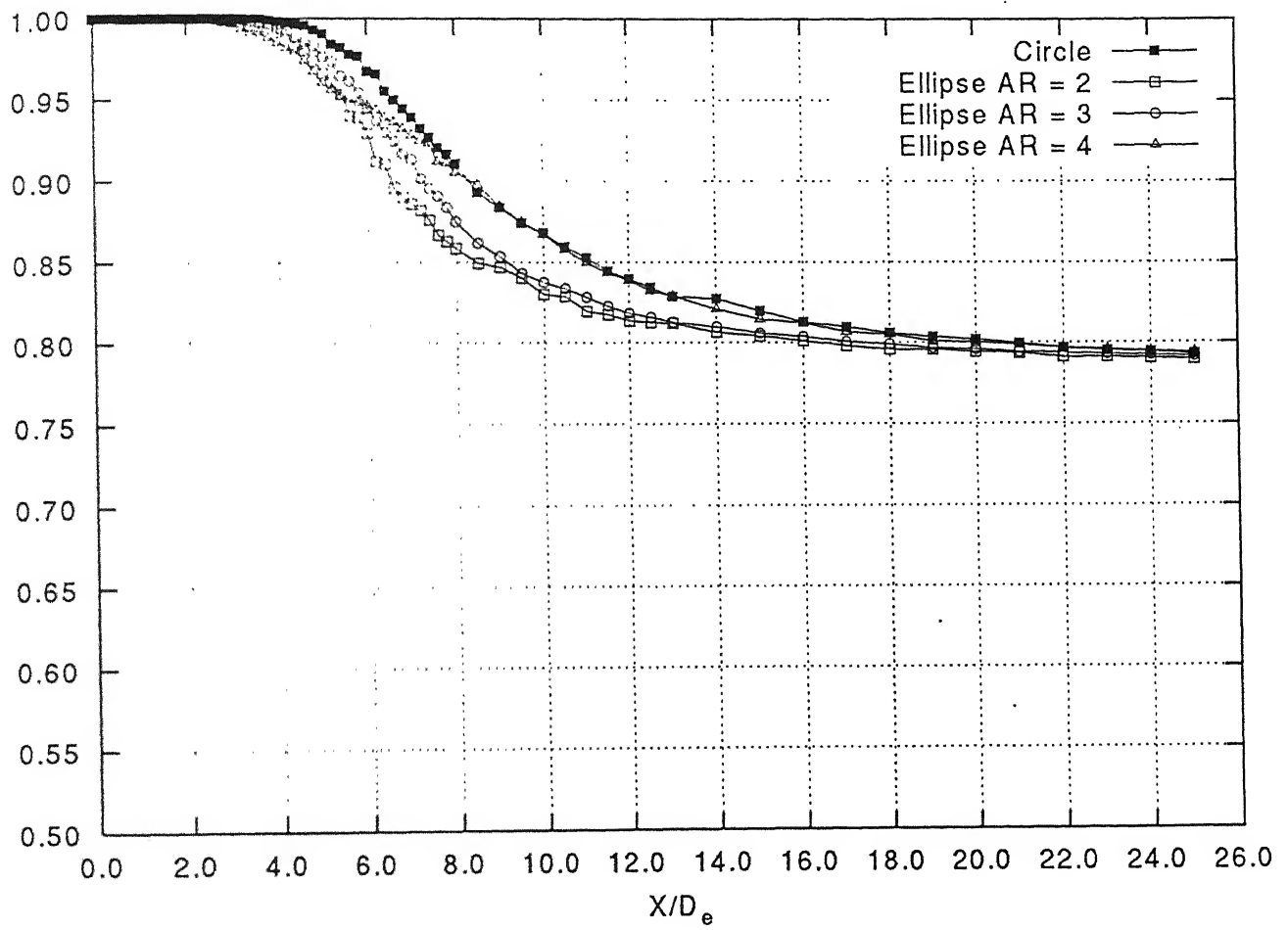
Figure. 4.3 Centerline Pressure Decay for M = 0.6
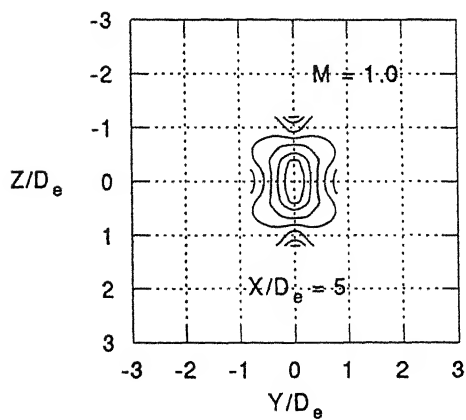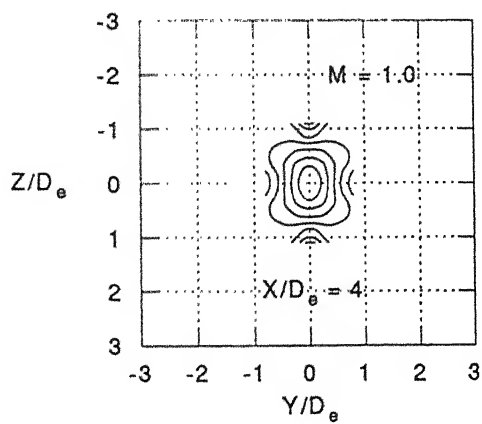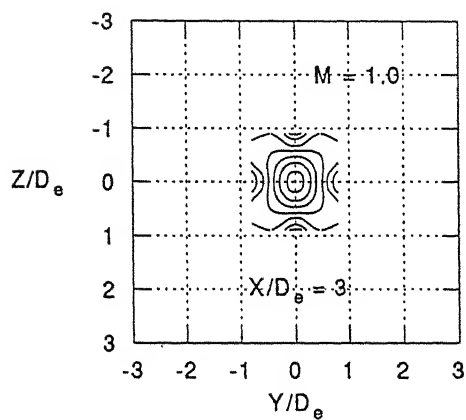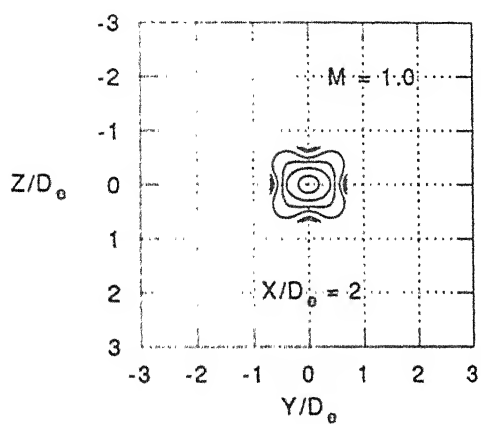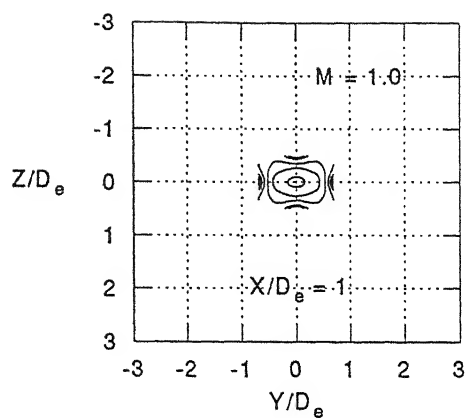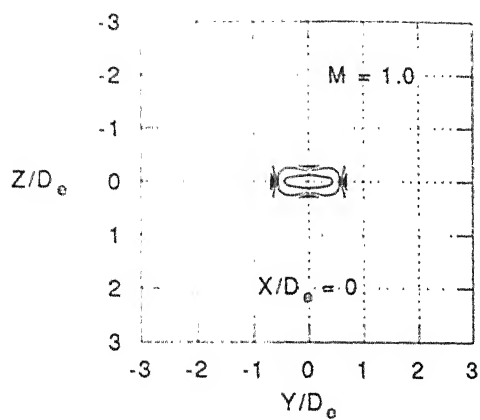
Figure. 4.4 Iso-velocity (V/Vc) profiles for AR = 2 ellipse. The innermost is for V/Vc = 1.0 and the outermost is for V/Vc = 0.2
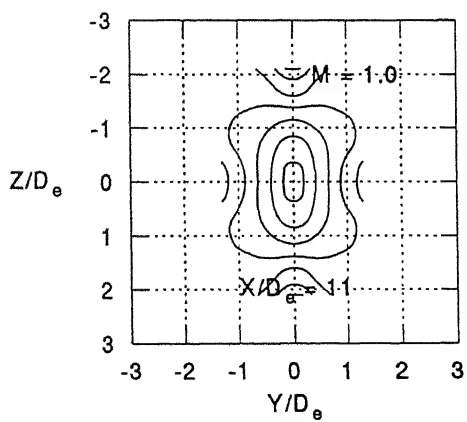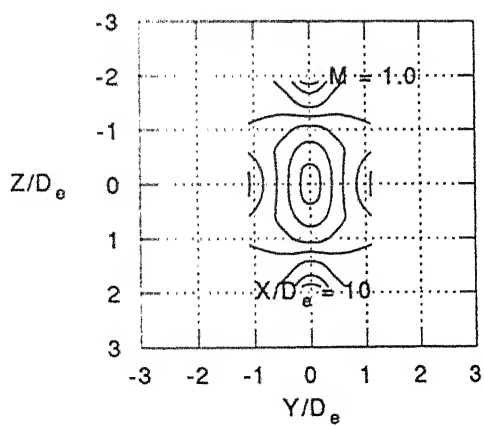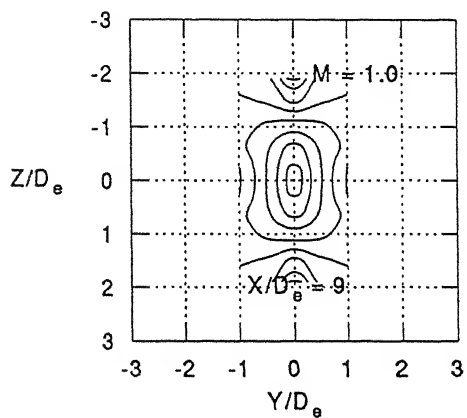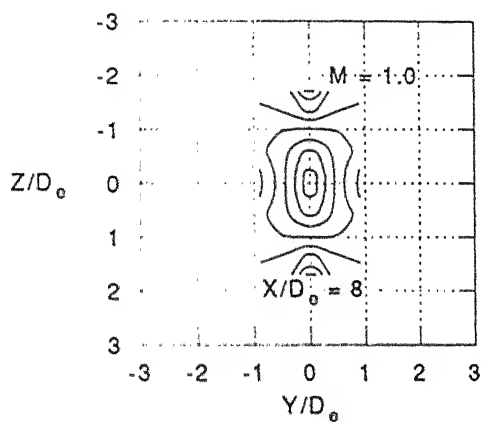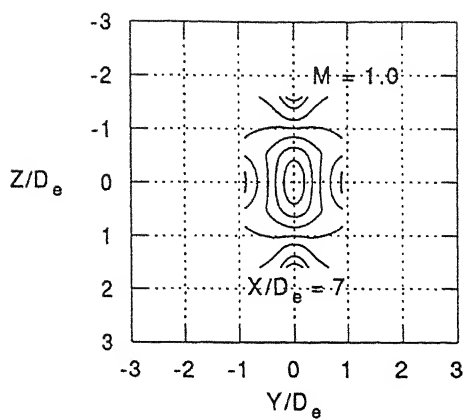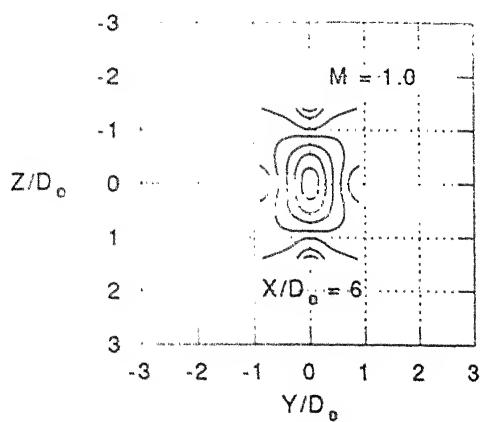
Figure. 4.4 (contd) Iso-velocity (V/Vc) profiles for AR = 2 ellipse. The innermost is for V/Vc = 1.0 and the outermost is for V/Vc = 0.2
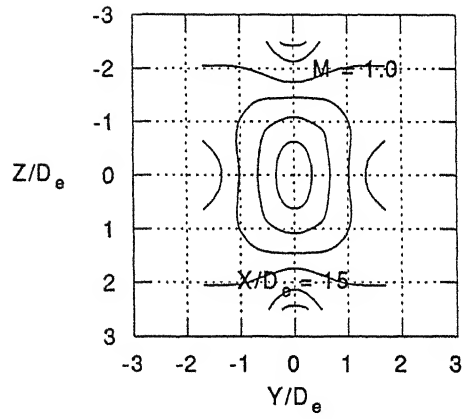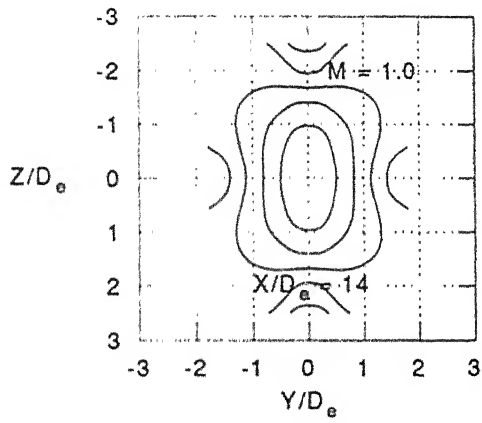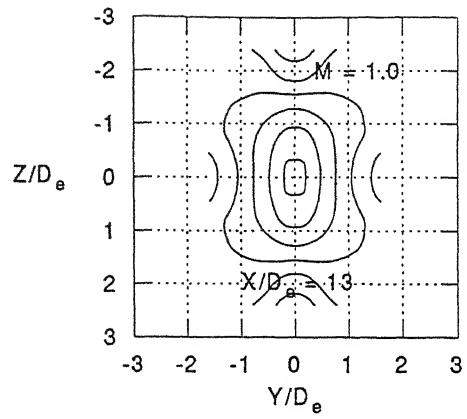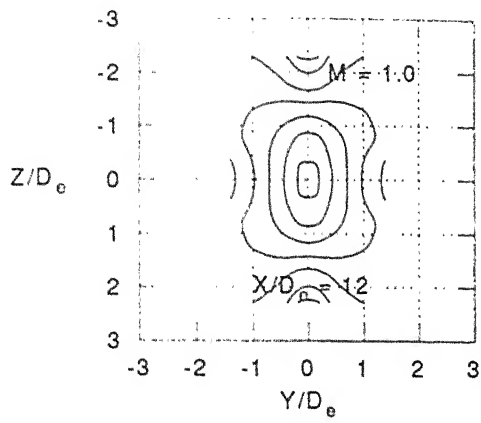
Figure. 4.4 (contd) Iso-velocity (V/Vc) profiles for AR = 2 ellipse. The innermost is for V/Vc = 1.0 and the outermost is for V/Vc = 0.2
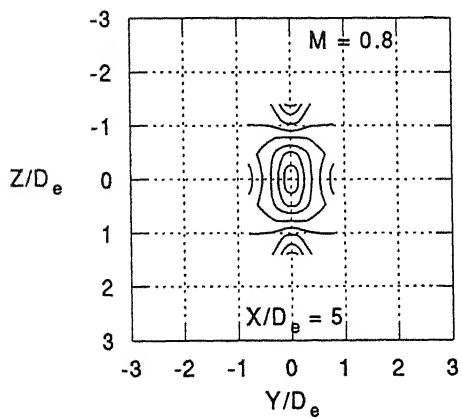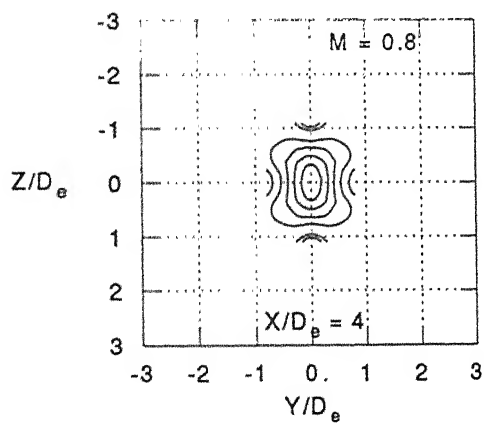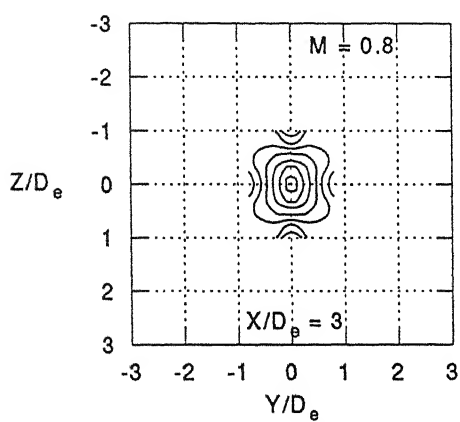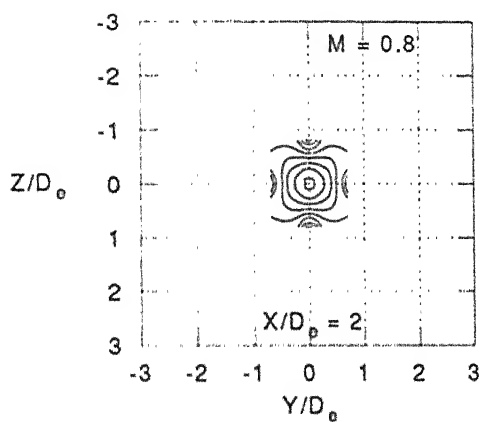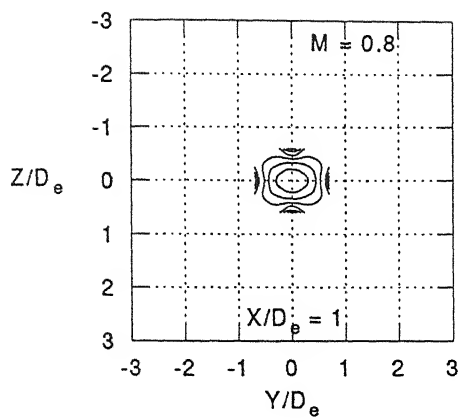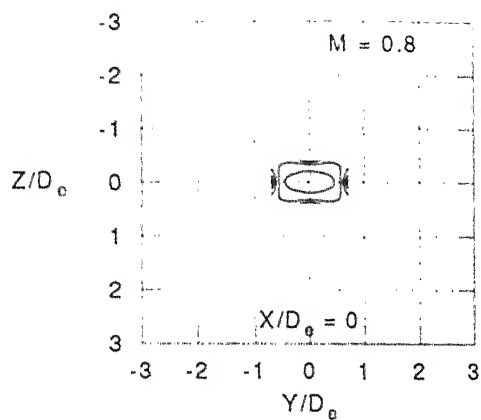
Figure. 4.5 Iso-velocity (V/Vc) profiles for AR = 2 ellipse. The innermost
is for V/Vc = 1.0 and the outermost is for V/Vc = 0.2
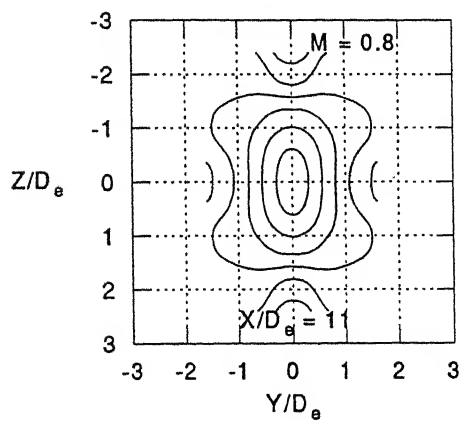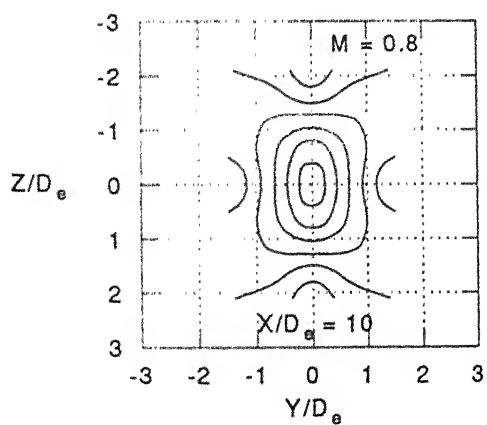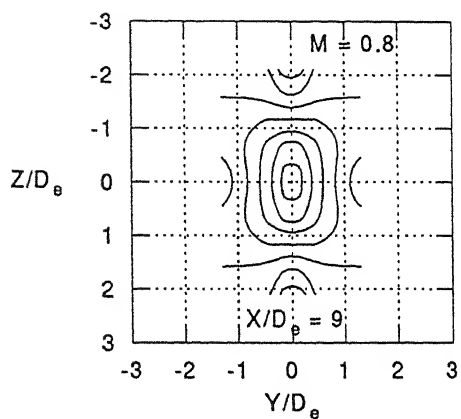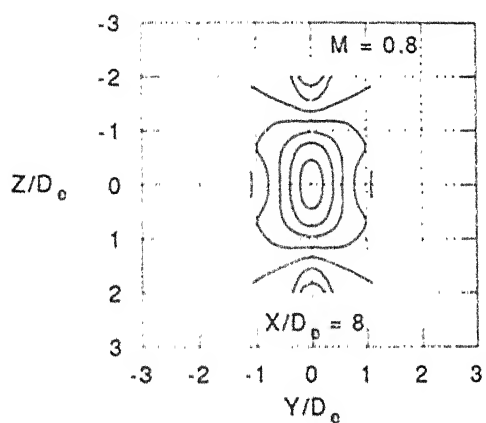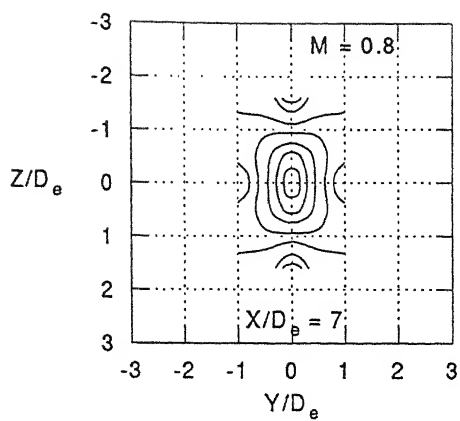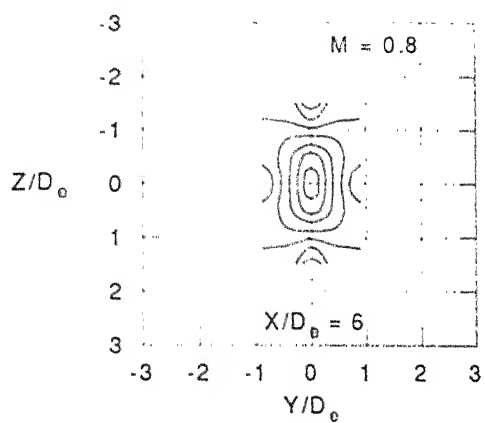
Figure. 4.5 (contd) Iso-velocity (V/Vc) profiles for AR = 2 ellipse. The innermost
is for V/Vc = 1.0 and the outermost is for V/Vc = 0.2

38
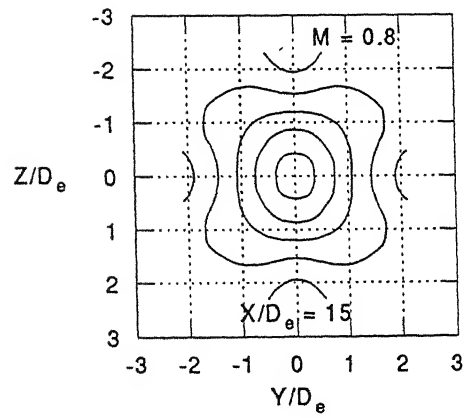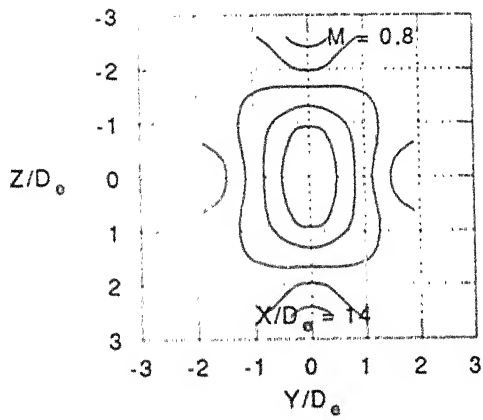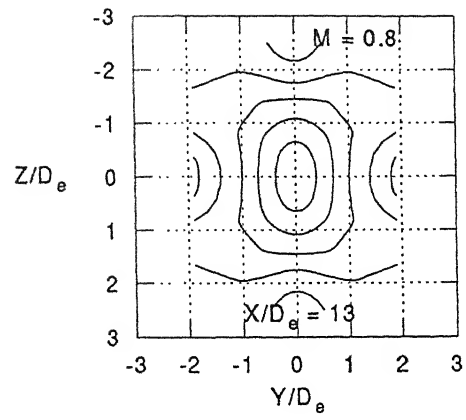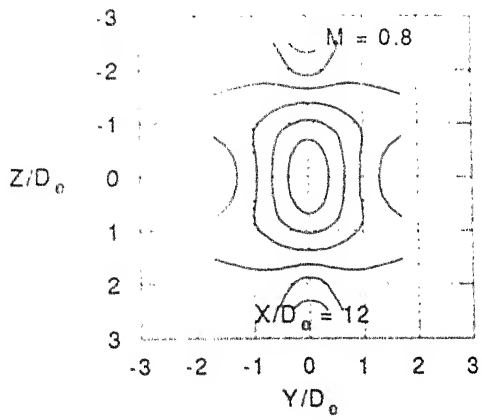
Figure. 4.5 Iso-velocity (V/Vc) profiles for AR = 2 ellipse. The innermost
is for V/Vc = 1.0 and the outermost is for V/Vc = 0.2
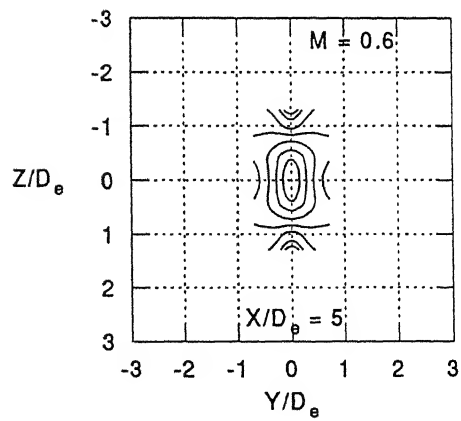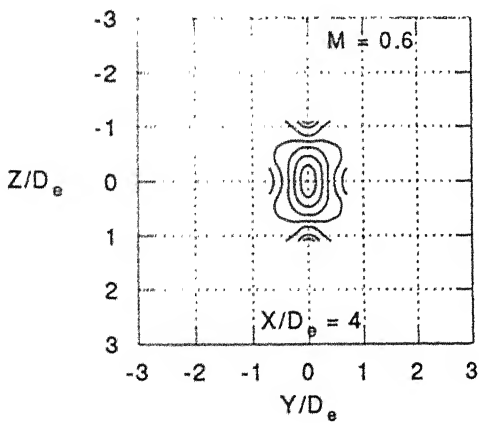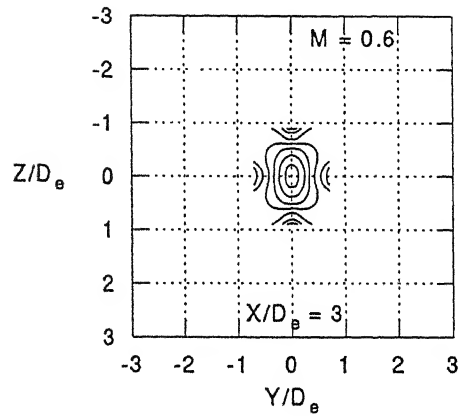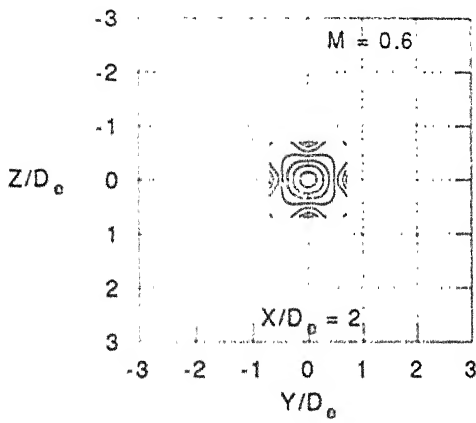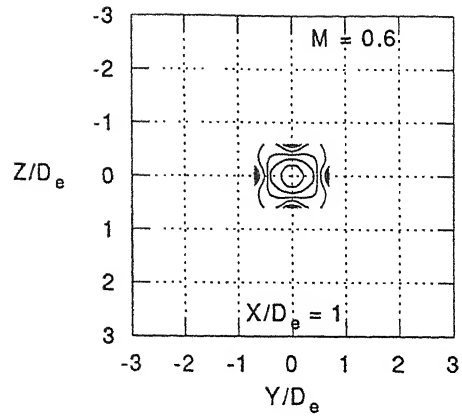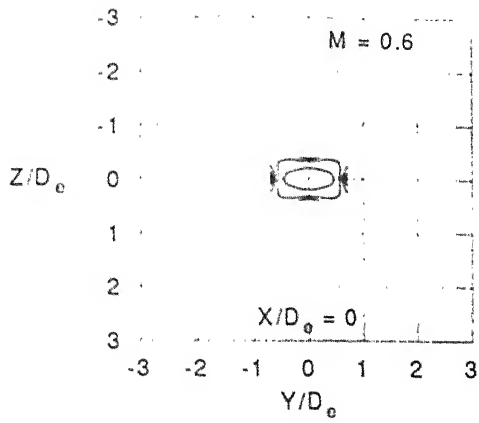
Figure. 4.6 Iso-velocity (V/Vc) profiles for AR = 2 ellipse. The innermost
is for V/Vc = 1.0 and the outermost is for V/Vc = 0.2
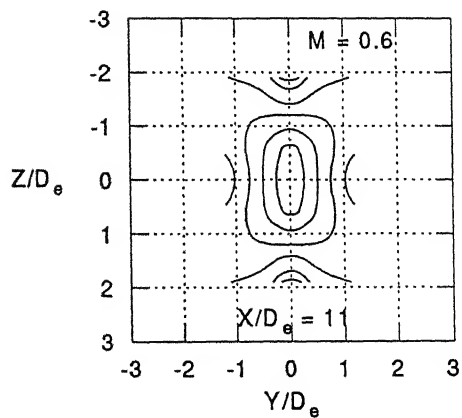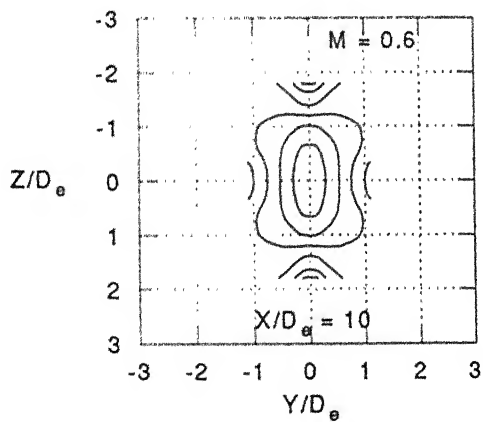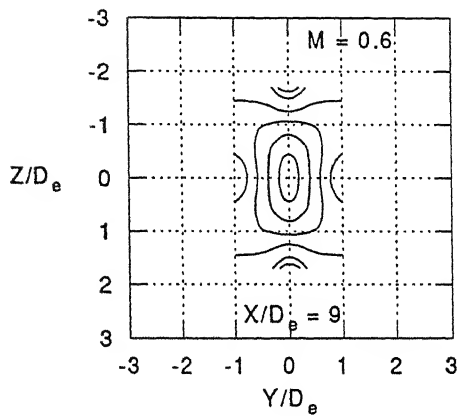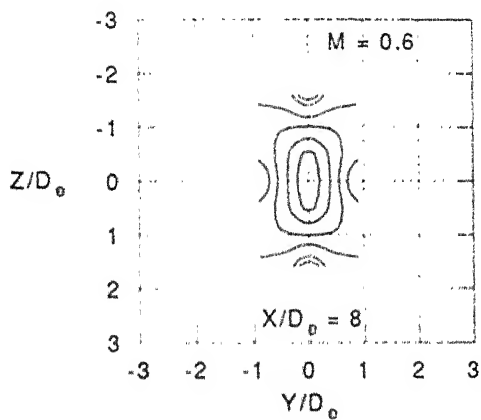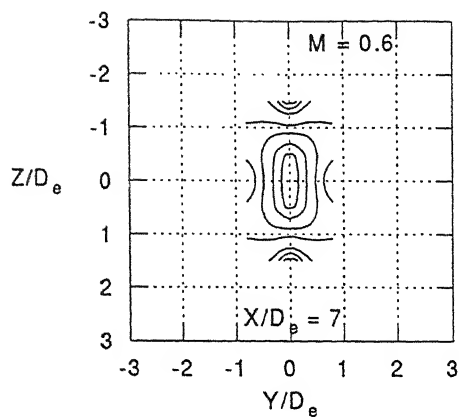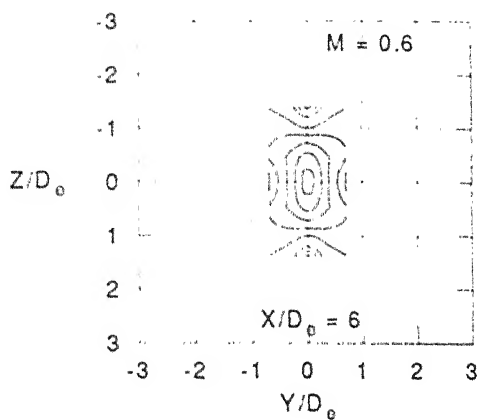
Figure. 4.6 (contd) Iso-velocity (V/Vc) profiles for AR = 3 ellipse. The innermost is for V/Vc = 1.0 and the outermost is for V/Vc = 0.2

41
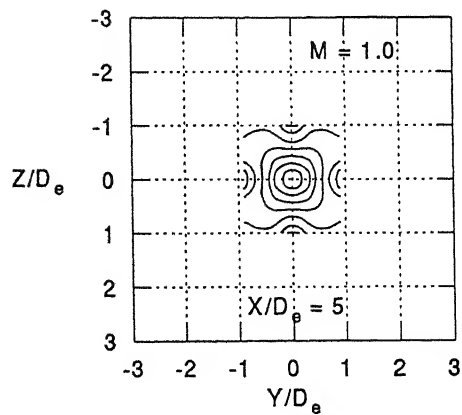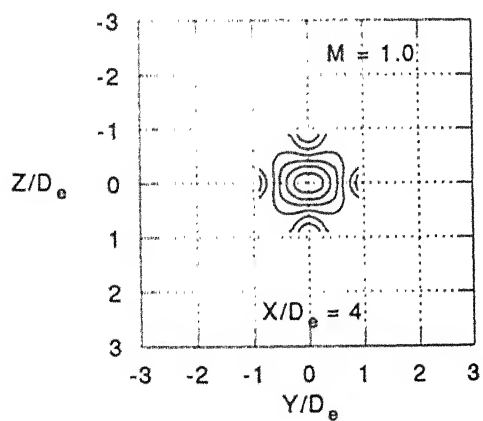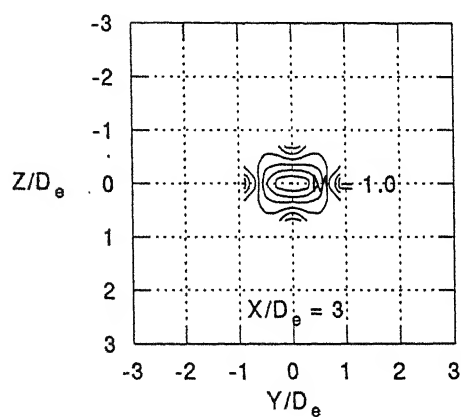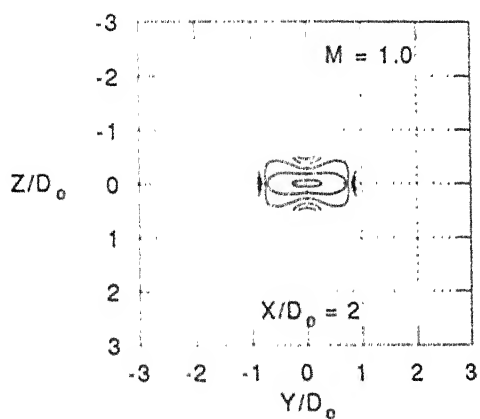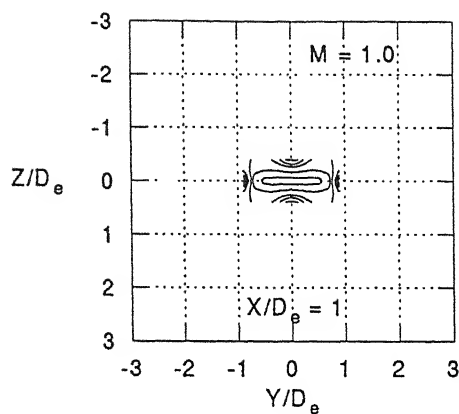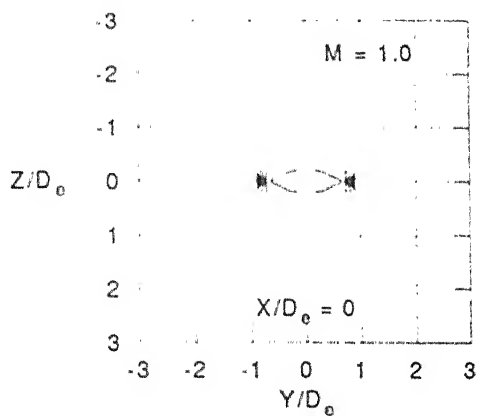
Figure. 4.7 Iso-velocity (V/Vc) profiles for AR = 3 ellipse. The innermost
is for V/Vc = 1.0 and the outermost is for V/Vc = 0.2

42
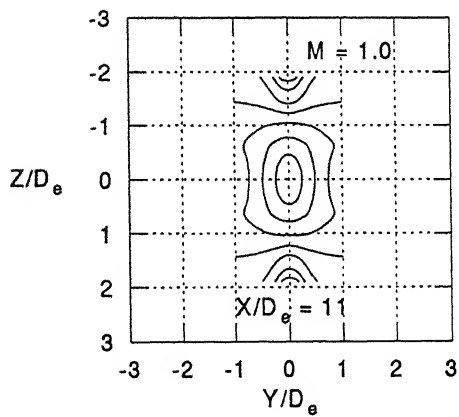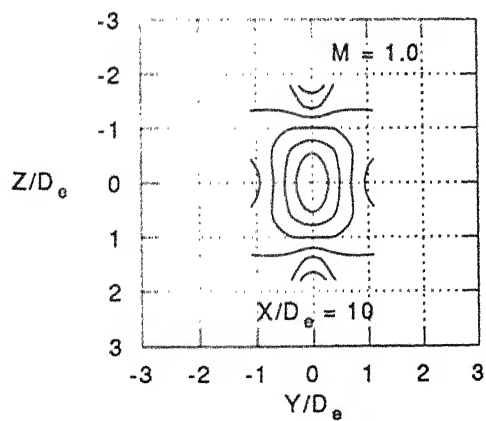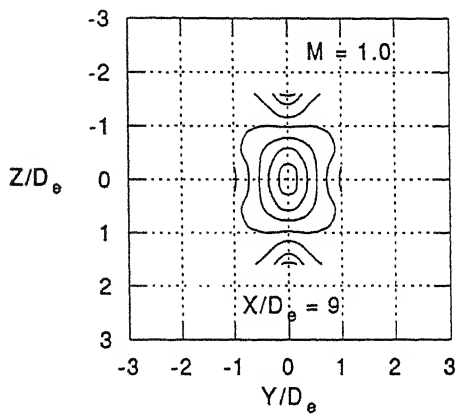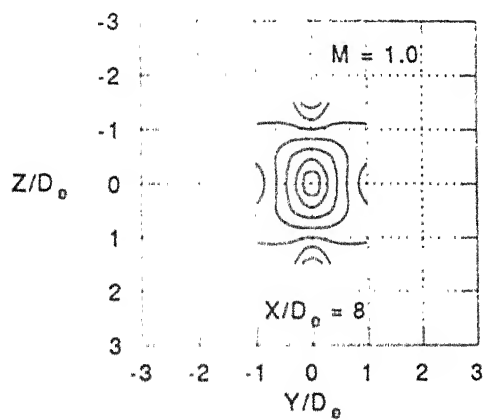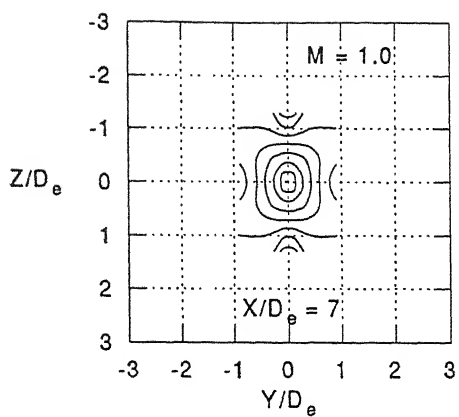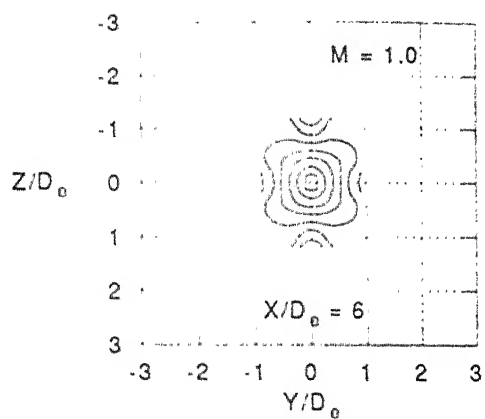
Figure. 4.7 (contd) Iso-velocity (V/Vc) profiles for AR = 3 ellipse. The innermost
is for V/Vc = 1.0 and the outermost is for V/Vc = 0.2
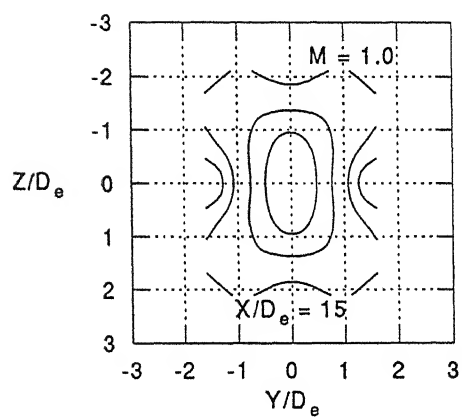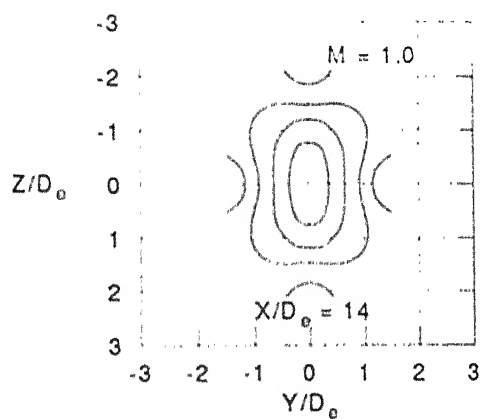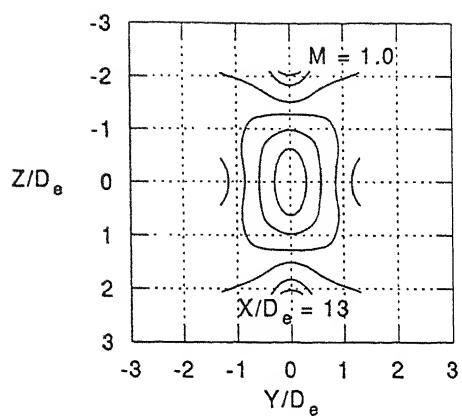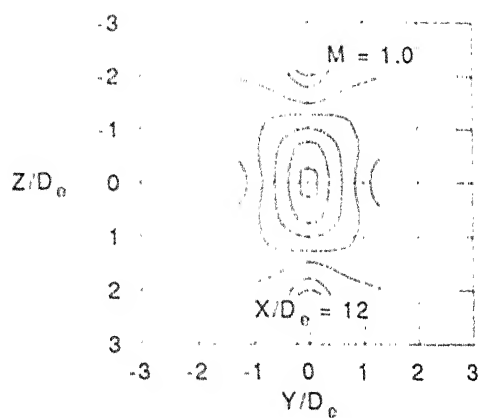
Figure. 4.7 (contd) Iso-velocity (V/Vc) profiles for AR = 3 ellipse. The innermost
is for V/Vc = 1.0 and the outermost is for V/Vc = 0.2
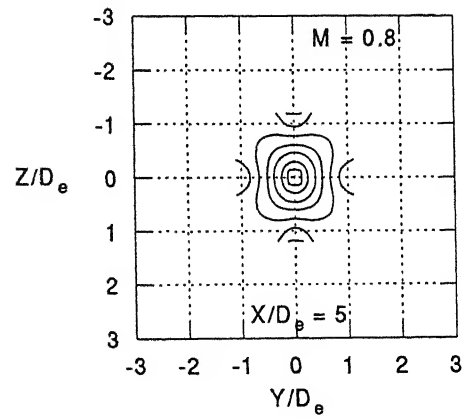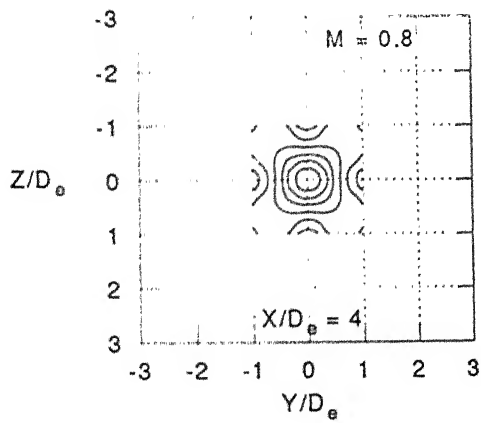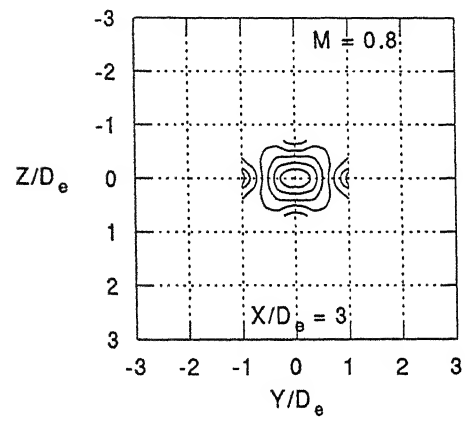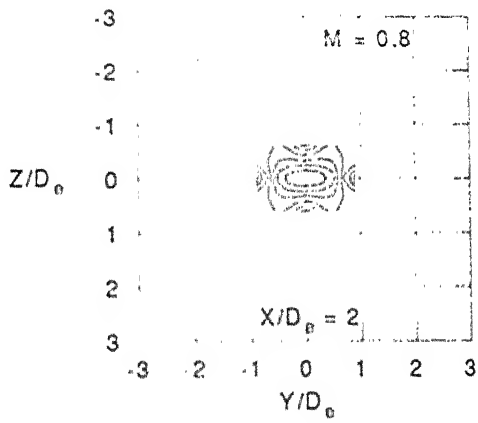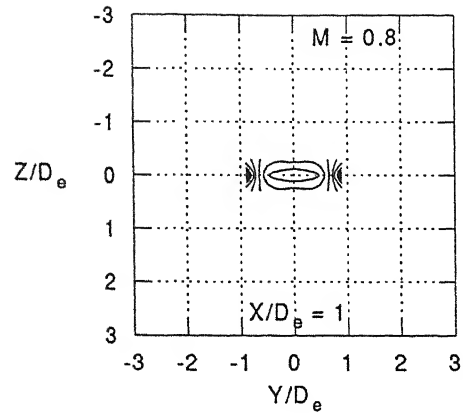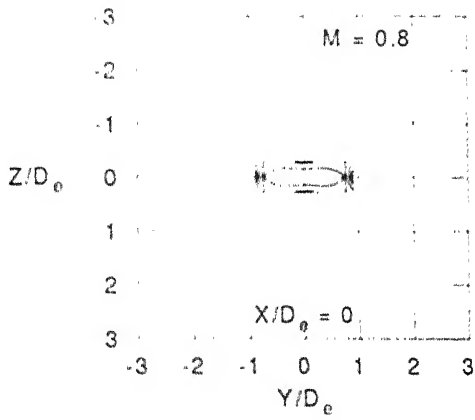
Figure. 4.8 Iso-velocity (V/Vc) profiles for AR = 3 ellipse. The innermost
is for V/Vc = 1.0 and the outermost is for V/Vc = 0.2

Figure. 4.8 (contd) Iso-velocity (V/Vc) profiles for AR = 3 ellipse. The innermost
is for V/Vc = 1.0 and the outermost is for V/Vc = 0.2

Figure. 4.8 (contd) Iso-velocity (V/Vc) profiles for AR = 3 ellipse. The innermost is for V/Vc = 1.0 and the outermost is for V/Vc = 0.2

47

Figure. 4.9 (contd) Iso-velocity (V/Vc) profiles for AR = 3 ellipse. The innermost
is for V/Vc = 1.0 and the outermost is for V/Vc = 0.2

49
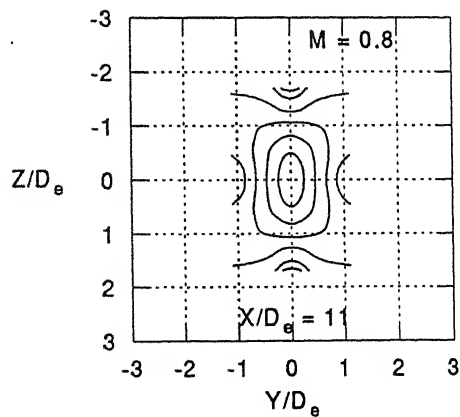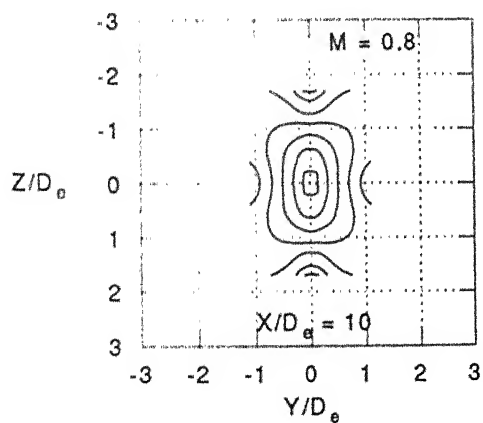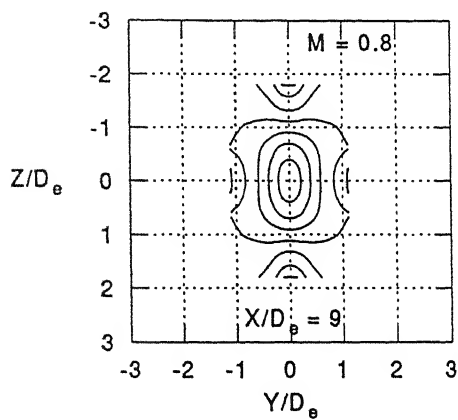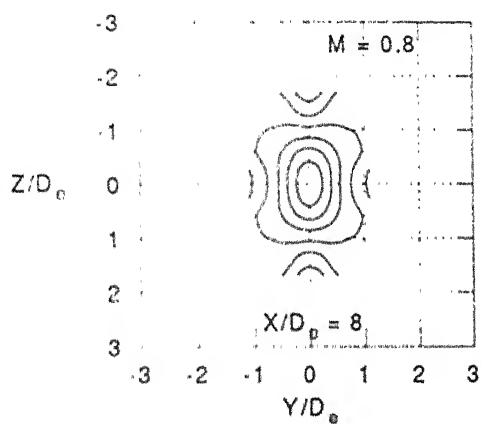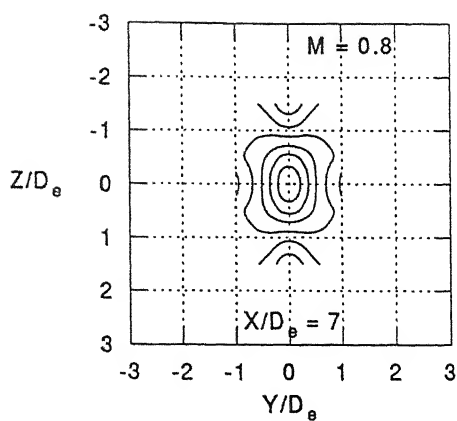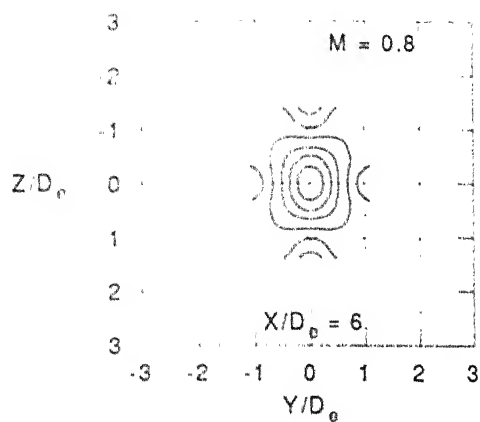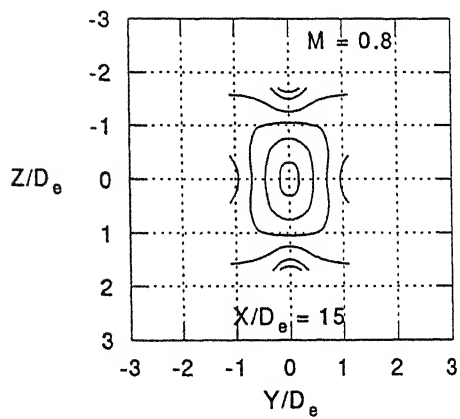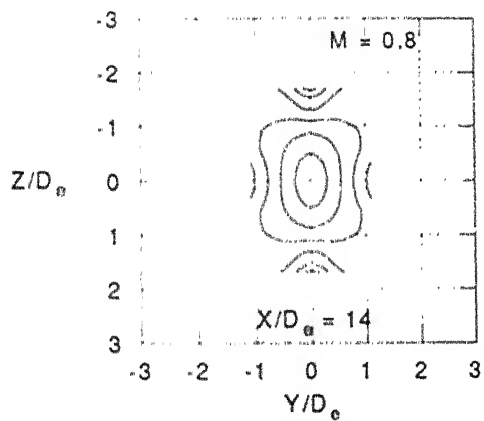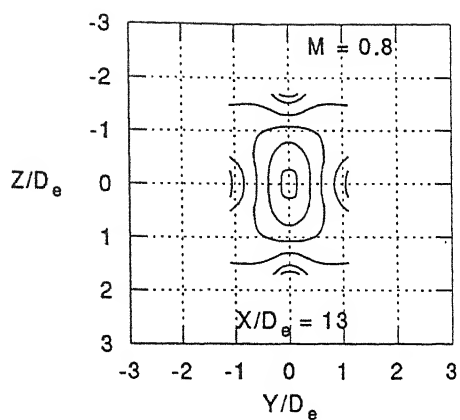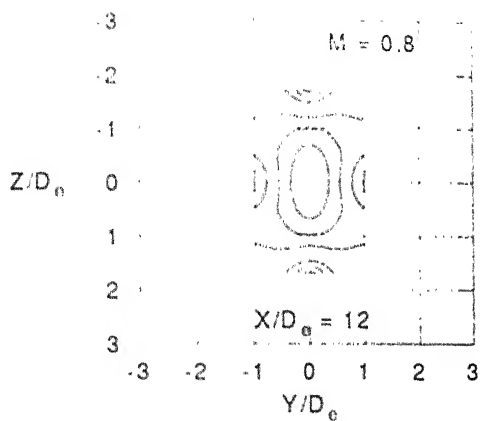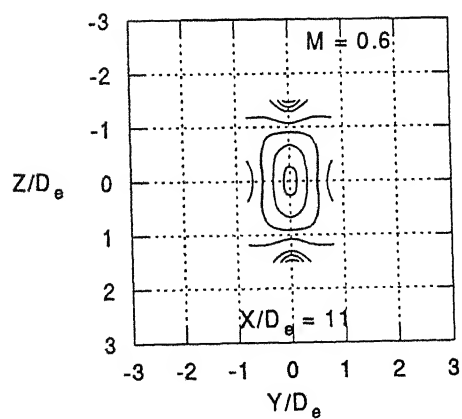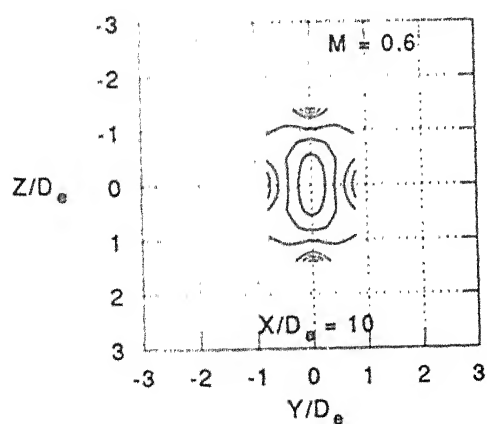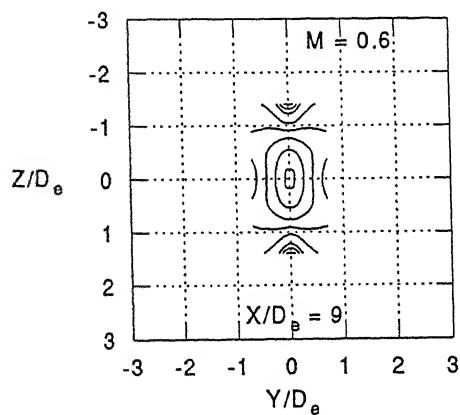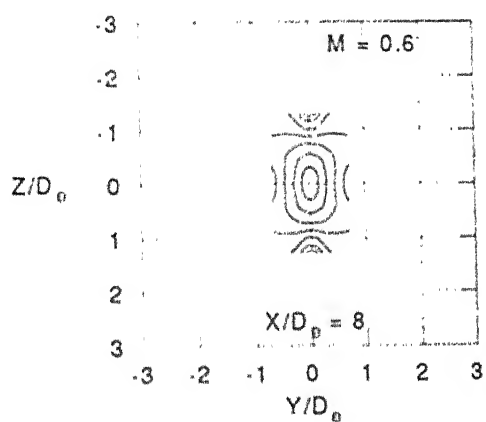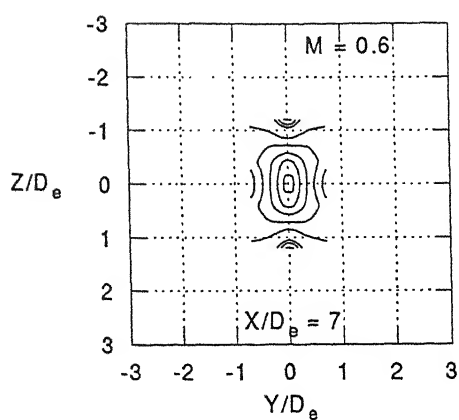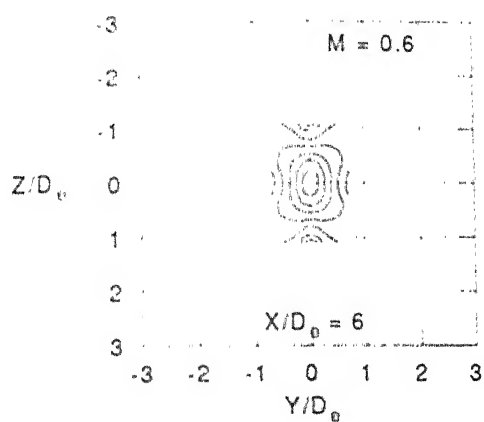
Figure. 4.9 (contd) Iso-velocity (V/Vc) profiles for AR = 3 ellipse. The innermost
is for V/Vc = 1.0 and the outermost is for V/Vc = 0.2
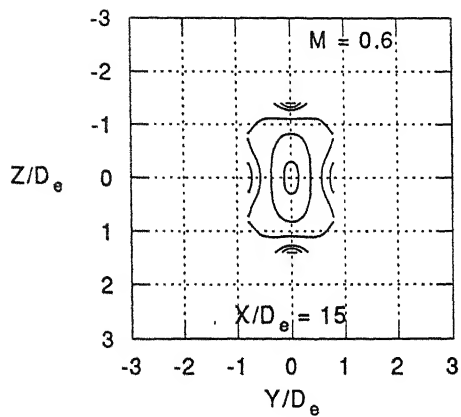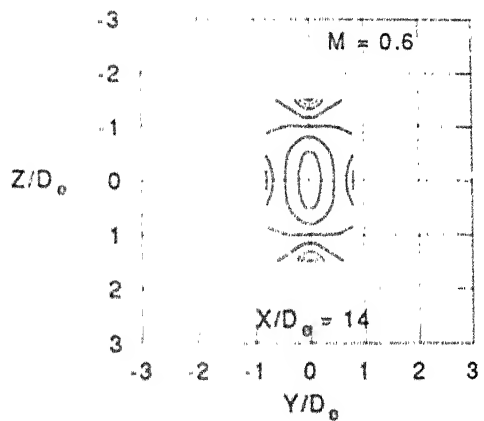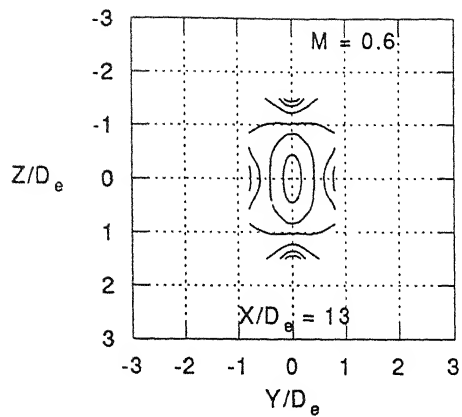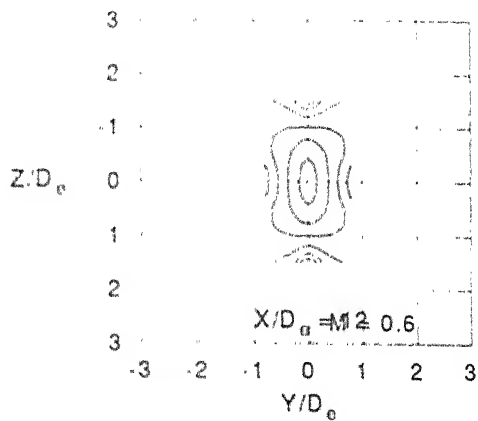
Figure. 4.9 (contd) Iso-velocity (V/Vc) profiles for AR = 3 ellipse. The innermost is for V/Vc = 1.0 and the outermost is for V/Vc = 0.2
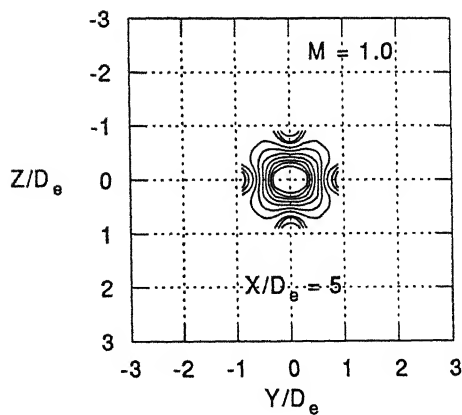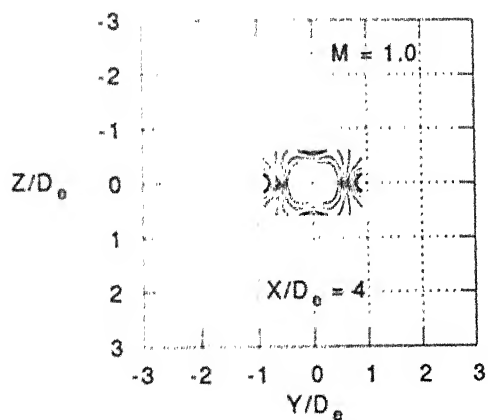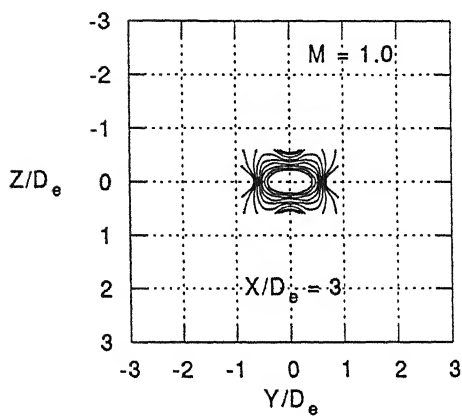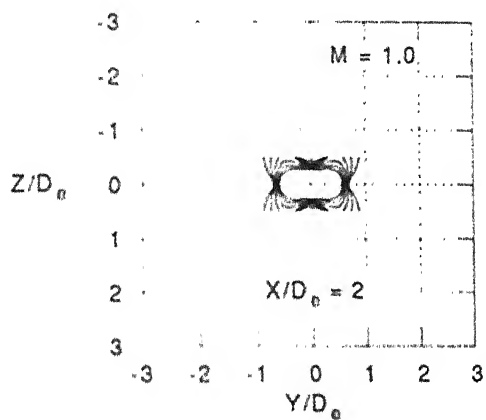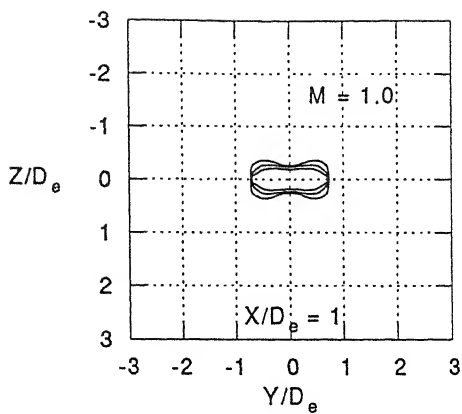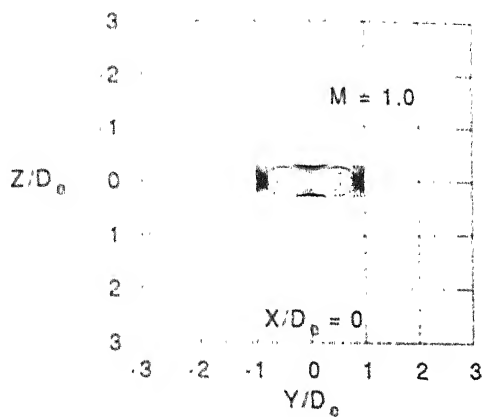
Figure. 4.10 Iso-velocity (V/Vc) profiles for AR = 4 ellipse. The innermost
is for V/Vc = 1.0 and the outermost is for V/Vc = 0.2

51
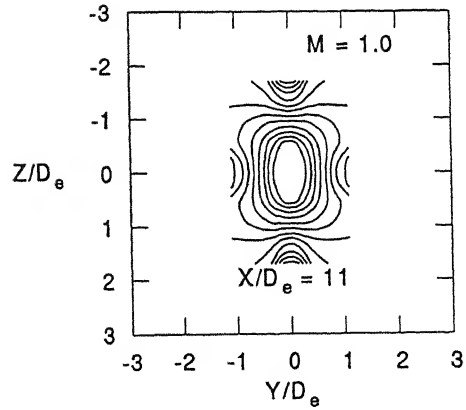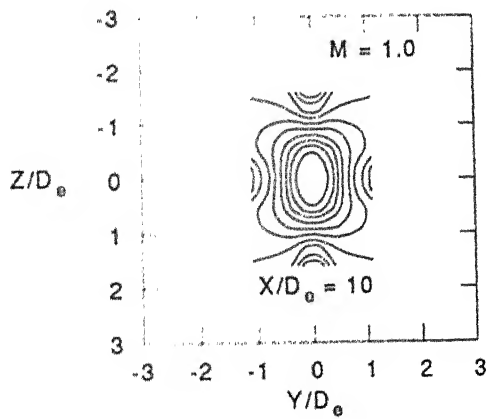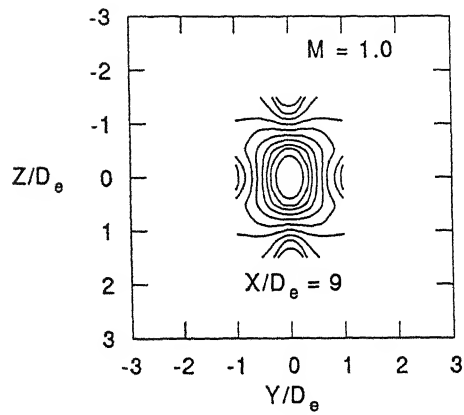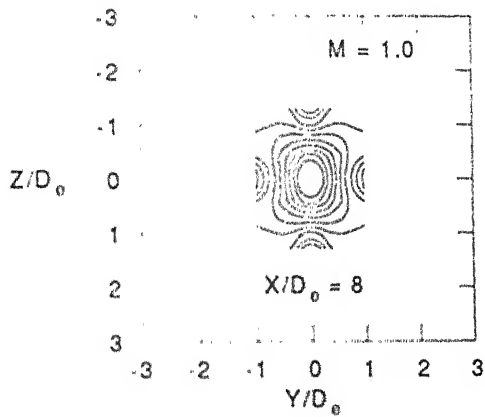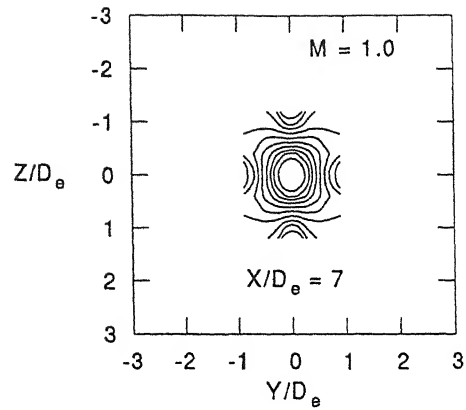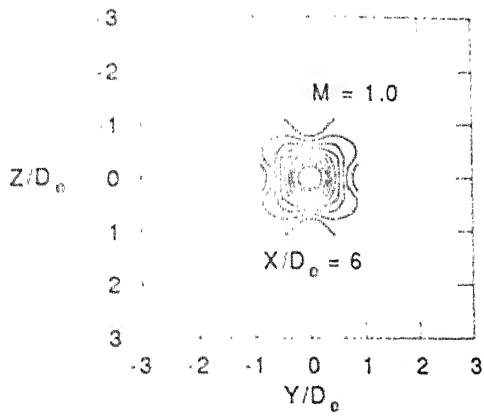
Figure. 4.10 (contd) Iso-velocity (V/Vc) profiles for AR = 4 ellipse. The innermost is for V/Vc = 1.0 and the outermost is for V/Vc = 0.2
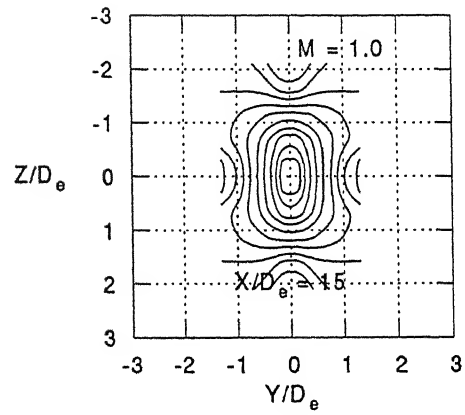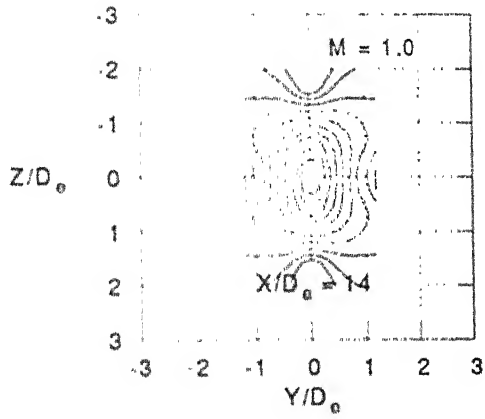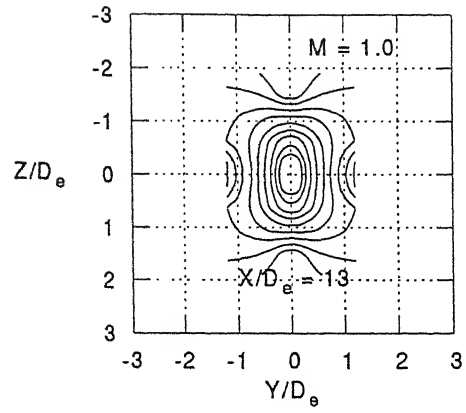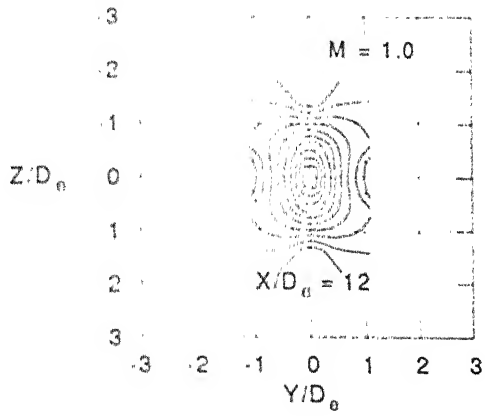
Figure. 4.10 (contd) Iso-velocity (V/Vc) profiles for AR = 4 ellipse. The innermost
is for V/Vc = 1.0 and the outermost is for V/Vc = 0.2
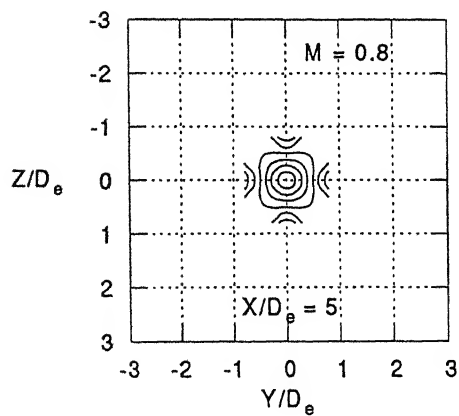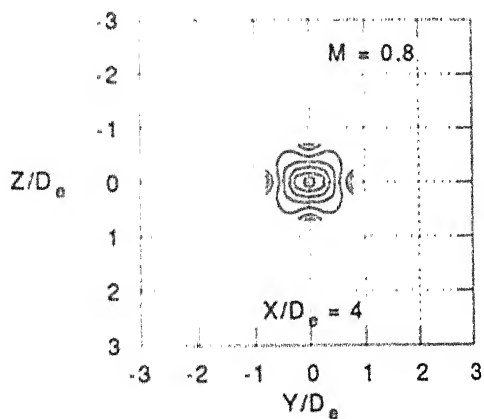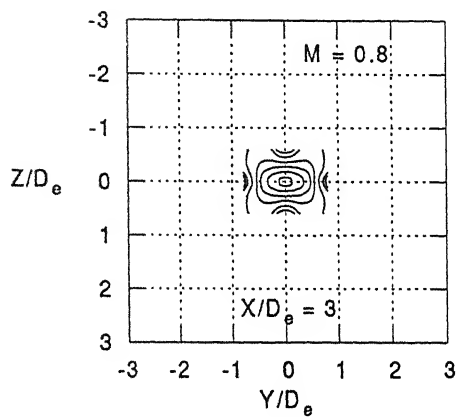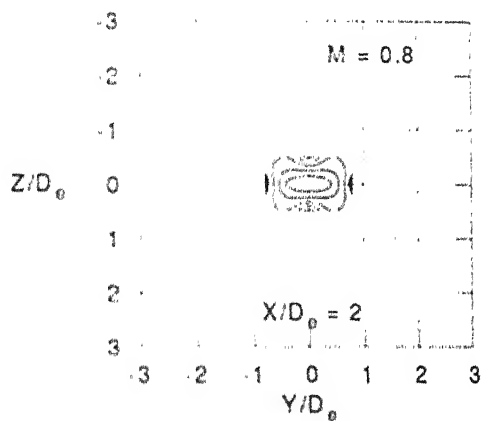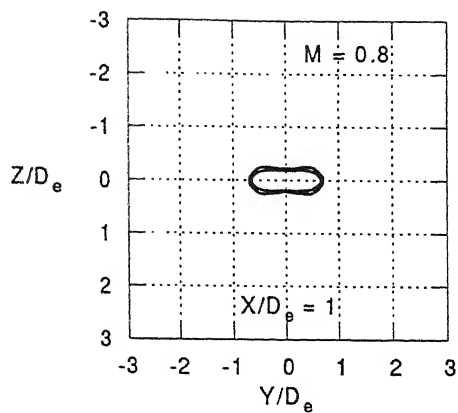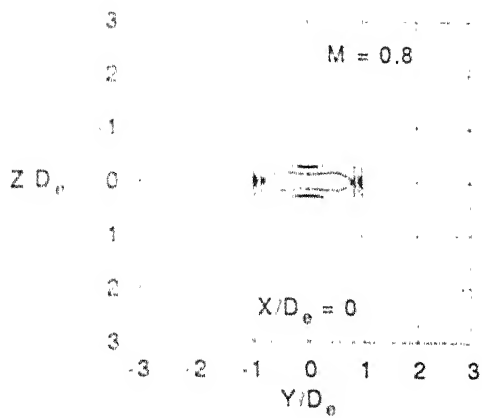
Figure. 4.11 Iso-velocity (V/Vc) profiles for AR = 4 ellipse. The innermost
is for V/Vc = 1.0 and the outermost is for V/Vc = 0.2
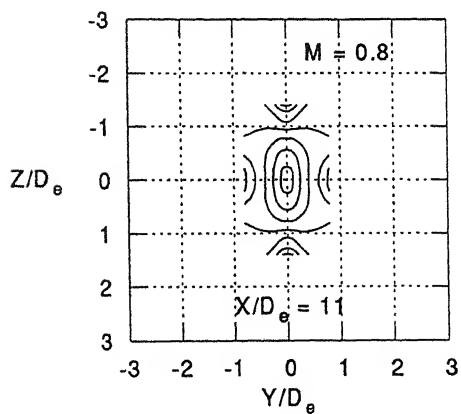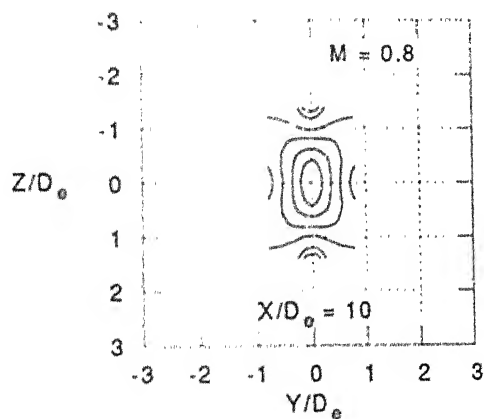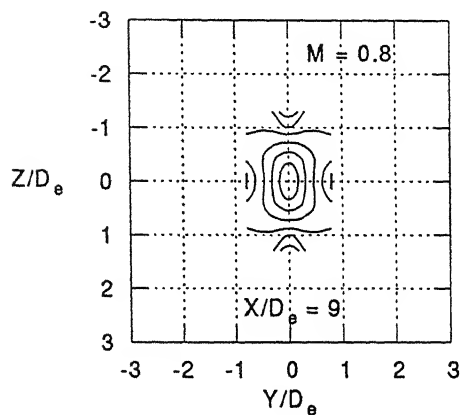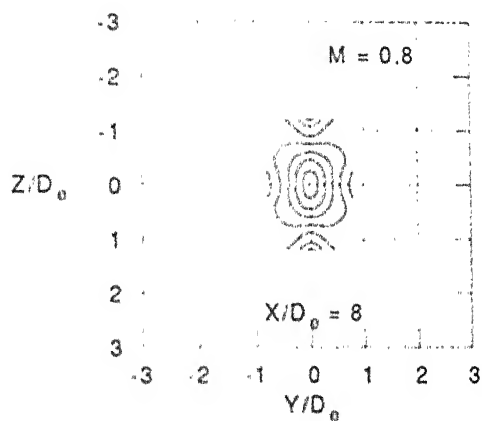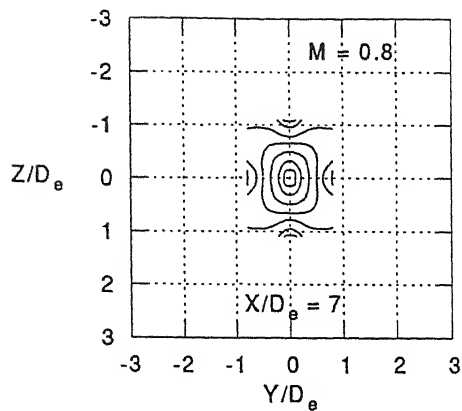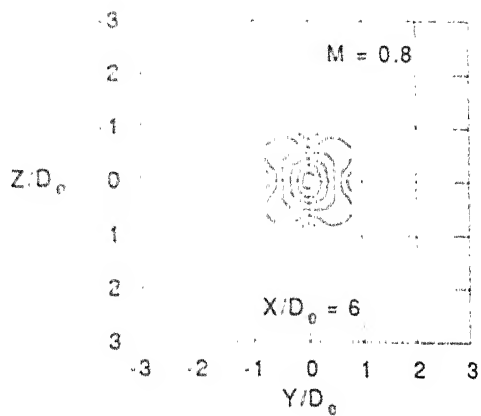
Figure. 4.11 (contd) Iso-velocity (V/Vc) profiles for AR = 4 ellipse. The innermost is for V/Vc = 1.0 and the outermost is for V/Vc = 0.2
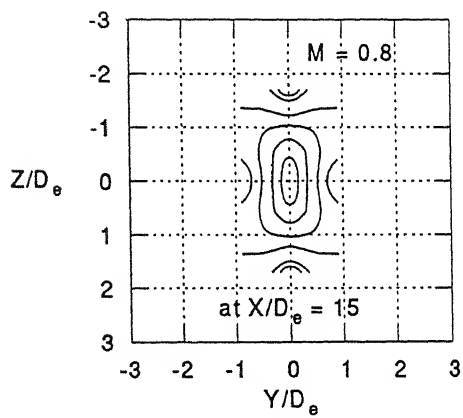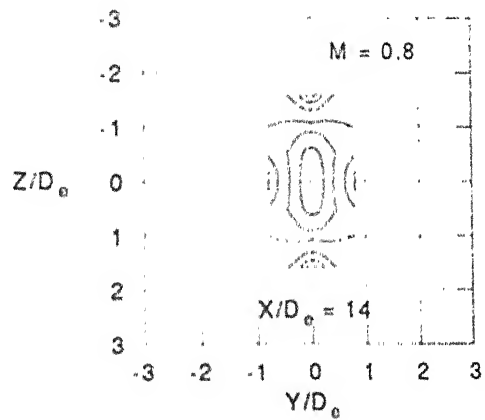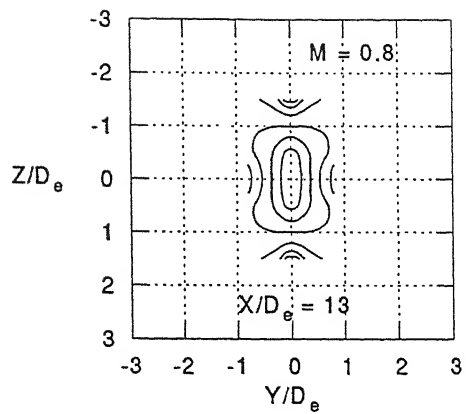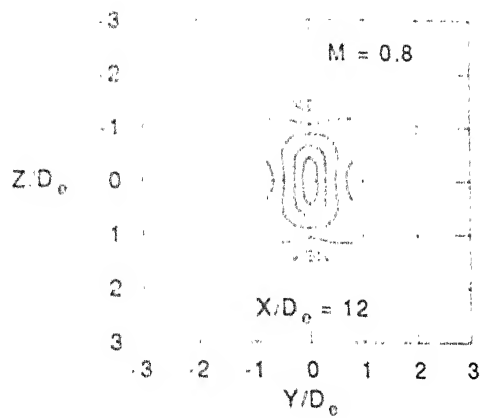
Figure. 4.11 (contd) Iso-velocity (V/Vc) profiles for AR = 4 ellipse. The innermost
is for V/Vc = 1.0 and the outermost is for V/Vc = 0.2
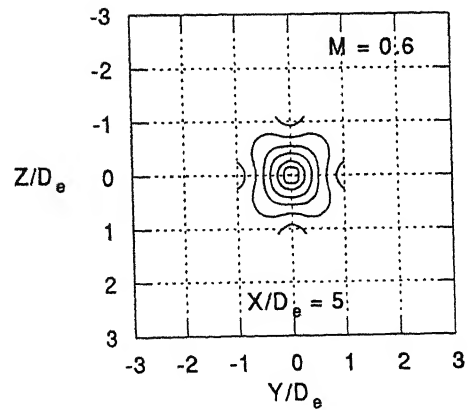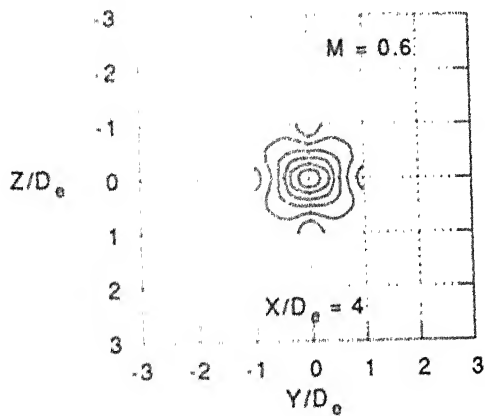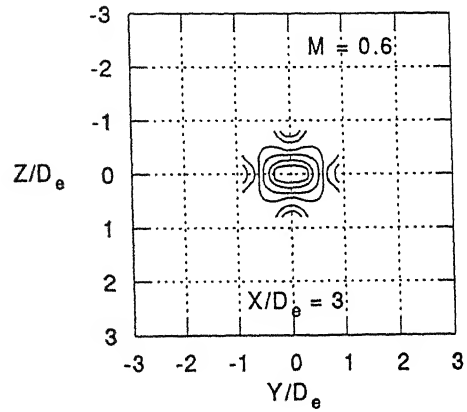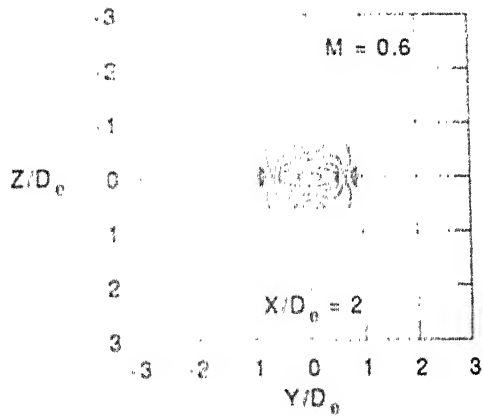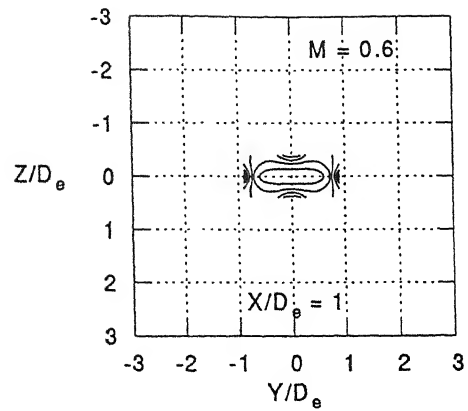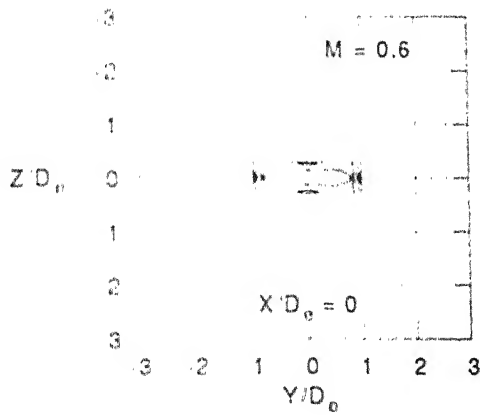
Figure. 4.12 Iso-velocity (V/Vc) profiles for AR = 4 ellipse. The innermost
is for V/Vc = 1.0 and the outermost is for V/Vc = 0.2
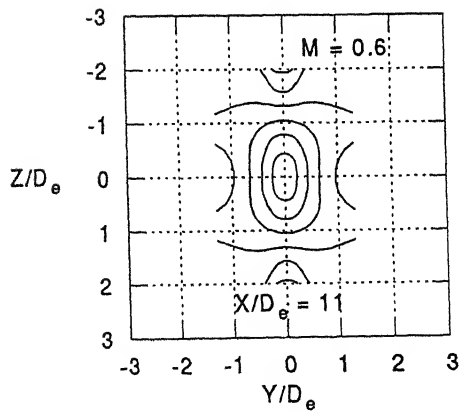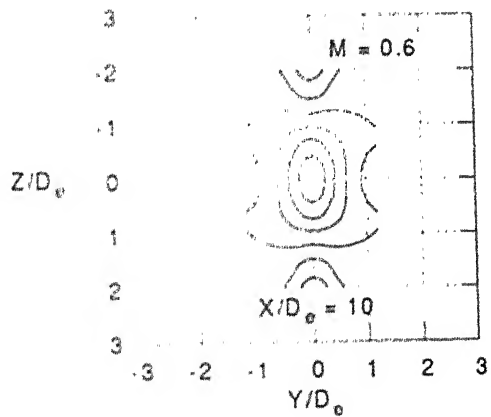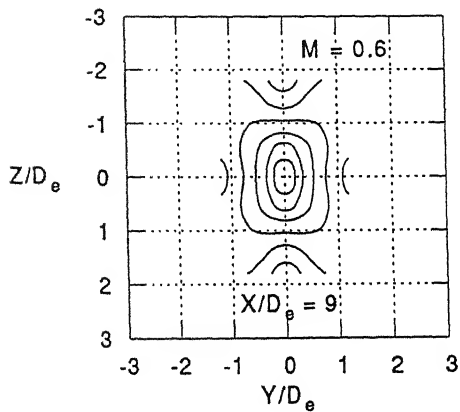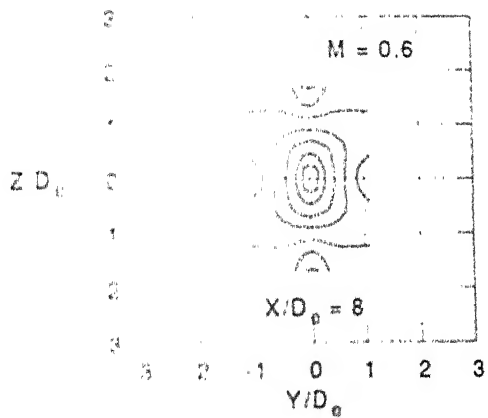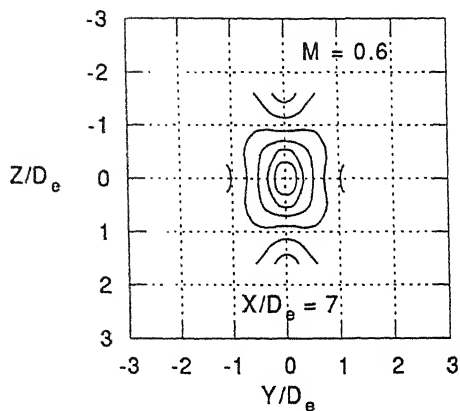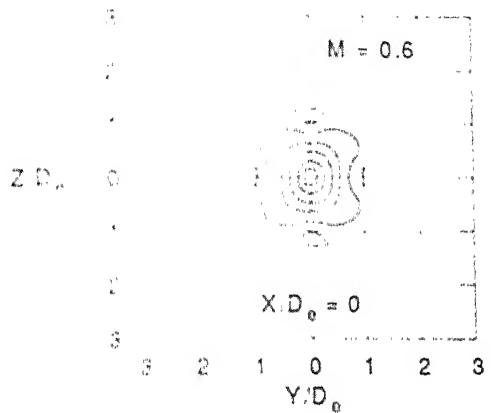
Figure. 4.12 (contd) Iso-velocity (V/Vc) profiles for AR = 4 ellipse. The innermost is for V/Vc = 1.0 and the outermost is for V/Vc = 0.2
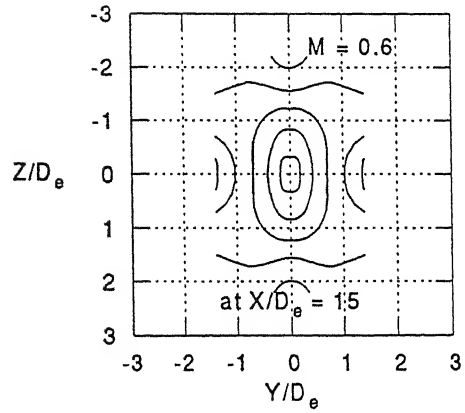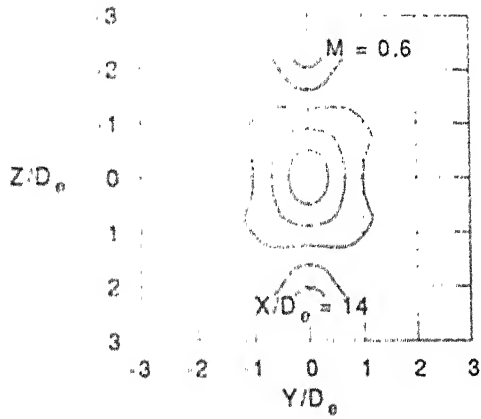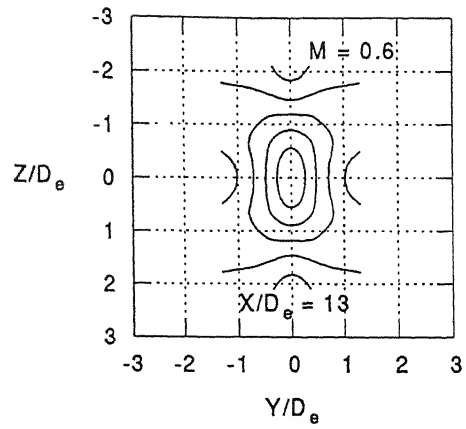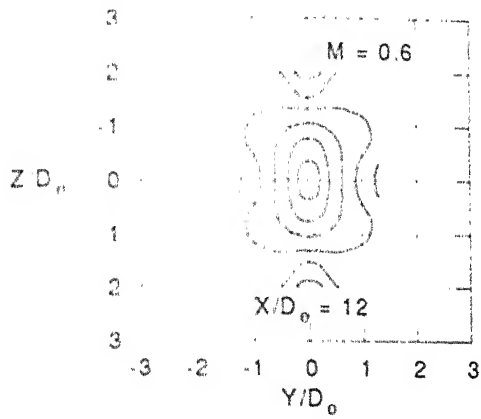
Figure. 4.12 (contd) Iso-velocity (V/Vc) profiles for AR = 4 ellipse. The innermost is for V/Vc = 1.0 and the outermost is for V/Vc = 0.2
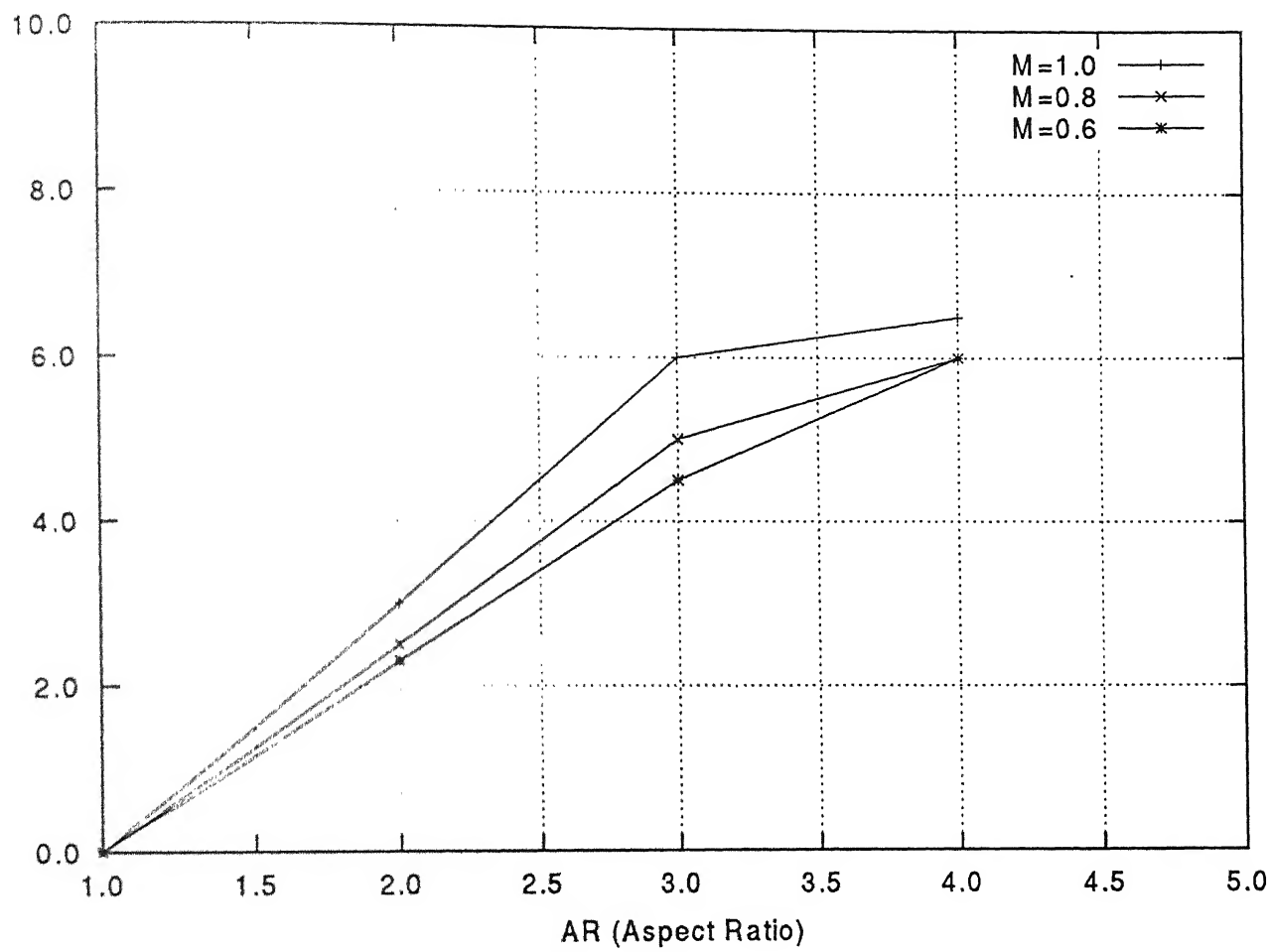
Figure. 4.13 Aspect ratio Vs Axis switching locations
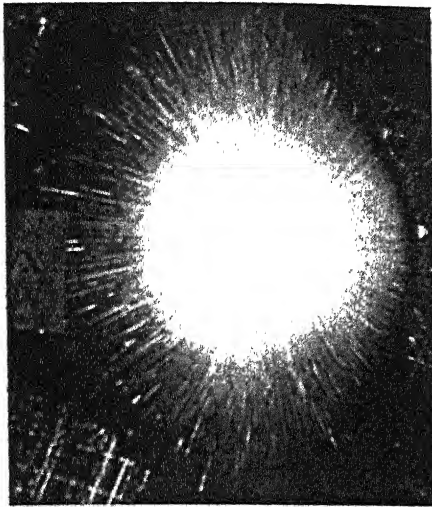
(a). $X/D_e = 1.0$
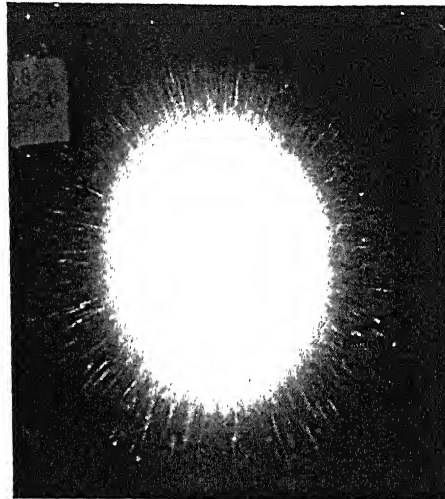
(b). $X/D_e = 2.0$
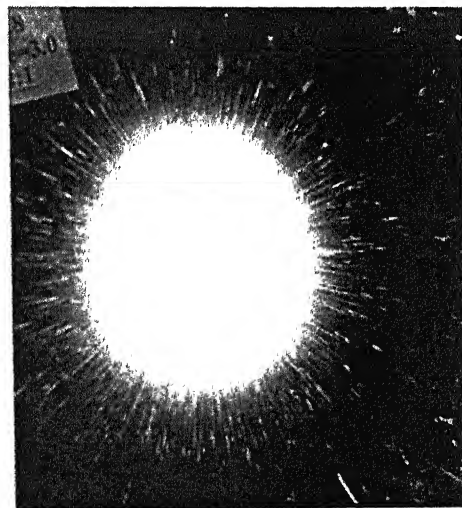
(c). $X/D_e = 3.0$

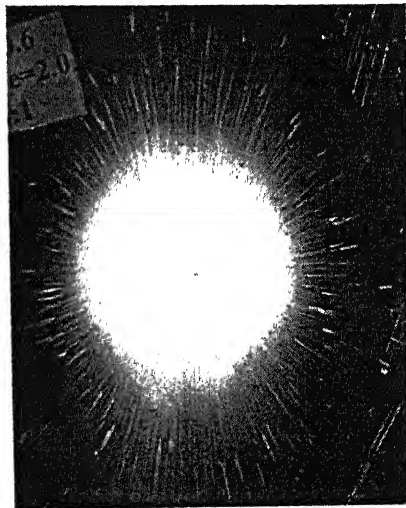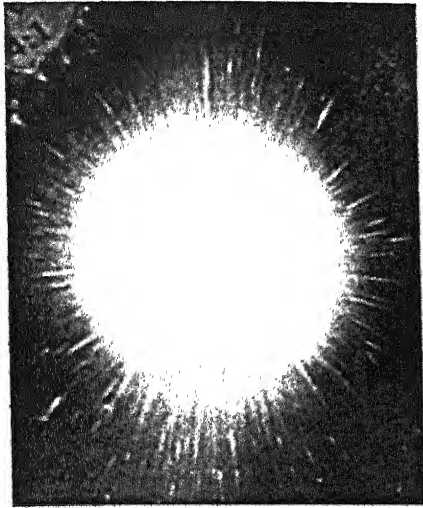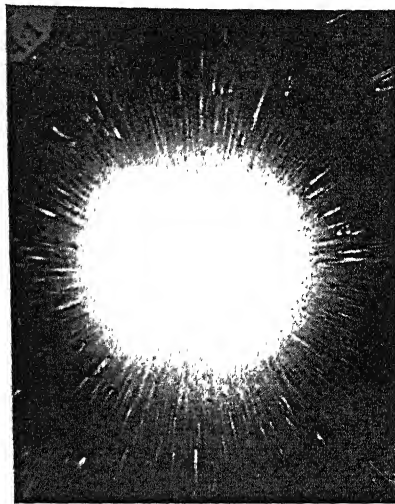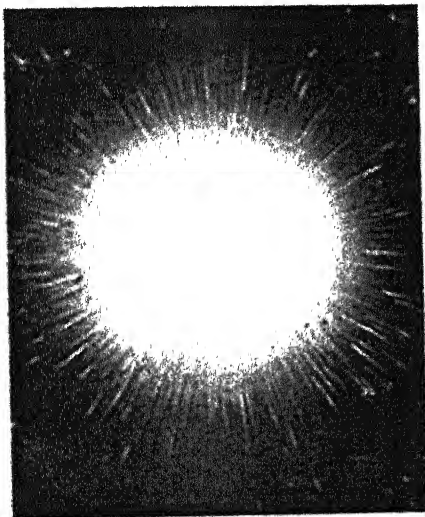Figure. 4.15 Flow Visualization for Elliptical Jet (AR=2) at M = 0.8
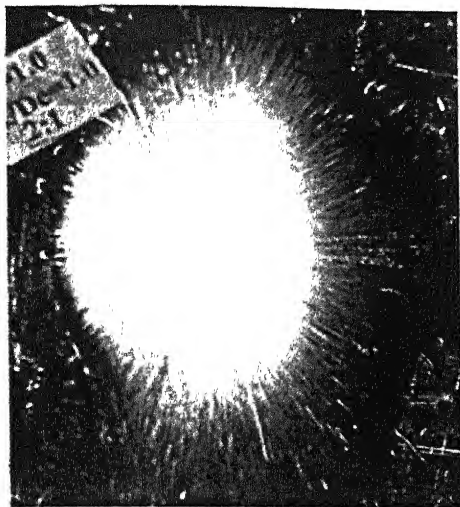
(a). $X/D_e = 1.0$
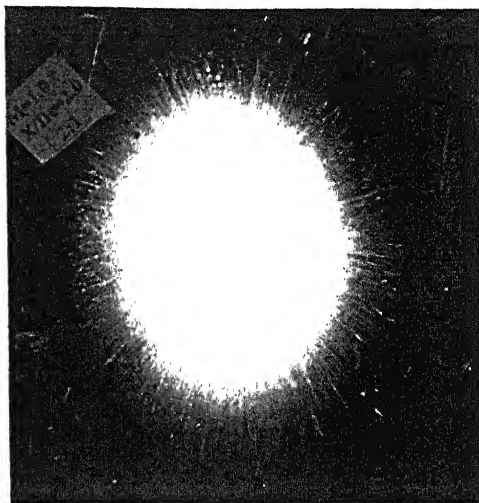
(b). $X/D_e = 2.0$
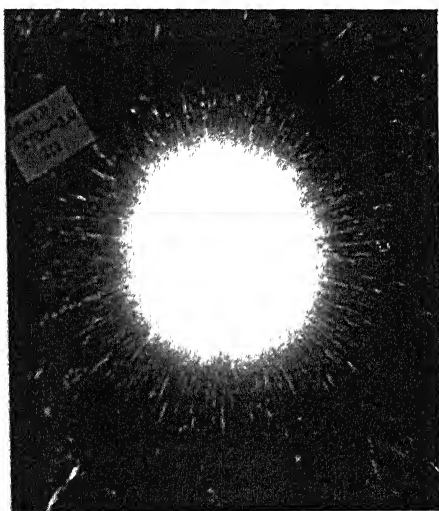
(c). $X/D_e = 3.0$

Figure. 4.14 Flow Visualization for Elliptical Jet (AR=2) at M =1.0
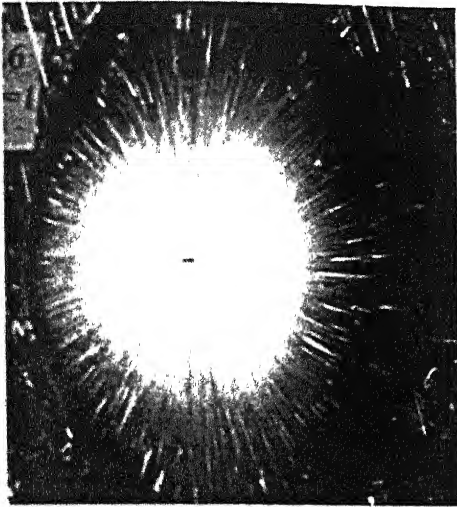
(a). $X/D_e = 1.0$
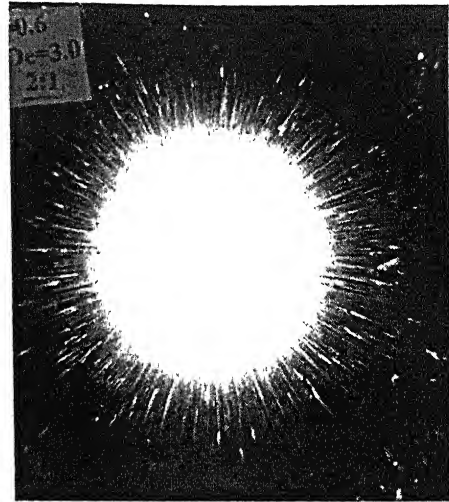
(b). $X/D_e = 2.0$
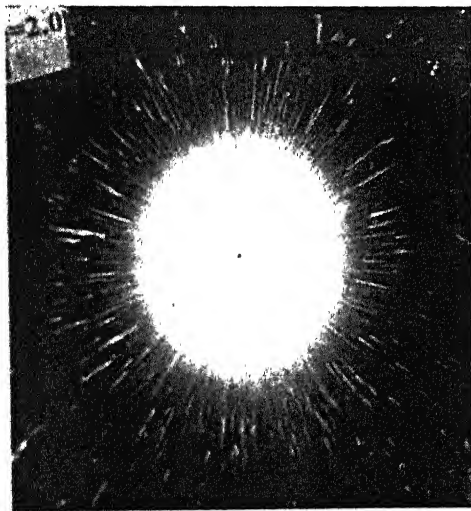
(c). $X/D_e = 3.0$

Figure. 4.16 Flow Visualization for Elliptical Jet (AR=2) at M = 0.6
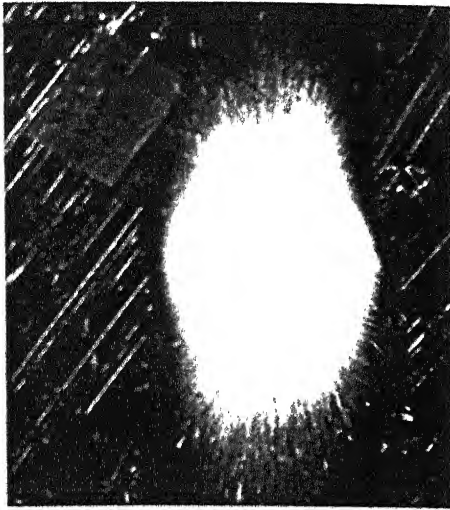
(a). X/D$_e$ = 1.0
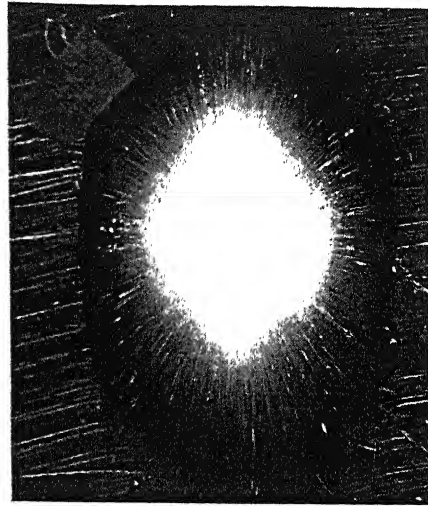
(b). X/D$_e$ = 2.0
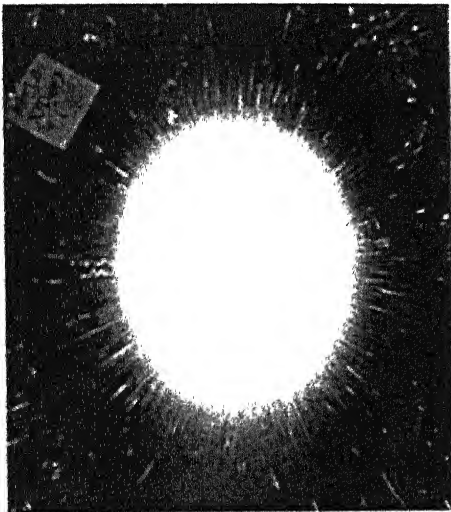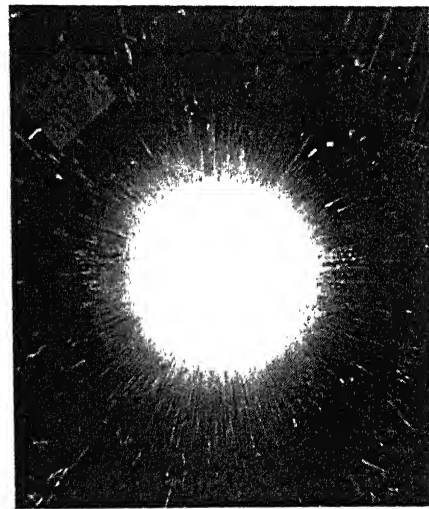
(c). X/D$_e$ = 3.0

(d). X/D$_e$ = 4.0

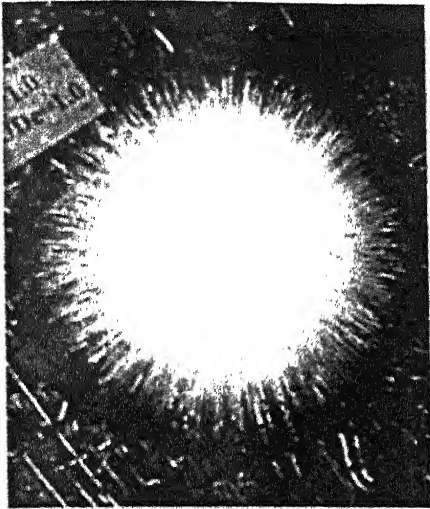Figure. 4.17 Flow Visualization for Elliptical jet (AR = 3) at M = 1.0
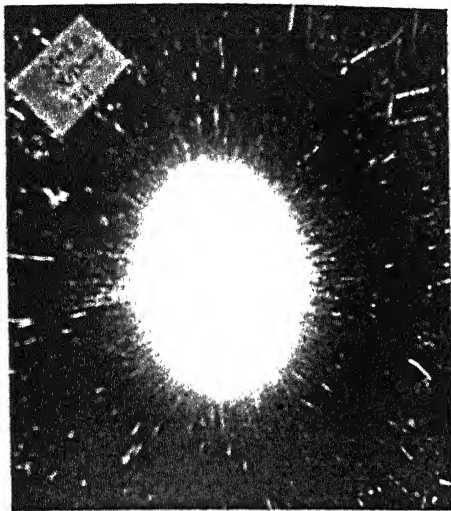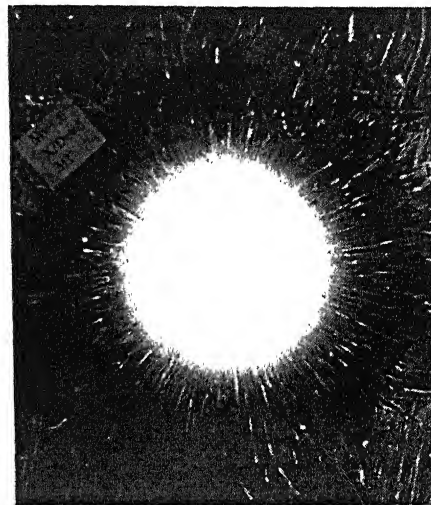
(e). $X/D_e = 5.0$ (f). $X/D_e = 6.0$
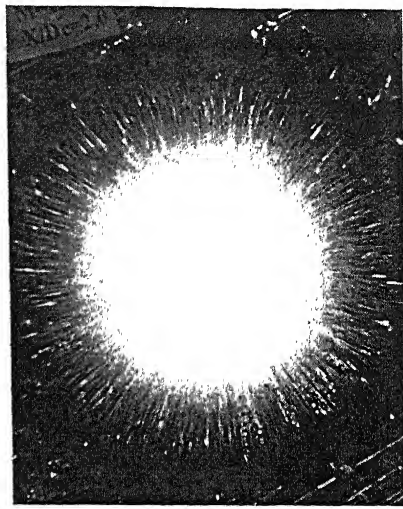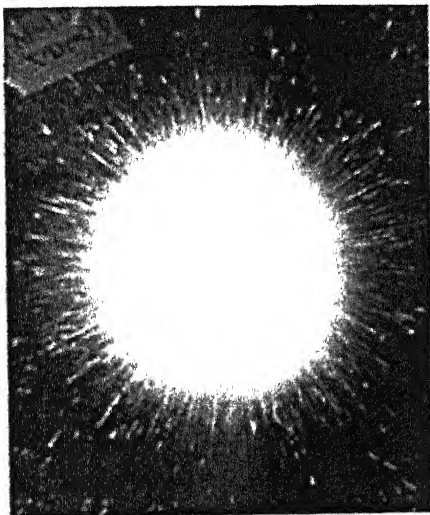
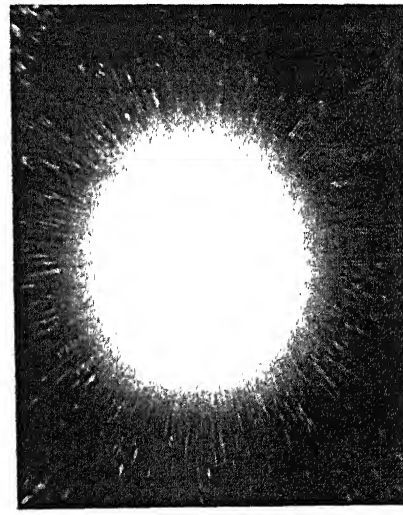Figure. 4.17 (Contd) Flow Visualization for Elliptical jet (AR = 3) at M = 1.0

(a). $X/D_e = 1.0$
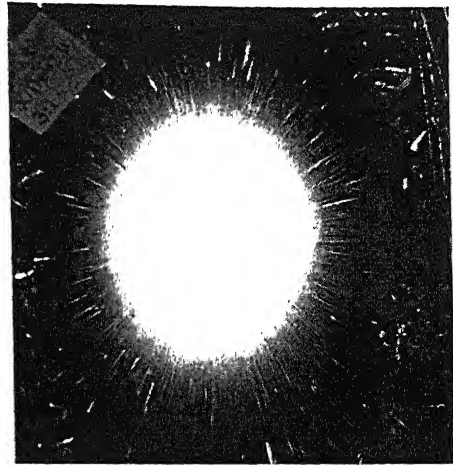
(b). $X/D_e = 2.0$
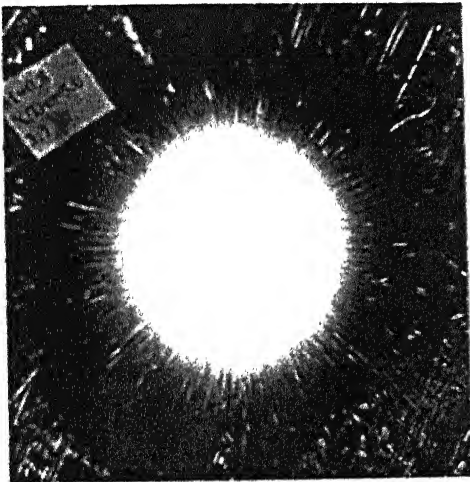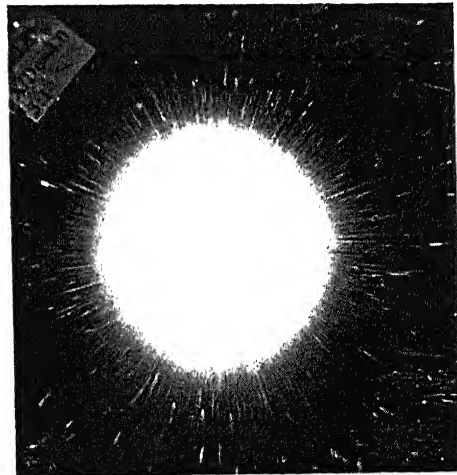
(c). $X/D_e = 3.0$

(d). $X/D_e = 4.0$

Figure. 4.18 Flow Visualization for Elliptic Jet (AR=3) at M = 0.8
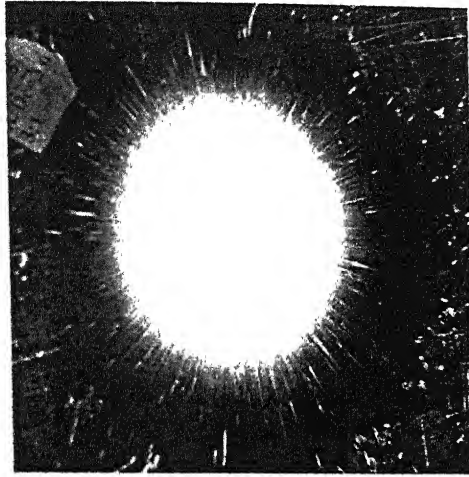
(e). $X/D_e = 5.0$

Figure 4.18 (Contd) Flow Visualization for Elliptic Jet (AR=3) at M = 0.8
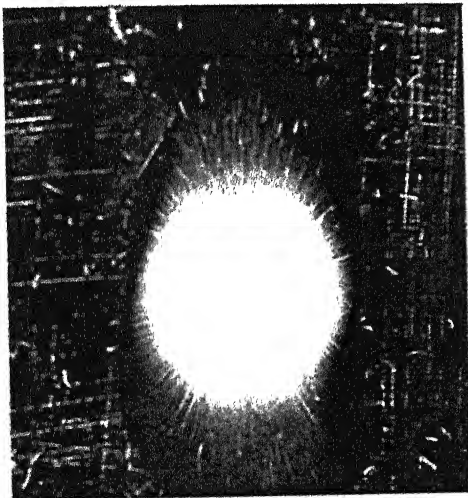
(a). $X/D_e = 1.0$
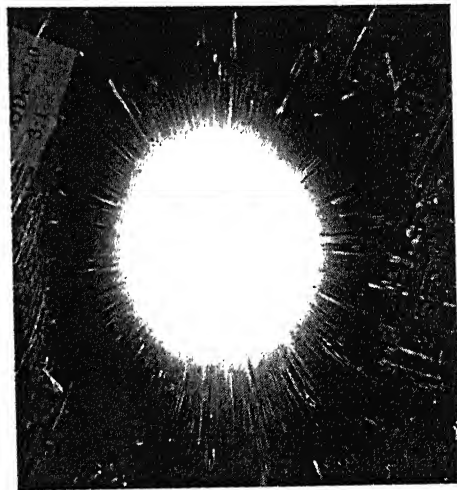
(b). $X/D_e = 2.0$

Figure. 4.19 Flow Visualization for Elliptical Jet (AR = 3) at M = 0.6
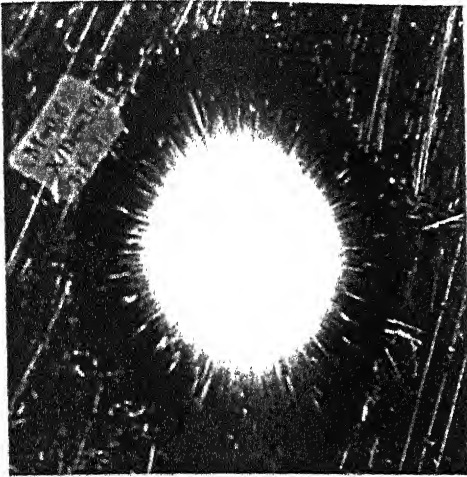
(c). $X/D_e = 3.0$
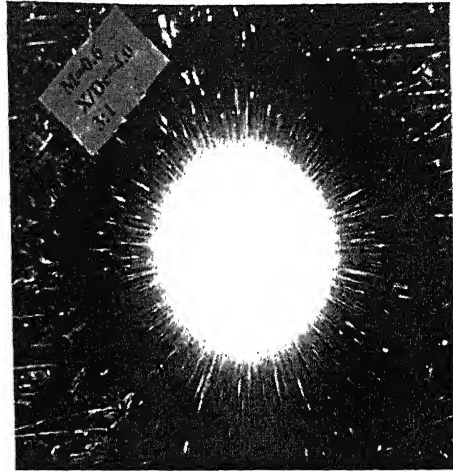
(d). $X/D_e = 4.0$
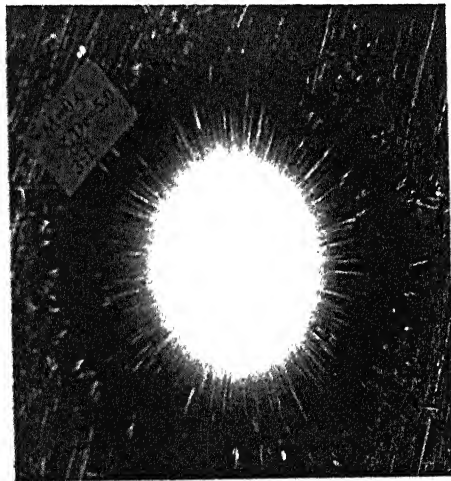
(e). $X/D_e = 5.0$

Figure. 4.19 (Contd) Flow Visualization for Elliptical Jet (AR=3)
at M = 0.6
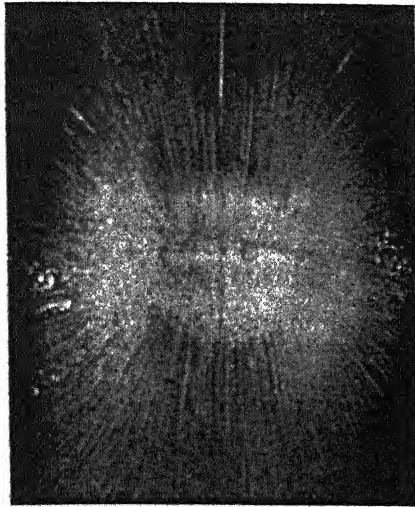
(a). $X/D_e = 1.0$
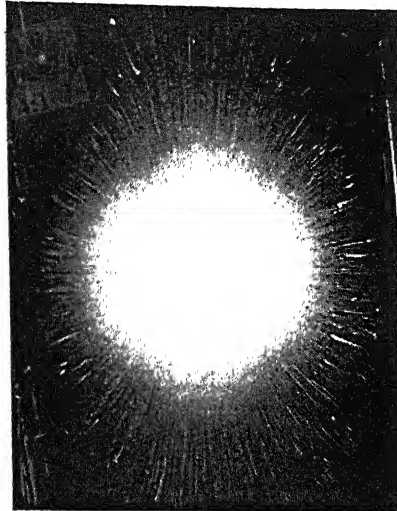
(b). $X/D_e = 2.0$
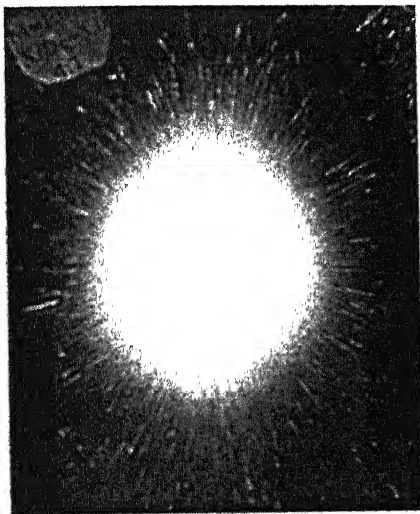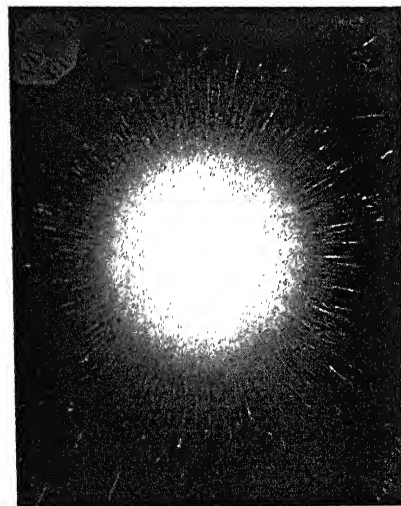
(c). $X/D_e = 3.0$

(d). $X/D_e = 4.0$

Figure. 4.20 Flow Visualization for Elliptical Jet (AR = 4) at M =1.0

69
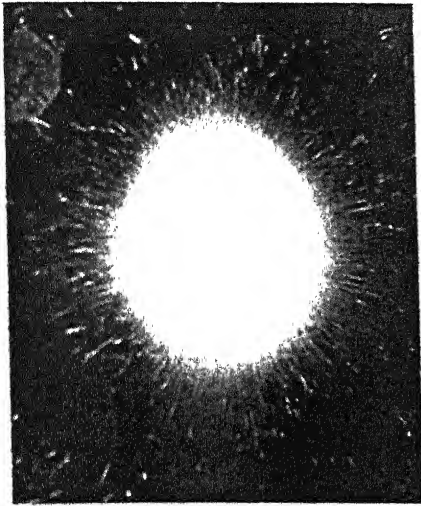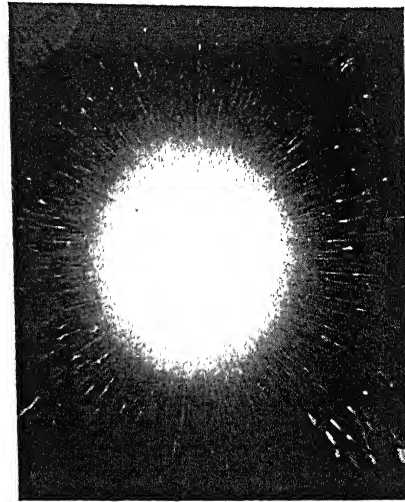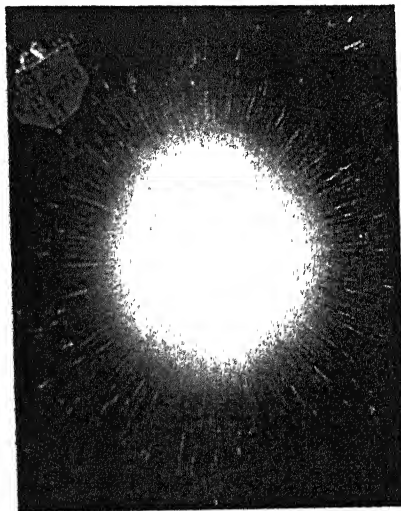
(e). $X/D_e = 5.0$

(f). $X/D_e = 6.0$

(g). $X/D_e = 7.0$

Figure. 4.20 (Contd) Flow Visualization for Elliptical Jet (AR = 4)
at M =1.0
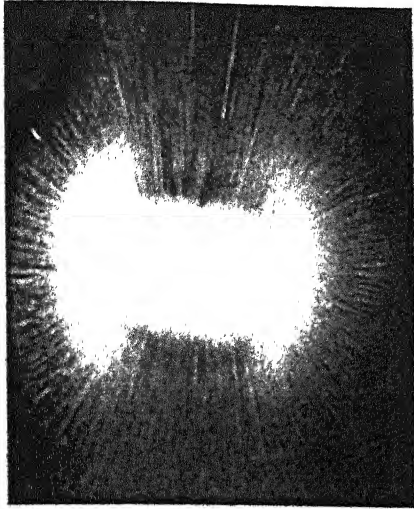
(a). X/D$_e$ = 1.0
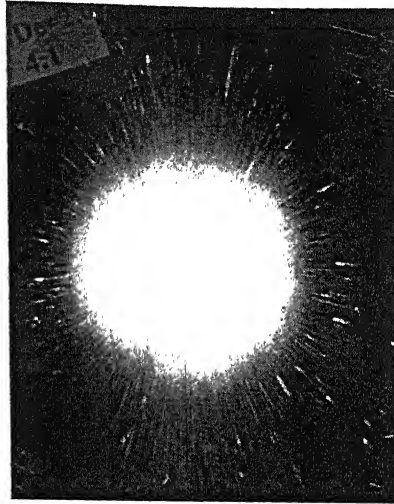
(b). X/D$_e$ = 2.0
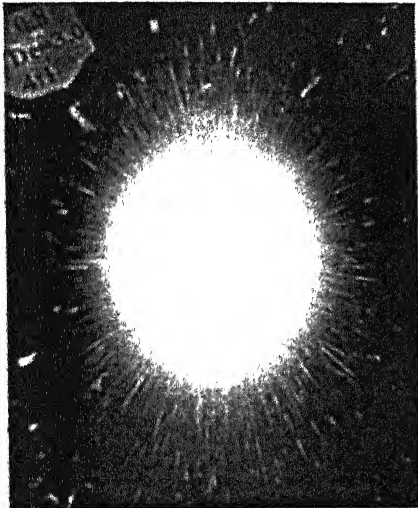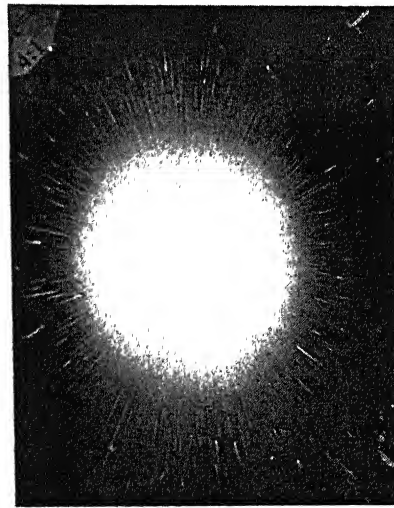
(c). X/D$_e$ = 3.0

(d). X/D$_e$ = 4.0

Figure. 4.21 Flow Visualization for Elliptical Jet (AR = 4) at M = 0.8
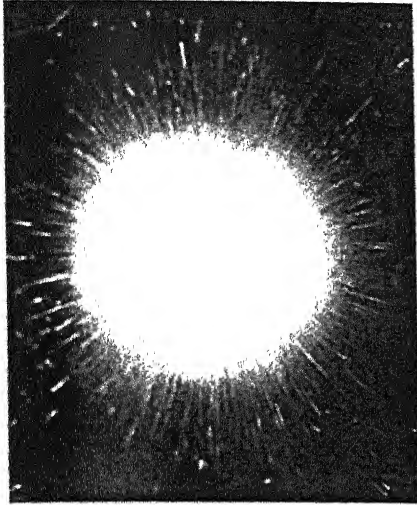
(e). $X/D_e = 5.0$
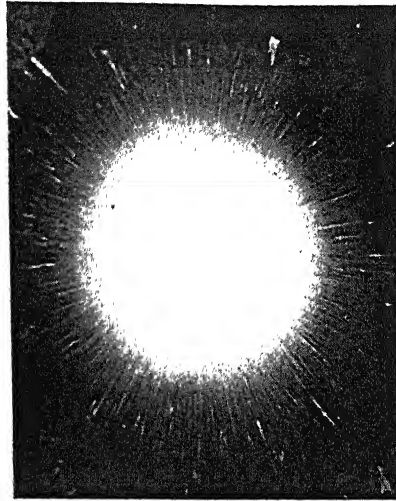
(f). $X/D_e = 6.0$

Figure. 4.21 (Contd) Flow Visualization for Elliptical Jet (AR = 4) at M = 0.8
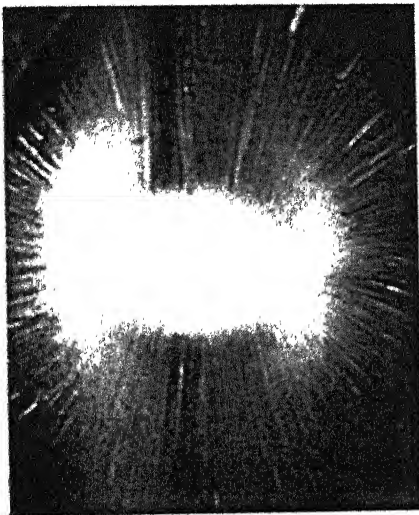
(a). $X/D_e = 1.0$

(b). $X/D_e = 2.0$

Figure. 4.22 Flow Visualization for Elliptical Jet (AR = 4) at M = 0.6

(c). $X/D_e = 3.0$

(d). $X/D_e = 4.0$

(e). $X/D_e = 5.0$
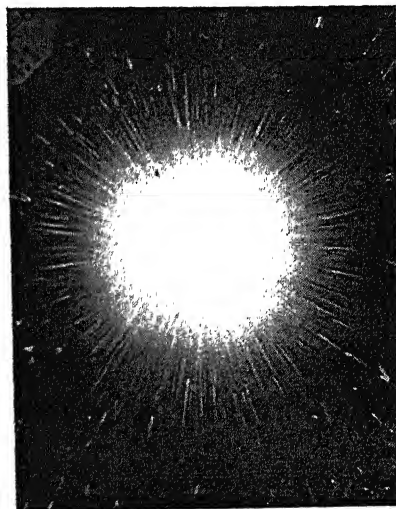
(f). $X/D_e = 6.0$

Figure. 4.22 (Contd) Flow Visualization for Elliptical Jet (AR = 4)
at M = 0.6

73

(a). $X/D_e = 1.0$

(b). $X/D_e = 2.0$

(c). $X/D_e = 3.0$

(d). $X/D_e = 4.0$

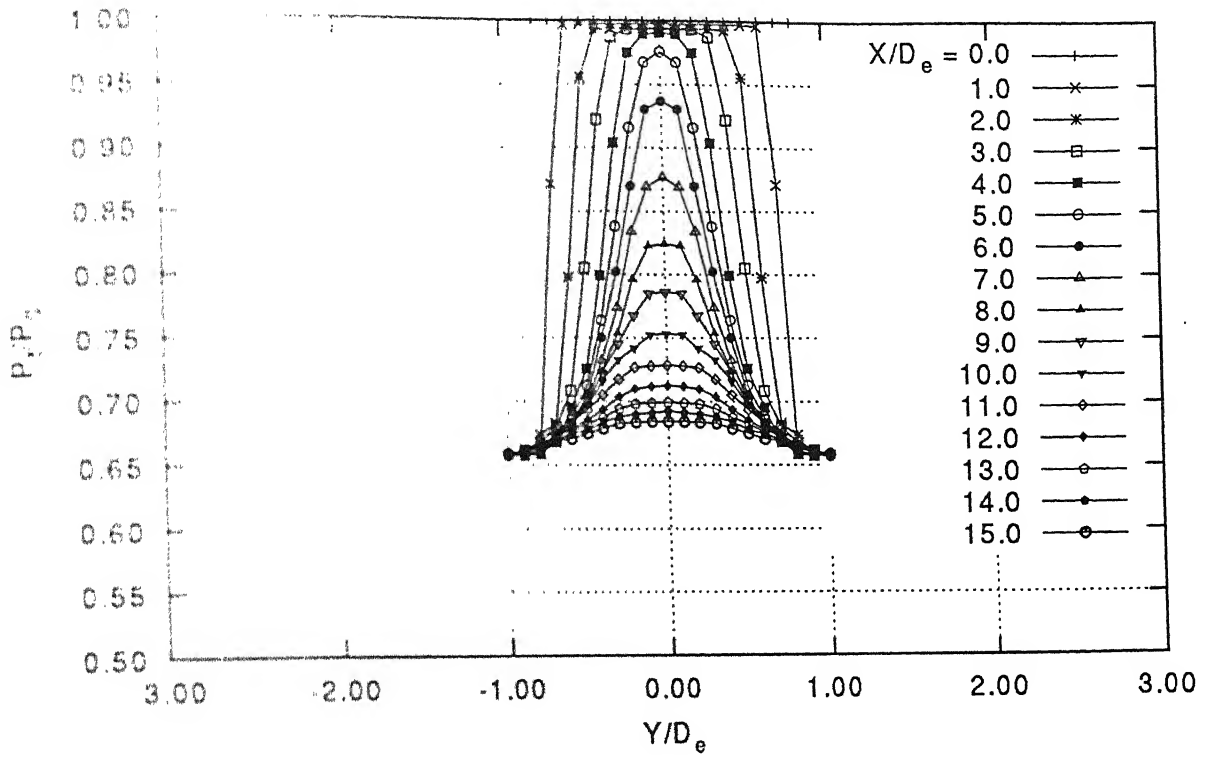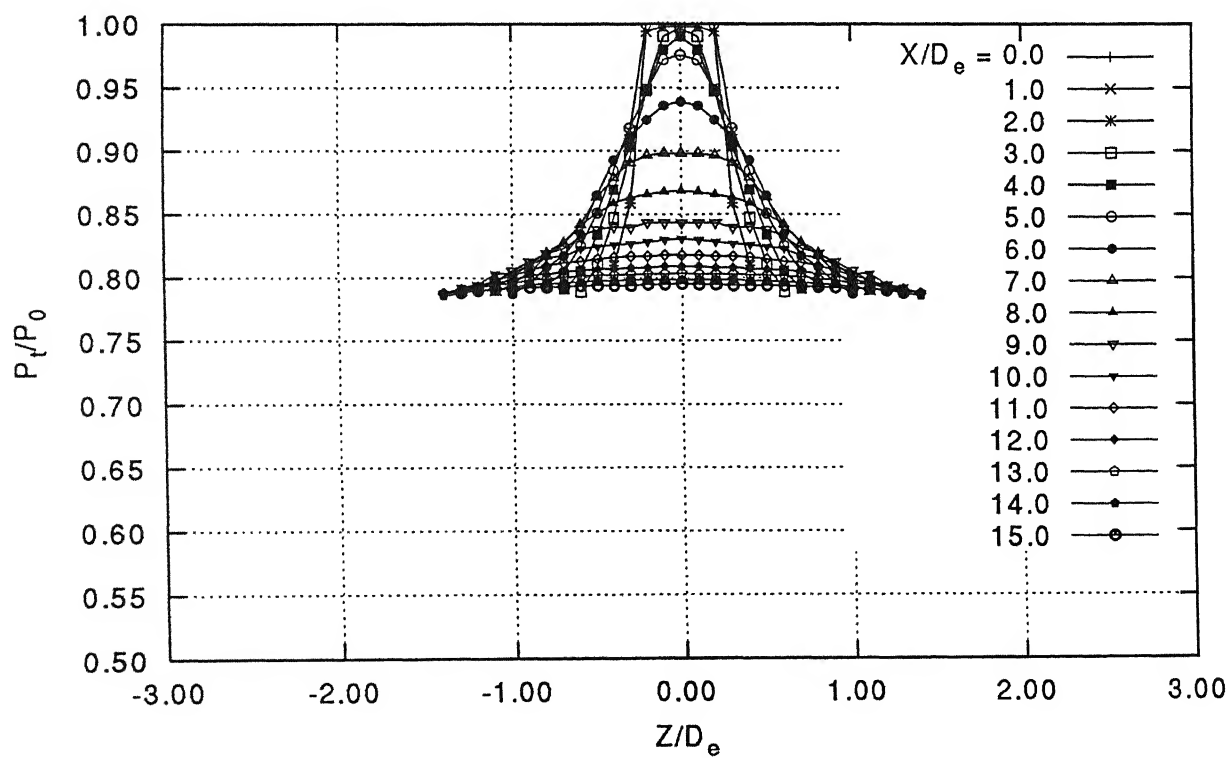Figure. 4.23 Flow Visualization for Circular Jet at $M = 1.0$
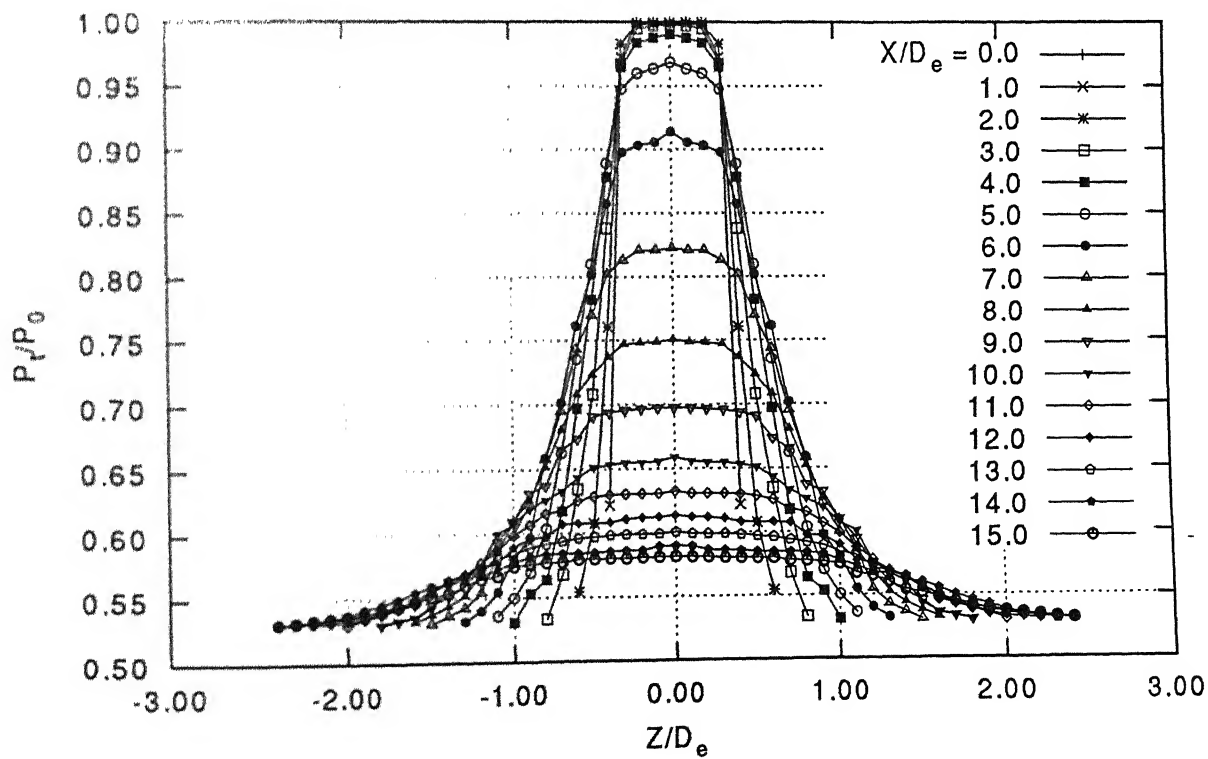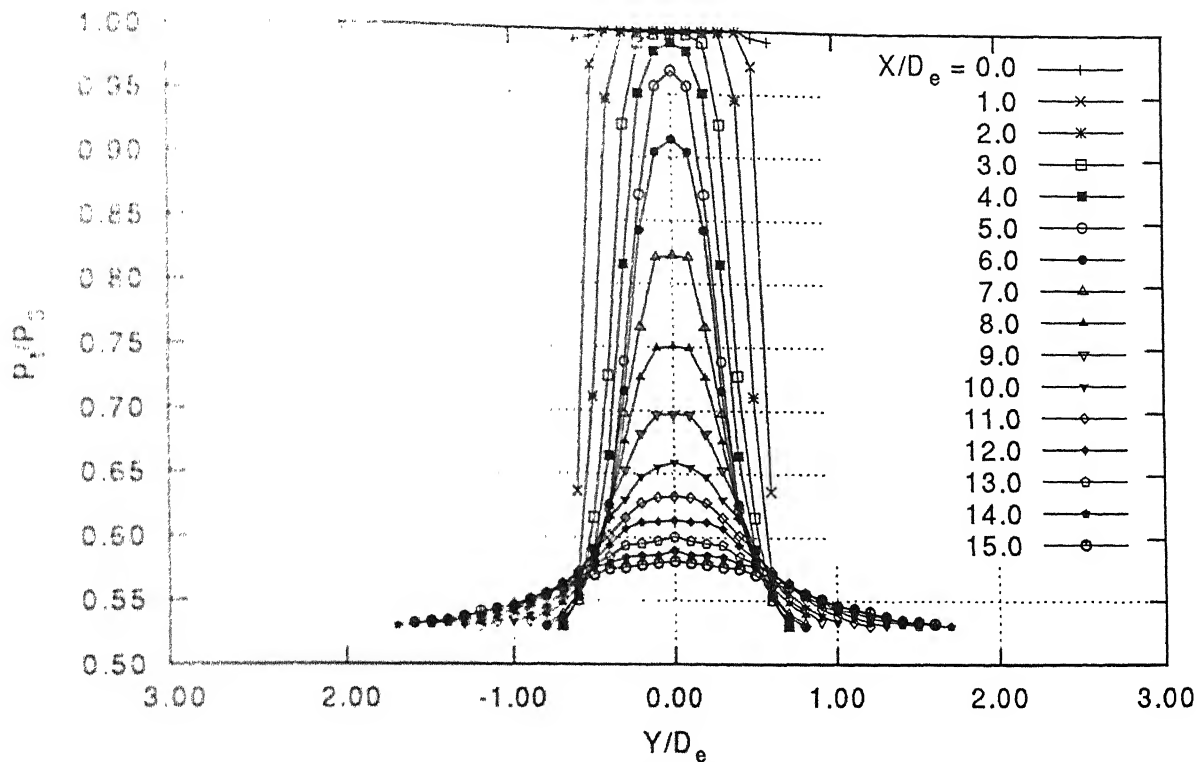
Figure. 4.24a Pressure profile Ellipse AR = 2 at M = 1.0
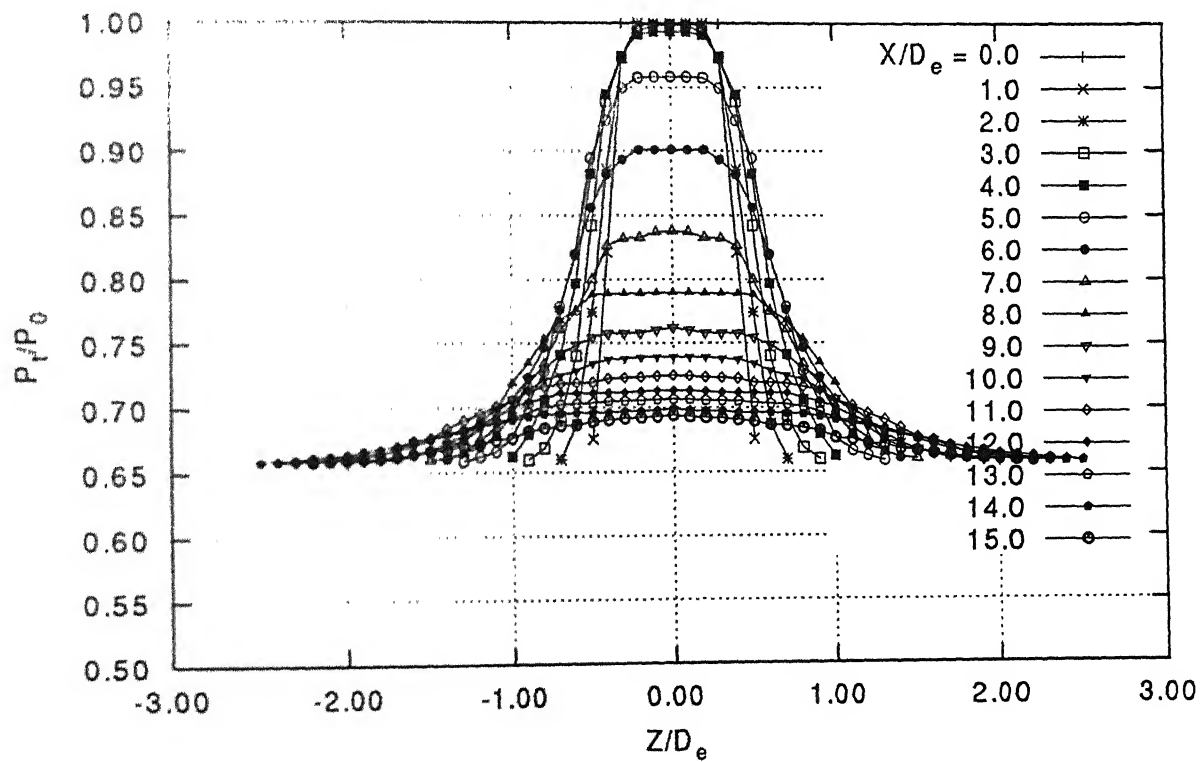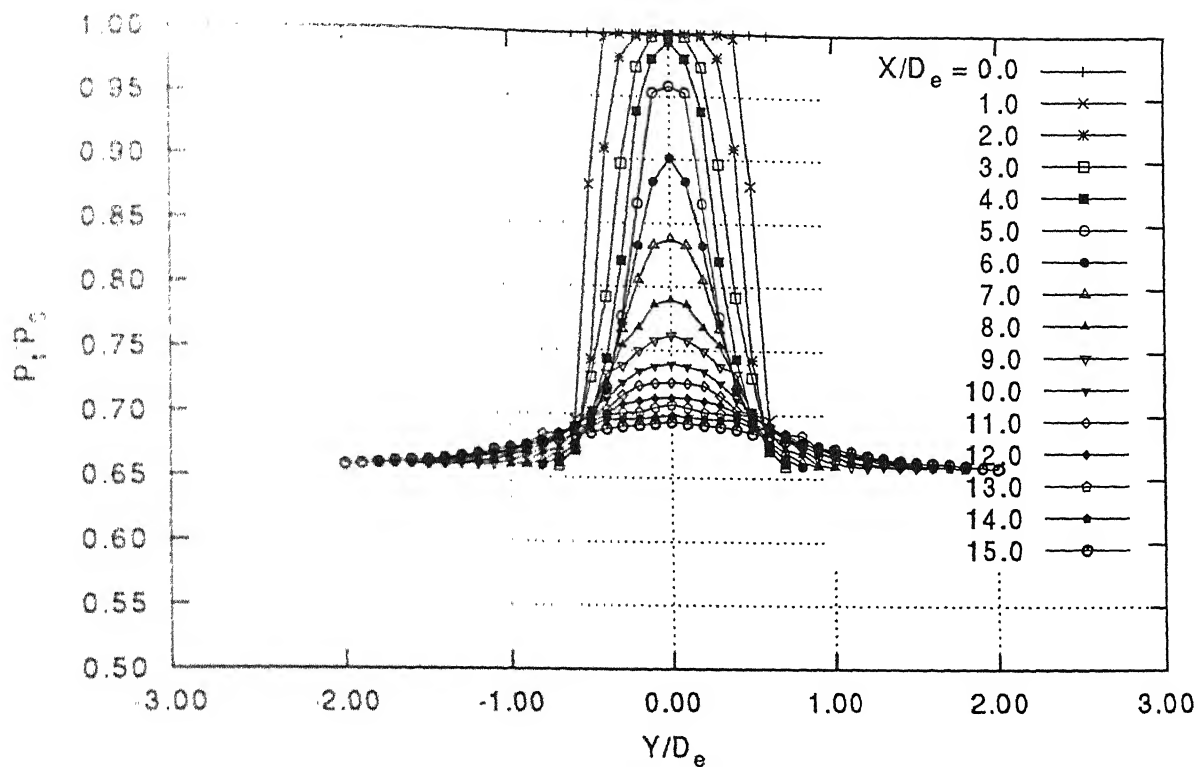
Figure. 4.24b Pressure profile Ellipse AR = 2 at M = 0.8
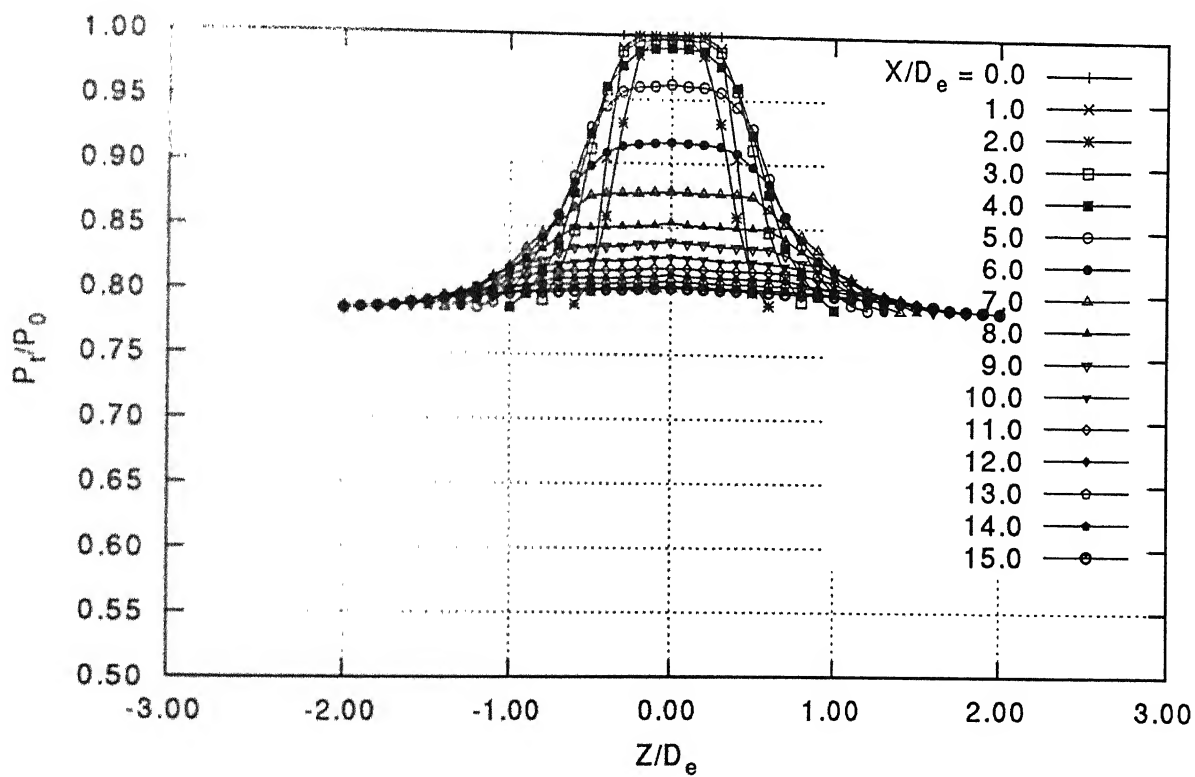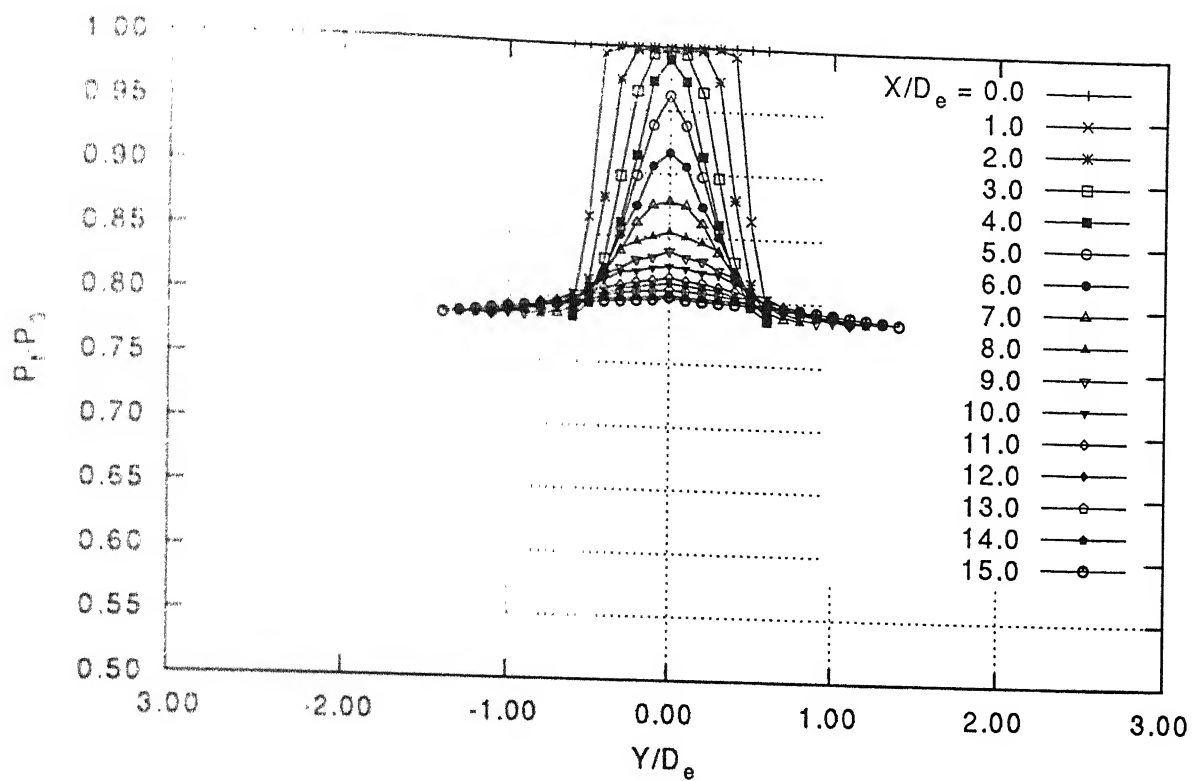
Figure. 4.24c Pressure profile Ellipse AR = 2 at M=0.6
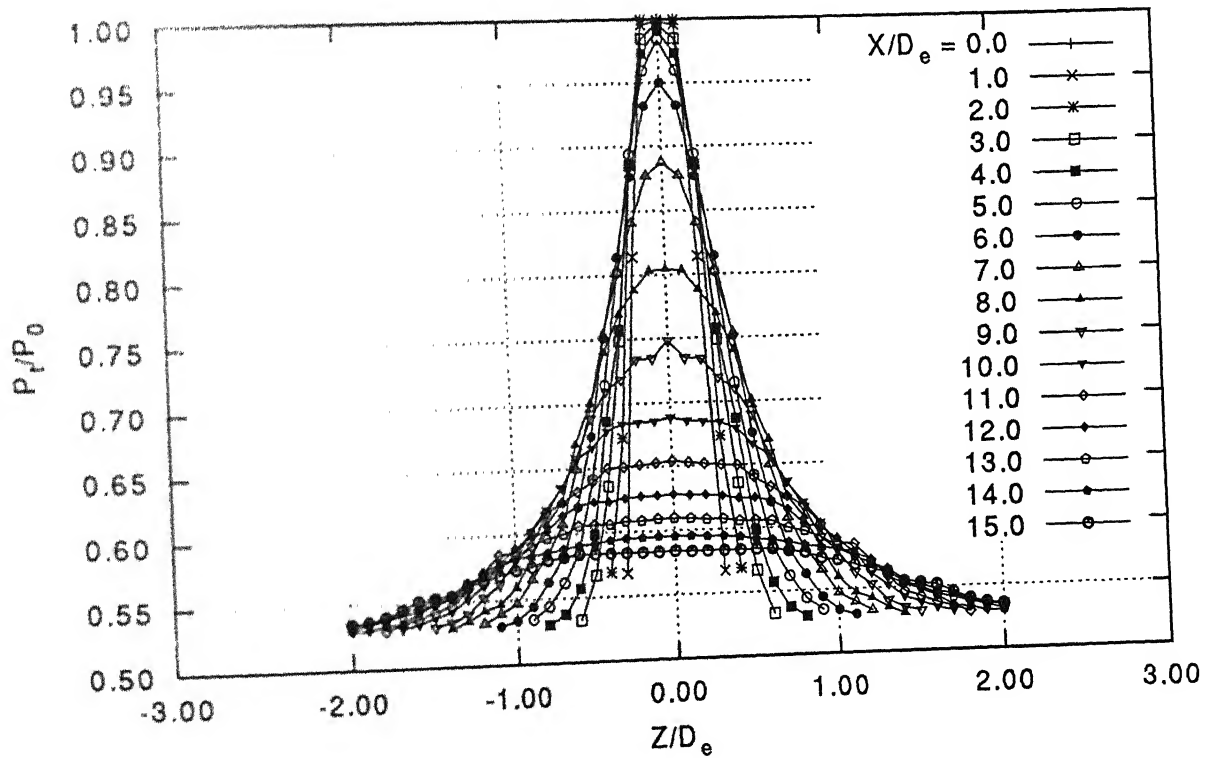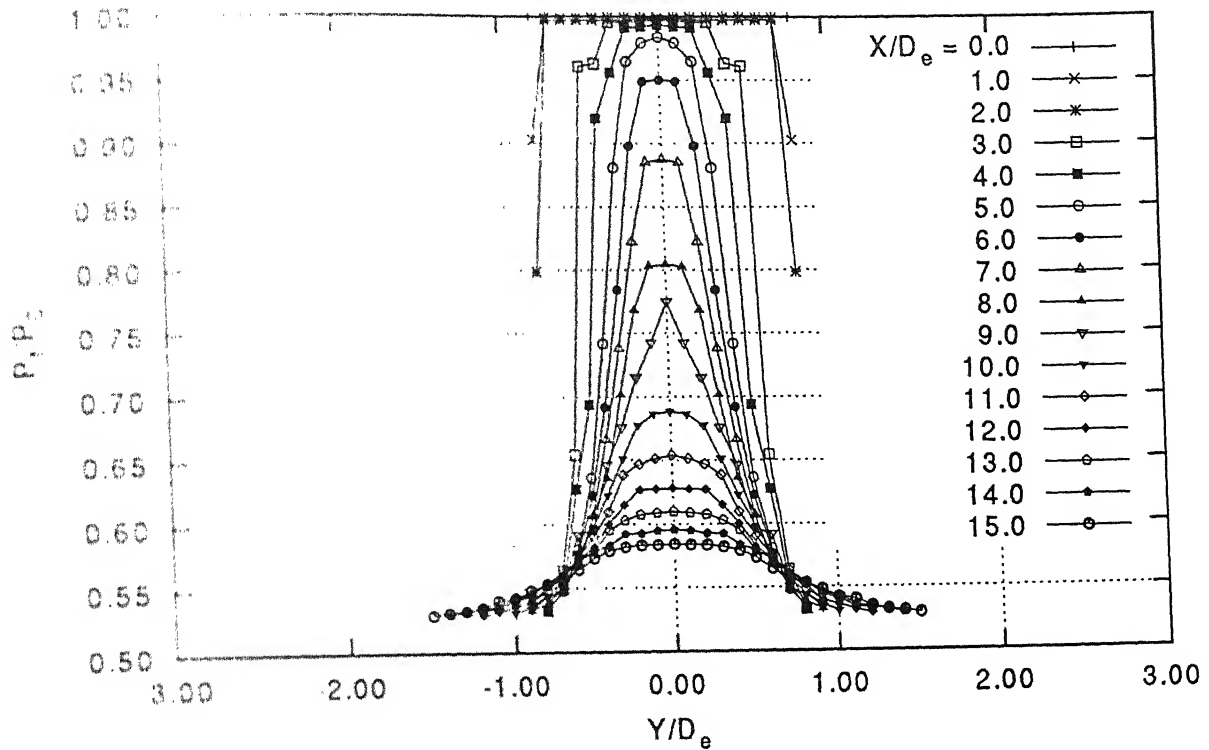
Figure. 4.25a Pressure profile Ellipse AR = 3 at M = 1.0
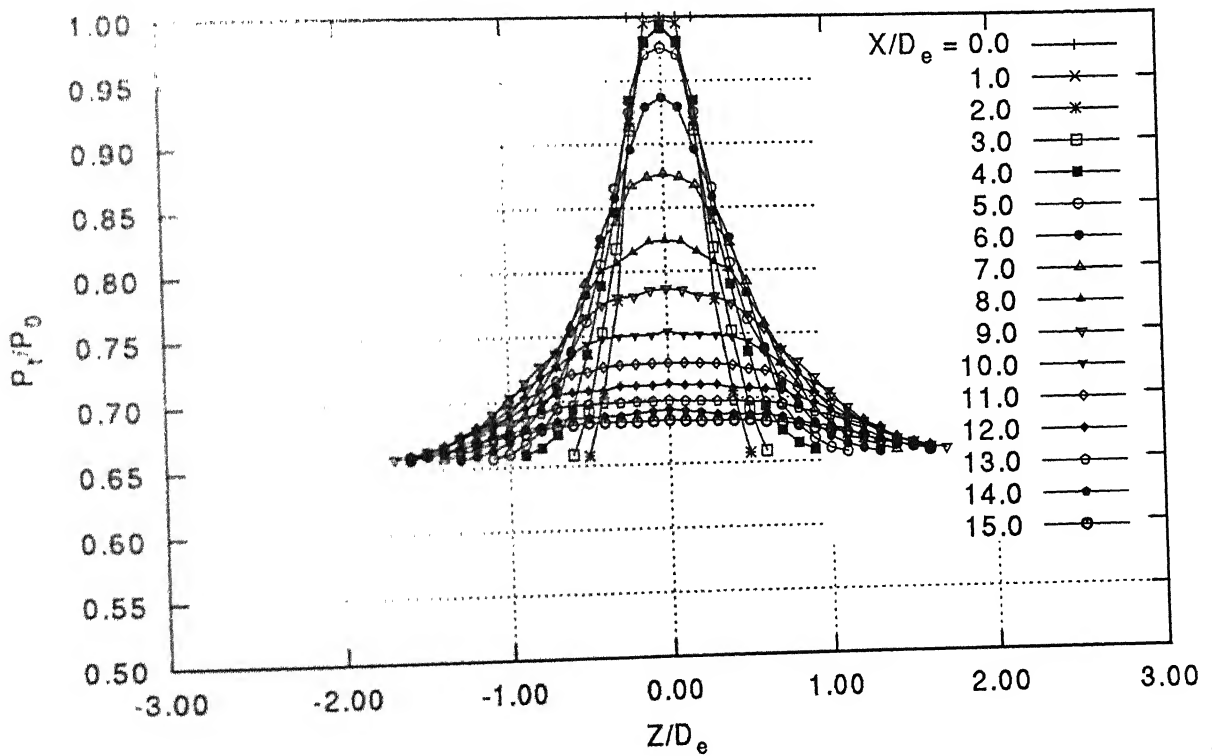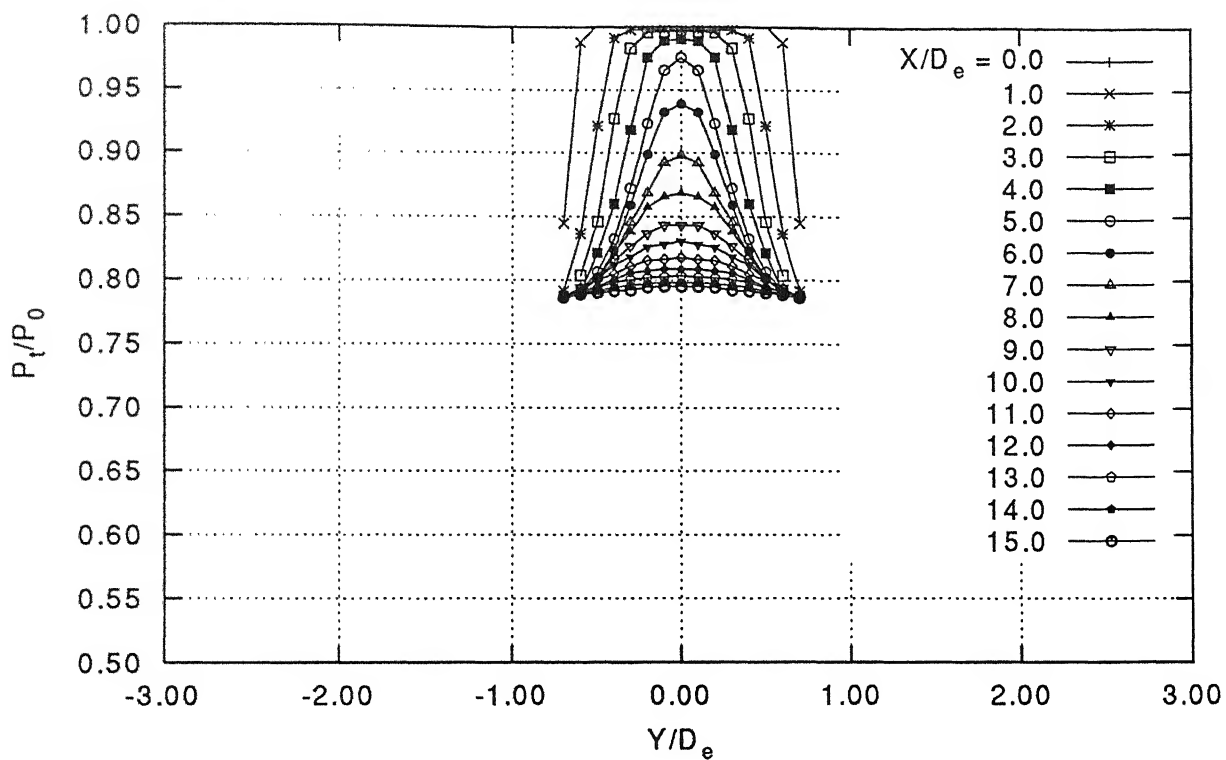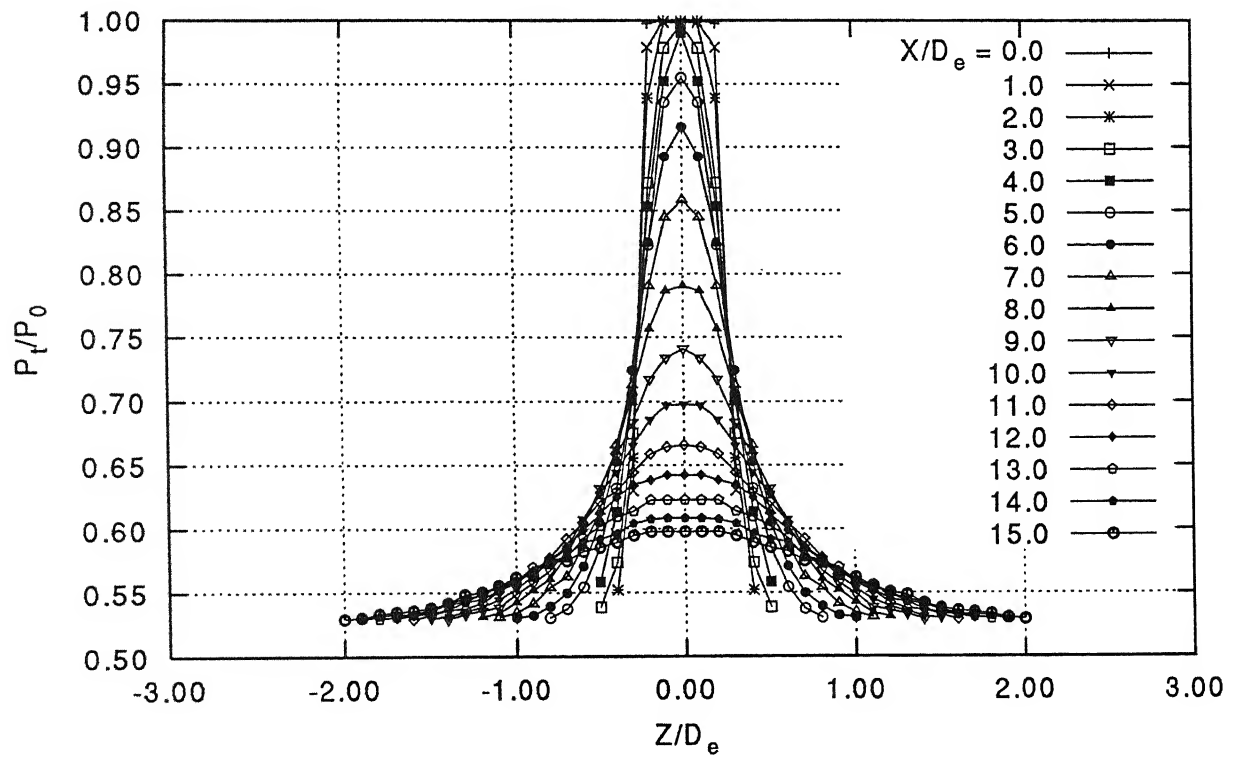
Figure. 4.25b Pressure profile Ellipse AR = 3 at M = 0.8

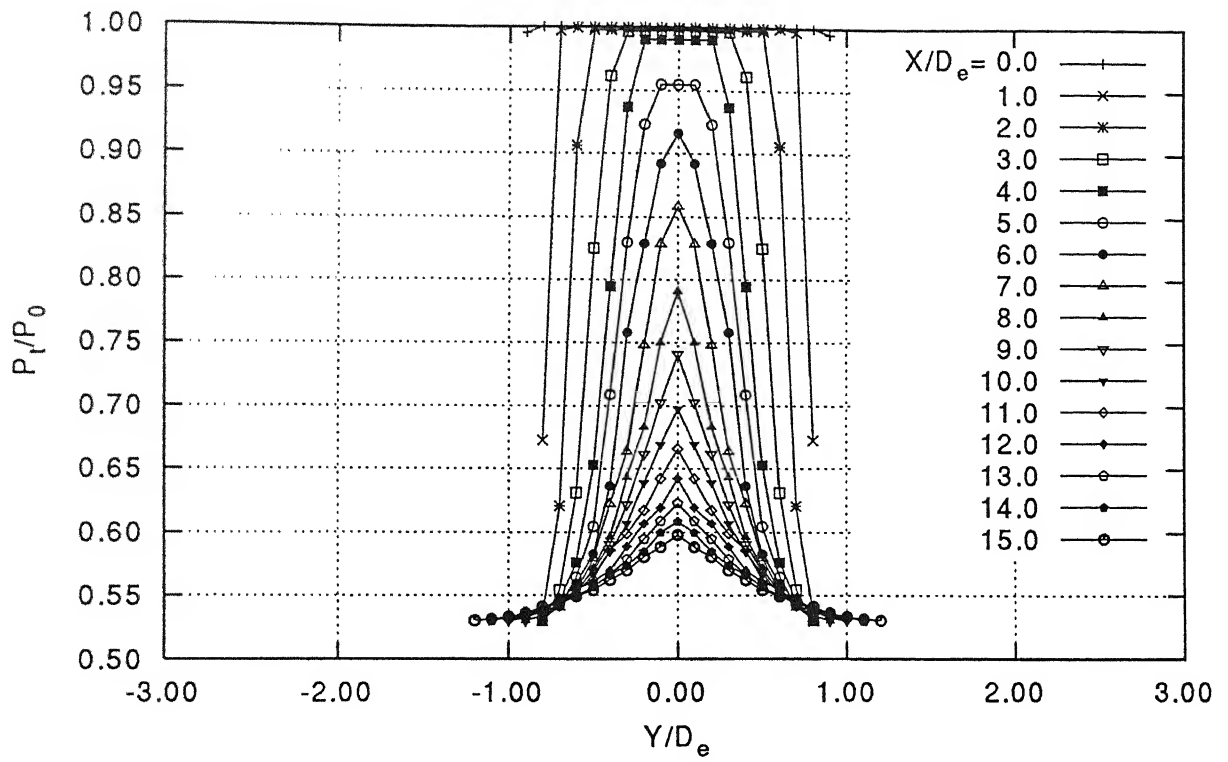Figure. 4.25c Pressure profile Ellipse AR = 3 at M=0.6

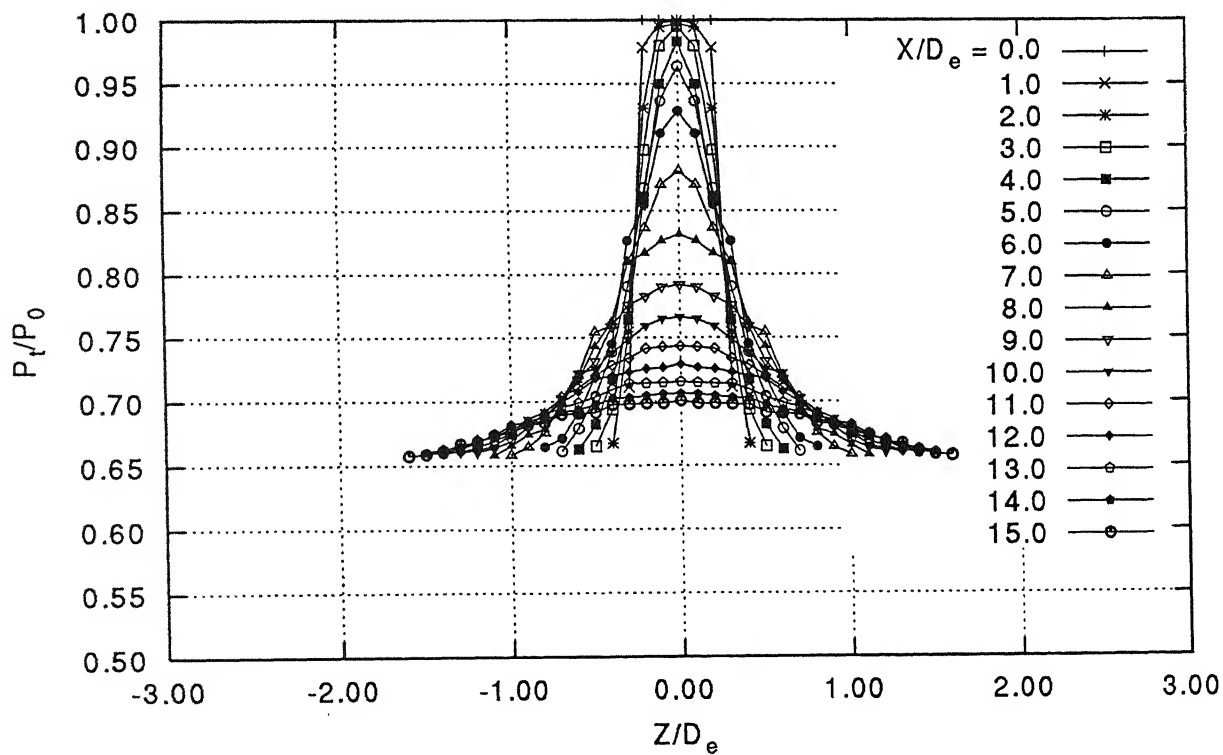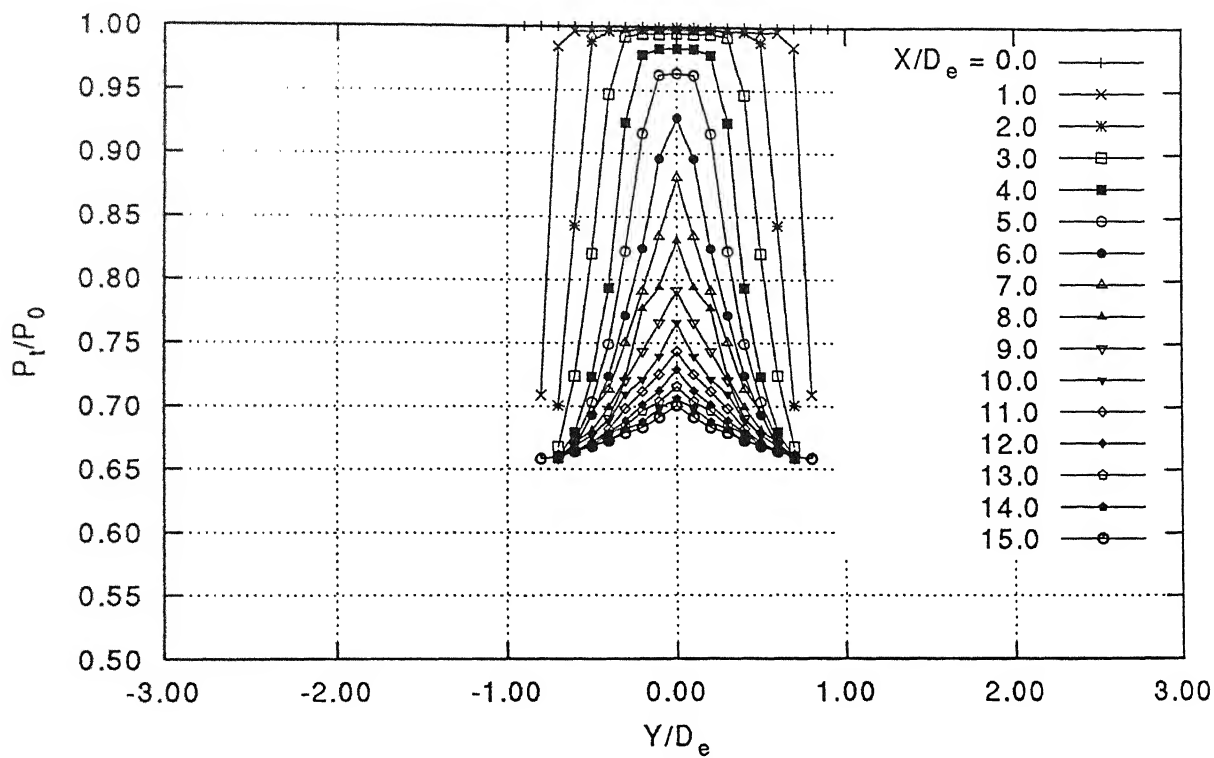Figure. 4.26a Pressure profile for Ellipse AR = 4 at M = 1.0

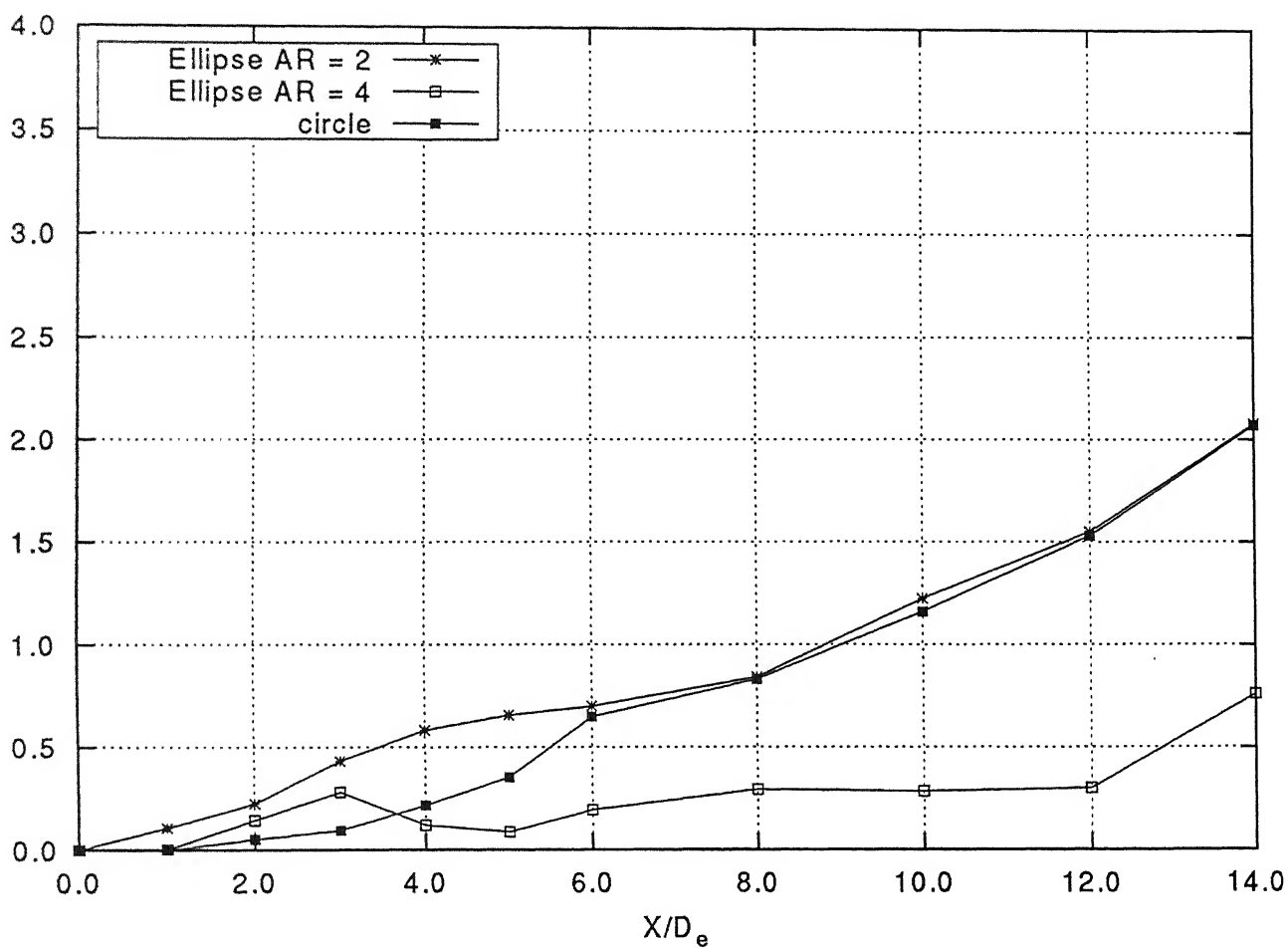Figure. 4.26b Pressure profile Ellipse AR = 4 at M = 0.8

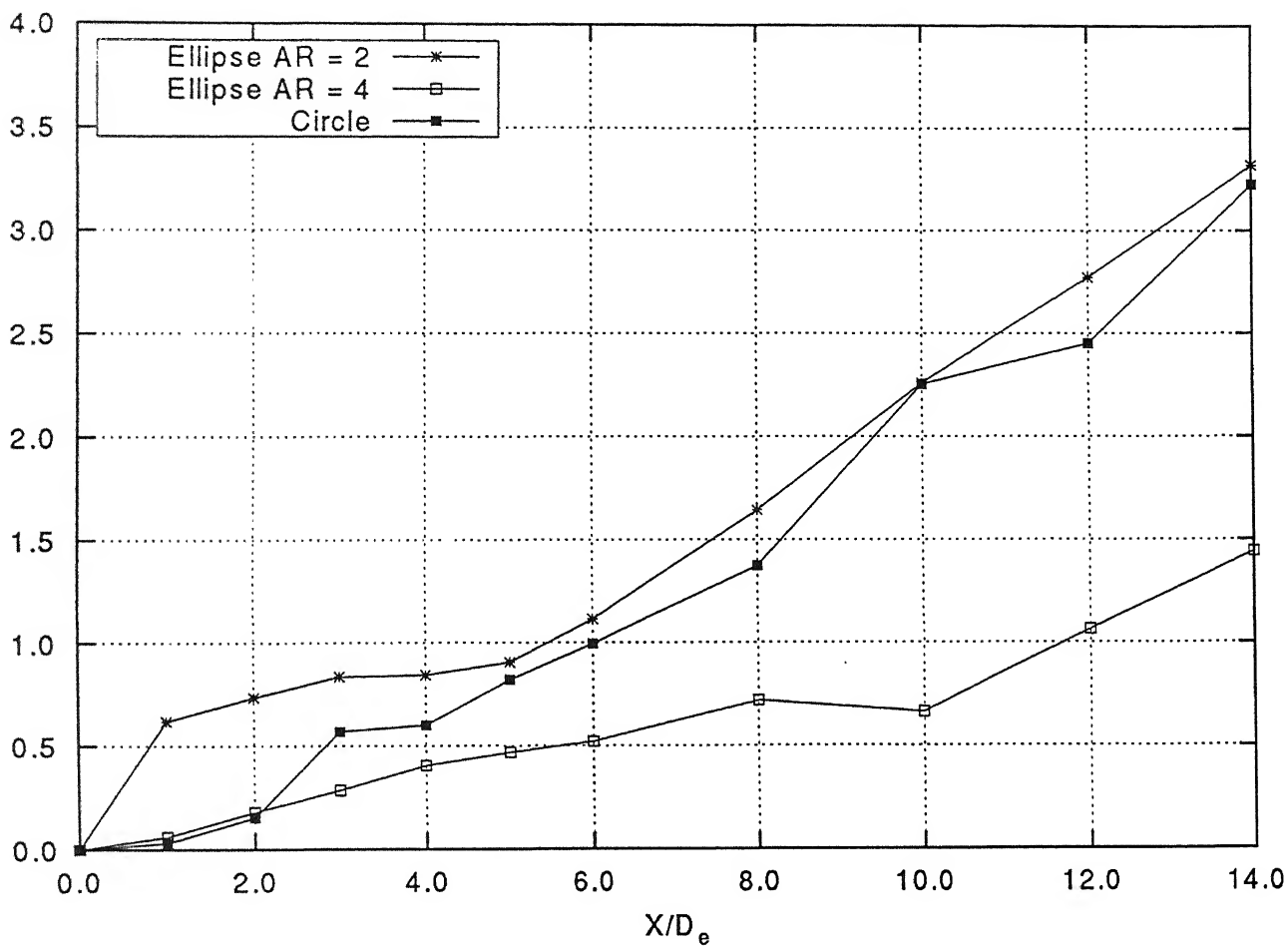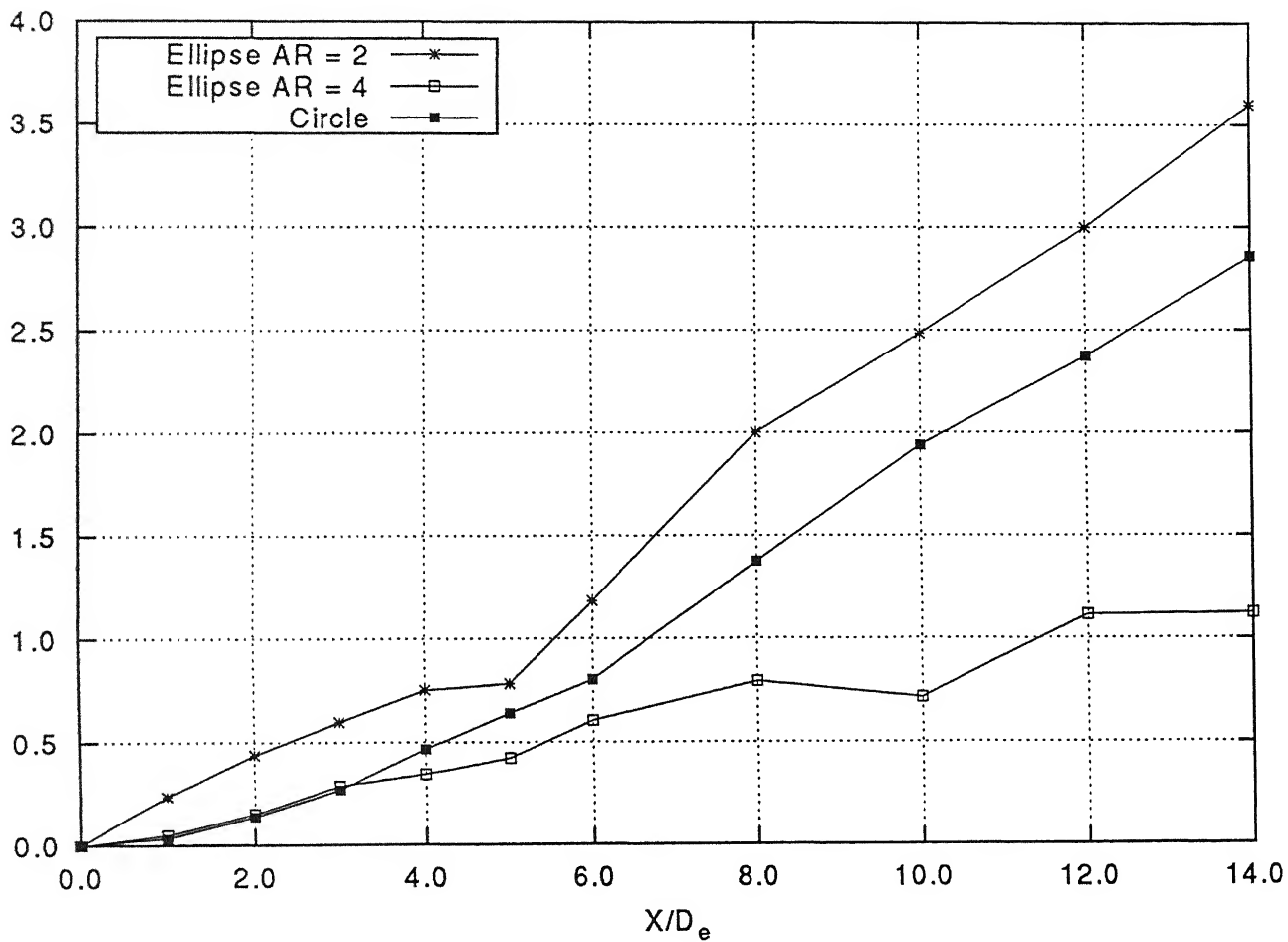Figure. 4.27 Mass entrainment profile at Mach 1.0

83

Figure. 4.28 Mass entrainment profile at Mach 0.8

Figure. 4.29 Mass entrainment profile at Mach 0.6